

**SYNTHESIS AND IN VITRO STUDIES OF
POLYCAPROLACTONE-COATED
SUPERPARAMAGNETIC IRON OXIDE NANOPARTICLES
FOR MAGNETIC HYPERTHERMIA THERAPY**

ZIBA HEDAYAT NASAB

**FACULTY OF ENGINEERING
UNIVERSITY OF MALAYA
KUALA LUMPUR**

2020

**SYNTHESIS AND IN VITRO STUDIES OF
POLYCAPROLACTONE-COATED
SUPERPARAMAGNETIC IRON OXIDE
NANOPARTICLES FOR
MAGNETIC HYPERTHERMIA THERAPY**

ZIBA HEDAYAT NASAB

**THESIS SUBMITTED IN FULFILMENT OF THE
REQUIREMENTS FOR THE DEGREE OF
DOCTOR OF PHILOSOPHY**

**FACULTY OF ENGINEERING
UNIVERSITY OF MALAYA
KUALA LUMPUR**

2020

UNIVERSITY OF MALAYA
ORIGINAL LITERARY WORK DECLARATION

Name of Candidate : Ziba Hedayat Nasab
Matric No : KHA150004
Name of Degree : Doctor of Philosophy

Title of Project Paper/Research Report/Dissertation/Thesis ("this Work"):

**Synthesis and In Vitro Studies of Polycaprolactone-Coated Superparamagnetic
Iron Oxide Nanoparticles for Magnetic Hyperthermia Therapy**

Field of Study: Advanced Materials & Technology

I do solemnly and sincerely declare that:

- (1) I am the sole author/writer of this Work;
- (2) This Work is original;
- (3) Any use of any work in which copyright exists was done by way of fair dealing and for permitted purposes and any excerpt or extract from, or reference to or reproduction of any copyright work has been disclosed expressly and sufficiently and the title of the Work and its authorship have been acknowledged in this Work;
- (4) I do not have any actual knowledge nor do I ought reasonably to know that the making of this work constitutes an infringement of any copyright work;
- (5) I hereby assign all and every rights in the copyright to this Work to the University of Malaya ("UM"), who henceforth shall be owner of the copyright in this Work and that any reproduction or use in any form or by any means whatsoever is prohibited without the written consent of UM having been first had and obtained;
- (6) I am fully aware that if in the course of making this work I have infringed any copyright whether intentionally or otherwise, I may be subject to legal action or any other action as may be determined by UM.

Candidate's Signature

Date: 7.08.2020

Subscribed and solemnly de

Witness's

Date: 7.08.2020

Name:

Designation:

SYNTHESIS AND IN VITRO STUDIES OF POLYCAPROLACTONE-COATED SUPERPARAMAGNETIC IRON OXIDE NANOPARTICLES FOR MAGNETIC HYPERTHERMIA THERAPY

ABSTRACT

Research has garnered a great interest in utilization of superparamagnetic iron oxide nanoparticles (SPIONs) as magnetic nano-heating agents in hyperthermia cancer therapy by profiting from high apoptosis vulnerability of cancer cells at elevated temperatures. However, low oxidation resistance and high agglomeration tendency negatively affect magnetic characteristics of nanoparticles and subsequently their clinical efficiency. Particle surface modifications are potential approaches to endow SPIONs a range of desirable properties including high colloidal dispersity, low aggregation tendency, cytocompatibility, and high oxidation resistance. Currently, polymer coating has led to decrease magnetic hyperthermia efficiency through formation of intermediate layer between nanoheating agents and targeted cells. This research aimed to stabilize the negatively-charged SPIONs through a cationic surfactant, followed by surface coating using thermosensitive biopolymer to improve particles dispersibility, cytocompatibility, functionality and in-vitro cytotoxicity under hyperthermia condition. In this study, synthesis condition was optimized via investigating the effects of two alkaline reagents as well as two synthesis environments on various SPIONs characteristics. Thereafter, the possibility of synthesizing SPIONs using a single iron precursor was examined to decrease synthesis complexity, save expenses, eschew wasting materials and improve their properties. The SPIONs were then stabilized by the surfactant, followed by focusing on preparation of biopolymer-coated SPIONs and assessing their physicochemical, thermal and magnetic properties as well as in-vitro hyperthermia performance on human hepatocellular carcinoma (HepG2) cells under the exposure of an alternating magnetic

field (AMF). The obtained results indicated that SPIONs could be synthesized using a single precursor through precipitation protocol under oxidative experimental condition with significant improvement in crystallinity and magnetic features in comparison with those of SPIONs produced using two precursors. Investigation of the surfactant showed its negligible effect on magnetic behaviors while enhanced dispersibility in a controlled micellar conformation, then biopolymer core-shell SPIONs showed an improvement in hyperthermia efficacy via their enhanced stealth characteristics to avoid rapid clearance by immune system and improved activity towards AMF due to melting of protective shell under hyperthermia condition. The findings indicated that combination of SPIONs and AMF rendered SPIONs highly cytotoxic to liver cancer cells; therefore, they would be a step-change into research as potential targeted nanoheating agent for new therapeutic options.

Keywords: Superparamagnetic iron oxide nanoparticles, Synthesis conditions, Specific absorption rate, In-vitro magnetic hyperthermia, Cytotoxicity assay.

**SINTESIS DAN KAJIAN IN VITRO NANOZARAH BESI OKSIDA
SUPERPARAMAGNETIK YANG BERSALUT POLYCAPROLACTONE
UNTUK TERAPI HIPERTERMIA MAGNETIK**

ABSTRAK

Kajian telah mengumpul minat yang besar dalam penggunaan nanozarah besi oksida superparamagnetik (SPIONs) sebagai agen nano-pemanasan magnetik dalam terapi kanser hipertermia dengan memaparkan kerentanan apoptosis yang tinggi pada suhu yang tinggi. Walaubagaimanapun, rintangan pengoksidaan yang rendah dan kebarangkalian aglomerasi yang tinggi akan menjejaskan ciri-ciri magnetik zarah secara negatif dan juga efisiensi klinikal. Modifikasi permukaan nanozarah merupakan cara yang berpotensi dalam menyumbangkan pelbagai ciri-ciri SPIONs yang baik seperti penyebaran koloid tinggi, kebarangkalian aglomerasi rendah, sito-keserasian dan rintangan pengoksidaan tinggi. Pada masa ini, teknik modifikasi permukaan semasa telah mengurangkan efisiensi terapi hipertermia magnetik melalui formasi lapisan pertengahan di antara agen nano-pemanasan dan sel sasaran. Kajian ini bertujuan untuk menstabilkan SPIONs yang bercas negatif dengan menggunakan bahan permukaan kation, seterusnya salutan permukaan melalui termosensitif biopolimer untuk meningkatkan penyebaran zarah, sito-keserasian, ciri fungsi dan in-vitro sitotoksity di bawah keadaan hipertermia. Kajian pertama fokus dalam pengoptimuman keadaan sintesis dengan menyiasat kesan jenis alkali dan alam sekitar sintesis pada ciri-ciri SPIONs. Dalam bahagian kedua, kemungkinan SPIONs sintesis menggunakan satu prekursor besi telah dikaji untuk mengurangkan kerumitan, menjimatkan perbelanjaan dan mengelakkan pembaziran bahan. SPIONs telah menstabilkan dengan menggunakan permukaan seterusnya, fokus pada sintesis SPIONs yang bersalut biopolimer dan penilaian ciri-ciri fizikokimia dan magnetik nanozarah dan juga prestasi hipertermia in-vitro pada sel karsinoma

hepatoselular manusia (HepG2) di bawah pendedahan medan magnet bergilir (AMF). Hasil kajian menunjukkan SPIONs boleh disintesis menggunakan satu prekursor melalui protokol pemendakan di bawah keadaan eksperimen oksidatif dengan peningkatan yang ketara dalam kehabluran dan pemagnetan dibanding dengan SPIONs yang dihasilkan melalui dua prekursor. Kajian permukaan menunjukkan tiada pengaruh pada ciri-ciri magnetik dan kehabluran zarah di samping menghasilkan zarah yang penyebaran tinggi dalam kawalan bentuk micellar, kemudian, biopolimer cangkerang-teras SPIONs menunjukkan peningkatan yang ketara dalam keberkesanan terapi hyperthermia magnetik secara melalui peningkatan ciri senyap untuk mengelakkan pelepasan pantas oleh sistem imun dan peningkatan aktiviti terhadap AMF disebabkan oleh leburan cangkerang pelindung di bawah keadaan hipertermia. Penemuan menunjukkan bahawa gabungan dari SPIONs dan AMF menjadikan SPIONs sangat sitotoksik kepada sel kanser hati; oleh itu, ia akan menjadi suatu penambahbaikan didalam kajian sebagai potensi sasaran agen nanopemanasan untuk pilihan terapeutik baru.

Kata kunci: Nanozarah besi oksida superparamagnetik, keadaan sintesis, kadar penyerapan spesifik, hipertermia magnetik in-vitro, ujian sitotoksiti.

To The Memory Of My Beloved Parents, Mozafar & Parvaneh

*To My Beloved Husband, Mohammadreza, For His Constant Support,
Understanding & Endless Love*

University of Malaya

ACKNOWLEDGEMENTS

First and foremost, I would like to express my sincere gratefulness to my research advisors, Prof. Ir. Dr. Wan Mohd Ashri Wan Daud and Assoc. Prof. Dr. Faisal Abnisa. Their beliefs in me and my decision to extend my scientific skills during this Ph.D work in cancer treatment provided motivation to achieve goals that I would not have imagined possible.

I am grateful to the entire Faculty of Engineering and also Faculty of Dentistry and all staff of the Chemical Engineering Department for providing laboratory facilities and instruments for experimental work of this research.

In addition, I would like to acknowledge the Ministry of Higher Education for the generous financial support under University of Malaya Research Grant (UMRG)-Innovative Technology Research Cluster (ITRC) and also Postgraduate Research Grant (PPP) which assisted me in the completion of my study.

Finally, I would like to give my sincere thanks to my beloved brother 'Kambiz' for his encouragement, support, and unconditional love throughout my life as far as I can remember.

TABLE OF CONTENTS

Abstract	iii
Abstrak	v
Acknowledgements	viii
Table of Contents	ix
List of Figures	xiii
List of Tables	xvi
List of Symbols and Abbreviations	xvii
CHAPTER 1: INTRODUCTION	1
1.1 Research Background	1
1.2 Problem Statement	3
1.3 Aim and Objectives	5
1.4 Research Scope	6
1.5 Outline and Structure	7
1.6 Workflow of the Thesis	9
CHAPTER 2: LITERATURE REVIEW	10
2.1 Introduction	10
2.2 Classification of MNPs for Hyperthermia Application	14
2.2.1 Magnetic Alloy Nanoparticles	14
2.2.2 Magnetic Metal Oxide Nanoparticles	16
2.3 Magnetization in Hyperthermia Application	20
2.3.1 Types of Magnetism	20
2.3.1.1 Ferromagnetism	20
2.3.1.2 Ferrimagnetism	22

2.3.1.3	Superparamagnetism	23
2.3.2	Magnetic Properties	27
2.3.2.1	Intrinsic magnetic properties	27
2.3.2.2	Extrinsic magnetic properties	30
2.4	Hyperthermia Therapy	32
2.4.1	Magnetic-Mediated Hyperthermia Therapy	36
2.4.2	Magnetic Hyperthermia Therapy	39
2.4.2.1	Effect of coating on hyperthermia efficiency	41
2.4.2.2	Effects of particle size and shape of MNPs on hyperthermia efficiency	49
2.4.2.3	Effects of frequency and strength of AMF on hyperthermia efficiency	52
2.5	Conclusions and Outlook	66
CHAPTER 3: METHODOLOGY		68
3.1	Introduction	68
3.2	Synthesis of Highly Stable Superparamagnetic Iron Oxide Nanoparticles under Mild Alkaline Reagents and Anaerobic Condition	69
3.2.1	Materials	69
3.2.2	Synthesis Procedure	69
3.2.3	Characterization	70
3.2.4	Data Analysis	70
3.3	Synthesis and In-Vitro Characterization of Superparamagnetic Iron Oxide Nanoparticles Using a Sole Precursor for Hyperthermia Therapy	71
3.3.1	Materials	71
3.3.2	Synthesis Procedure	71
3.3.3	Characterization	73

3.3.4	Cell Viability Assay	74
3.3.5	Magnetic Induction Heating	75
3.3.6	In-Vitro Magnetic Hyperthermia on the HepG2 Cells	76
3.3.7	Data Analysis	77
3.4	Polycaprolactone-Coated Superparamagnetic Iron Oxide Nanoparticles Micelles for In-Vitro Magnetic Hyperthermia Therapy of Cancer	78
3.4.1	Materials	78
3.4.2	Synthesis Procedure	78
3.4.3	CTAB Functionalization of Iron Oxides	79
3.4.4	Preparation of Coated Particles	80
3.4.5	Characterization	81
3.4.6	Cell Viability Assay	82
3.4.7	Magnetic Induction Heating	82
3.4.8	In-Vitro Magnetic Hyperthermia on the HepG2 Cells	82
3.4.9	Data Analysis	82
CHAPTER 4: RESULTS AND DISCUSSION		83
4.1	Introduction	83
4.2	Synthesis of Highly Stable Superparamagnetic Iron Oxide Nanoparticles under Mild Alkaline Reagents and Anaerobic Condition	88
4.2.1	Physicochemical Characterization	88
4.2.2	Structural and Phase Analysis	89
4.2.3	Morphological Analysis	91
4.2.4	Magnetic Analysis	93
4.3	Synthesis and In-Vitro Characterization of Superparamagnetic Iron Oxide Nanoparticles Using a Sole Precursor for Hyperthermia Therapy	95
4.3.1	Physicochemical Characterization	95

4.3.2	Structural and Phase Analysis	96
4.3.3	Morphological Analysis	99
4.3.4	Magnetic Analysis	101
4.3.5	Cytotoxicity Assay	102
4.3.6	Magnetic Hyperthermia Studies	103
4.3.7	In-Vitro Hyperthermia Test on HepG2 Cells	107
4.4	Polycaprolactone-Coated Superparamagnetic Iron Oxide Nanoparticles Micelles for In-Vitro Magnetic Hyperthermia Therapy of Cancer	109
4.4.1	Conformational Characteristics and Micellar Solution Properties	109
4.4.2	Morphological Analysis	110
4.4.3	Structural and Phase Analysis	112
4.4.4	Chemical Structure Analysis	113
4.4.5	Thermal Analysis	116
4.4.6	Magnetic Analysis	118
4.4.7	Cytotoxicity Assay	119
4.4.8	Magnetic Hyperthermia Studies	120
4.4.9	In-Vitro Hyperthermia Test on HepG2 Cells	124
CHAPTER 5: CONCLUSION AND RECOMMENDATIONS		126
5.1	Conclusions	126
5.2	Recommendations.....	129
REFERENCES.....		130
List of Publications and Papers Presented		149

LIST OF FIGURES

Figure 1.1: Detailed workflow of the main research activities	9
Figure 2.1: Schematic of experimental setup for induction heating test.....	41
Figure 2.2: TEM images of (a) uncoated CoFe ₂ O ₄ and (b) coated CoFe ₂ O ₄ (Ashwini B. Salunkhe, Khot, Ruso, & Patil, 2016).....	43
Figure 2.3: Different types of coatings	46
Figure 2.4: Various structures of coated MNPs.....	46
Figure 2.5: Trends of T _H and SAR of coated and uncoated Fe ₃ O ₄ at various strengths (Shete et al., 2014)	49
Figure 2.6: TEM images of (a) star-shaped CoFe ₂ O ₄ (L. T. Lu et al., 2015), (b) polyhedron-shaped MnFe ₂ O ₄ (Zeng, Rice, Wang, & Sun, 2004), (c) cone-shaped ZnO nanocrystals and (d) ZnO nanorods (Joo, Kwon, Yu, & Hyeon, 2005), (e) spherical-shaped γ -Fe ₂ O ₃ and cubic-shaped γ -Fe ₂ O ₃ (Salazar-Alvarez et al., 2008), FI-shaped CoFe ₂ O ₄ (Joshi et al., 2009) and (h) MnO multipods (Zitoun, Pinna, Frolet, & Belin, 2005)	52
Figure 2.7: The effect of particle size on Ms and T _H . (A) spherical-shaped CoFe ₂ O ₄ : (1) 6 nm; (2) 10 nm, (3) 15 nm, and (B) FI-shaped CoFe ₂ O ₄ : 12 nm, (2) 25 nm (Joshi et al., 2009)	52
Figure 2.8: The effects of varied strengths (20, 40, 50, 60 KA/m) on T _H and SAR of CS-MnFe ₂ O ₄ (Oh et al., 2016)	55
Figure 3.1: Experimental setup to synthesize iron oxide under oxidative condition.....	73
Figure 3.2: The schematic of the in-vitro hyperthermia test.....	77
Figure 3.3: A schematic of the chemical reaction for functionalization of iron oxide with CATB cationic surfactant	79
Figure 3.4: A schematic of the attachment mechanism of PCL-d on CTAB-modified iron oxide.....	80
Figure 3.5: A schematic of the functionalization and coating of CTAB-modified iron oxides	81
Figure 4.1: The rates of pH rise during dropwise addition of alkaline reagent under four varied synthesis conditions	89
Figure 4.2: The XRD spectra of a) IO ₁ , b) IO ₂ , c) IO ₃ , and d) IO ₄	90

Figure 4.3: TEM images of a) IO ₁ , b) IO ₂ , c) IO ₃ , and d) IO ₄	92
Figure 4.4: The magnetization graph of IO ₁ , IO ₂ , IO ₃ , and IO ₄	94
Figure 4.5: The rates of pH rise during dropwise addition of alkaline reagent under four varied oxidative conditions	95
Figure 4.6: The XRD spectra of a) S ₃ , b) S ₄ , c) S ₅ , and d) S ₆	97
Figure 4.7: The TEM images of a) S ₃ , b) S ₄ , c) S ₅ , and d) S ₆ . The narrowest particle size distribution with minimal agglomeration tendency is observed in S ₅ possibly due to the optimal oxidative potency of synthesis environment with O ₂ :N ₂ flow ratio of 5:5	100
Figure 4.8: The magnetization graph of S ₃ , S ₄ , S ₅ , and S ₆ . The inset indicates the magnified view of the graph	102
Figure 4.9: Cell viability profiles of HepG2 cells treated with different SPIONs for 24 h	103
Figure 4.10: The thermal profiles of S ₅ with various concentrations a) 1 mg.ml ⁻¹ , b) 2 mg.ml ⁻¹ , c) 3 mg.ml ⁻¹ , d) 4 mg.ml ⁻¹ , and e) 5 mg.ml ⁻¹ exposed to five varied AMF strengths. The band illustrates the hyperthermia range.....	104
Figure 4.11: The SAR comparison of different S ₅ concentrations under exposure to five varied AMF strengths. The stronger AMF strengths and lower particles concentrations result in higher SAR values.....	106
Figure 4.12: The temperature profile of the HepG2 medium with S ₅ during exposure to varied AMF strengths. The minimal magnetic field of 31.47 kA.m ⁻¹ could only render S ₅ with adequate heating capability to retain the desirable T _H (the band area)	108
Figure 4.13: Cytotoxicity profiles of HepG2 cells treated with S ₅ exposed to varied AMF strengths, as quantified by MTT assay.....	108
Figure 4.14: Different configurations of surfactant molecules around the iron oxide particles at varied CTAB quantities. Three main micellar structures are determined based on alteration of the ζ values of samples	110
Figure 4.15: The TEM images of a) bare iron oxide, b) SPC ₁₅ , and c, d) PCL-SPC ₁₅ with different magnifications. The core-shell structure of PCL-SPC ₁₅ is obviously observed.....	111
Figure 4.16: The XRD patterns of a) bare iron oxide, b) SPC ₁₅ , and c) PCL-SPC ₁₅ . The peaks at 21.4° and 23.7°, which represent the crystallographic planes of PCL, indicated the formation of biopolymer coating on the nanoparticles surface.....	112
Figure 4.17: HRTEM images of a) bare iron oxide and b) PCL-SPC ₁₅	113

Figure 4.18: FTIR spectra of a) bare iron oxide, b) pure CTAB, c) SPC ₁₅ , d) PCL-d, and e) PCL-SPC ₁₅ . The *, ‡, and # symbols represent the specific bonds of iron oxide, CTAB, and PCL-d respectively, indicated the formation of their functional groups on the PCL-SPC ₁₅ surface.	114
Figure 4.19: The XPS spectra of PCL-SPC ₁₅ . a) Low-resolution survey spectrum, b) High-resolution C 1s XPS spectrum c) High-resolution O 1s XPS spectrum, and d) High-resolution Fe 2p XPS spectrum.....	116
Figure 4.20: The thermal behaviour of (a) DSC thermograms of pure PCL and PCL-SPC ₁₅ , and (b) TGA curves of pure PCL, SPC ₁₅ and PCL-SPC ₁₅	117
Figure 4.21: The magnetization graphs of bare SPIONs, SPC ₁₅ , and PCL-SPC ₁₅	119
Figure 4.22: Cell viability profiles of HepG2 cells treated with different concentrations of PCL-SPC ₁₅ for 24 and 48 h	120
Figure 4.23: The thermal profile of PCL-SPC ₁₅ at varied AMF strengths. The 31.49 kA.m ⁻¹ magnetic strength could only induce heating power within the secure hyperthermia range (the band area).....	123
Figure 4.24: The temperature profile of HepG2 cells with PCL-SPC ₁₅ during exposure to varied AMF strengths. The minimal magnetic field of 31.47 kA.m ⁻¹ could only render PCL-SPC ₁₅ with adequate heating capability to retain the desirable T _H (the band area)	124
Figure 4.25: Cytotoxicity profiles of HepG2 cells treated with PCL-SPC ₁₅ exposed to varied AMF strengths, as quantified by MTT assay	125

LIST OF TABLES

Table 2.1: Different types of MNPs	18
Table 2.2: Different types of magnetic behaviour	25
Table 2.3: Comparison of three different HT techniques	34
Table 2.4: Comparison of four main strategies of MHT	37
Table 2.5: Magnetic and in-vitro hyperthermia characteristics of varied MNPs	56
Table 3.1: The experimental conditions applied for the synthesis of iron oxide samples	73
Table 4.1: The phase structural characteristics of the iron oxide particles synthesized in varied synthesis conditions	91
Table 4.2: The initial and final pH values of the synthesis solutions as well as the ζ values of the particles produced in synthesis environments with varied oxidative potencies ...	96
Table 4.3: The phase structural characteristics of the iron oxide particles synthesized in varied oxidative environment	99
Table 4.4: The magnetic properties of SPIONs synthesized in four varied oxidative environments	101
Table 4.5: The achieved temperatures ($^{\circ}\text{C}$) in the nanofluids containing varied SPIONs concentrations exposed to different AMF strengths for 900 and 5400 s	106
Table 4.6: The comparison of the magnetic properties among bare SPIONs, CTAB-stabilized SPIONs and PCL-SPC ₁₅	118

LIST OF SYMBOLS AND ABBREVIATIONS

Symbols	:	
Ag	:	Silver
B	:	Full width at half maximum
C	:	Specific heat capacity
C_{do}	:	Concentration of the dissolved oxygen
Co	:	Cobalt
D	:	Crystallite size
dT/dt	:	Initial slop
f	:	Frequency
Fe	:	Iron
Fe_3O_4	:	Magnetite
H	:	Strength
h	:	Hour
H_c	:	Coercivity
i	:	Applied current
I_c	:	Optical values of sample
I_s	:	Optical values of cells
K_H	:	Henry's law constant
K_S	:	Shape factor of Scherrer
L	:	Coil diameter
m_{cd}	:	Mass of colloidal dispersion
m_{Fe}	:	Mass of iron in the fluid
min	:	Minutes
Mn	:	Manganese

M_r	:	Remanent magnetization
M_r/M_s	:	Relative remanence
M_s	:	Saturation magnetization
n	:	Coil turns
N_2	:	Nitrogen
Ni	:	Nickel
s	:	Second
t	:	Treatment time
T_B	:	Block temperature
T_C	:	Curie temperature
T_H	:	Hyperthermia temperature
ζ	:	Zeta potential
τ_B	:	Brownian relaxation
τ_N	:	Néel relaxation

Abbreviation :

AEH	:	Arterial embolization hyperthermia
AMF	:	Alternating magnetic field
BSA	:	Bovine serum albumin
CaMC	:	critical concentration for ad-micellar configuration
CS	:	Chitosan
CTAB	:	Cetyltrimethylammonium bromide
DEX	:	Dextran
DIH	:	Direct injection hyperthermia
DM	:	Diamagnetic
DMEM	:	Dulbecco's Modified Eagle Medium
DMSO	:	Dimethyl sulfoxide
DSC	:	Differential Scanning Calorimetry
FBS	:	Fetal bovine serum
FeCl ₂ ·4H ₂ O	:	ferrous chloride tetrahydrate
FeCl ₃ ·6H ₂ O	:	Ferric chloride hexahydrate
FI	:	Facet irregular
F _I M	:	Ferrimagnetic
F _O M	:	Ferromagnetic
FTIR	:	Fourier transform infrared spectroscopy
HepG2	:	Human hepatocellular carcinoma
HIFU	:	High Intensity Focused Ultrasound
HIS	:	Heating source insertion
HRTEM	:	High-resolution transmission electron microscopy
HT	:	Hyperthermia therapy
IIH	:	Interstitial implant hyperthermia

IH	:	Intracellular hyperthermia
IO ₁	:	Synthesis of iron oxide under NaOH.Air
IO ₂	:	Synthesis of iron oxide under NH ₄ OH.Air
IO ₃	:	Synthesis of iron oxide under NaOH.N ₂
IO ₄	:	Synthesis of iron oxide under NH ₄ OH.N ₂
IONPs	:	Iron oxide nanoparticles
MANPs	:	Magnetic alloy nanoparticles
MCA	:	Magneto-crystalline anisotropy
MHT	:	Magnetic hyperthermia therapy
MMHT	:	Magnetic-mediated hyperthermia therapy
MMONPs	:	Magnetic metal oxide nanoparticles
MMNPs	:	Metallic magnetic nanoparticles
MNPs	:	Magnetic nanoparticles
MRI	:	Magnetic resonance imaging
NaOH	:	Sodium hydroxide
NH ₄ OH	:	Ammonium hydroxide
OA	:	Oleic acid
PBS	:	Phosphate-buffered saline
PCL	:	Polycaprolactone
PCL-d	:	Polycaprolactone with diol terminal groups
PEG	:	Polyethylene glycol
PLA	:	Poly(lactic acid)
PLGA	:	Poly(glycolic acid)
PM	:	Paramagnetic
PU	:	Polyurethane
PVP	:	Polyvinylpyrrolidone

RES	:	Reticuloendothelial system
RF	:	Radiofrequency
SAR	:	Specific absorption rate
SD	:	Standard deviation
SPIONs	:	Superparamagnetic iron oxide nanoparticles
S ₃	:	Synthesis of SPIONs under oxygen pressure of 0.3 Pa
S ₄	:	Synthesis of SPIONs under oxygen pressure of 0.4 Pa
S ₅	:	Synthesis of SPIONs under oxygen pressure of 0.5 Pa
S ₆	:	Synthesis of SPIONs under oxygen pressure of 0.6 Pa
SPC ₁	:	SPIONs with 1mg CTAB
SPC ₅	:	SPIONs with 5mg CTAB
SPC ₁₀	:	SPIONs with 10mg CTAB
SPC ₁₅	:	SPIONs with 15mg CTAB
SPC ₂₀	:	SPIONs with 20mg CTAB
SPM	:	Superparamagnetic
SPMNPs	:	Superparamagnetic nanoparticles
SQUID	:	Superconducting quantum interference device
TEM	:	Transmission electron microscopy
TGA	:	Thermogravimetric analysis
VSM	:	Vibrating-sample magnetometry
W/O	:	Water-in-oil
WA	:	Wireless applicators
WB	:	Whole body
XPS	:	X-ray photoelectron spectroscopy
XRD	:	X-ray diffraction

CHAPTER 1: INTRODUCTION

1.1 Research Background

Superparamagnetic iron oxide nanoparticles (SPIONs) have increasingly exhibited a propitious opportunity in biomedical applications from magnetic resonance imaging (MRI) to drug delivery and magnetic hyperthermia therapy (MHT), due to their promising therapeutic and diagnostic capabilities. In particular, magnetite (Fe_3O_4) nanoparticles are considerably preferred choice thanks to their biocompatibility, pleomorphism, superior tunable magnetic properties, great saturation magnetization (M_s), low remanent magnetization (remanence; M_r) and coercivity (H_c), easy recycle through the metabolism pathways, facile synthesis, and low cost of mass production (Amirshaghghi et al., 2019; Hedayatnasab, Abnisa, & Wan Daud, 2017; Iacovita et al., 2016). Moreover, the US Food and Drug Administration has approved the application of Fe_3O_4 as contrast agents based on the fact that iron is a vital element to sustain the majority of the organism's cellular function e.g. hematopoiesis and to be the active center of ferredoxin and hemoglobin. (Muro-Cruces et al., 2019). However, in parallel to their diagnostic application, Fe_3O_4 could also be used as therapeutic agents to target the cancer biomarkers either in biopsies of tissues or even infusion of magnetic nanofluids in the presence of an external alternating magnetic field (AMF) in order to alter the metabolism of the heat shock proteins at the targeted tumor area, resulting in cellular degradation and apoptosis (Berry, Walker, Hoskins, Telling, & Price, 2019).

This cancer treatment approach which is called MHT, is based on the instant heating of the cancer cells via administration of SPIONs into the tumor region and their selective killing due to higher vulnerability of cancer cells at the hyperthermia temperatures (T_H ; 42-47 °C) compared to the healthy cells, mainly derived from low blood perfusion in the

tumor (Boyer et al., 2015; Dutz & Hergt, 2014). Thereby, SPIONs with dual therapeutic and diagnostic capabilities known as theranostics give rise to be recognized as a promising magnetic nanoheating agents in cancer therapy.

Magnetic nanoheating agents in cancer treatments necessitate adequate stability in aqueous media at neutral pH and physiological salinity. However, bare SPIONs are highly tendentious to self-agglomeration due to their strong electrostatic interactions, high surface energy, and vulnerability to air and moisture oxidation. The effective approach to provide higher colloidal stability is surfactant-based surface modification of nanoparticles (Elfeky, Mahmoud, & Youssef, 2017; Hedayatnasab et al., 2017). However, addition of excessive amounts of surfactants to the nanoparticle dispersions may induce agglomeration of fine particles through charge neutralization, bridging and formation of surfactant-particle surface or via a combination of these mechanisms. Thereby, a highly efficient surfactant with appropriate adsorption gives rise to surface saturation which not only prevents bridging and destabilization of nanoparticles but also controls particle size and improves dispersion (Abu-Jdayil, Ghannam, & Nasser, 2016; Günister et al., 2006).

In addition, a rapid opsonization and subsequent segregation by the immune system is another challenge during in-vivo application of SPIONs. Indeed, these nanoheating agents are easily recognized as foreign bodies by the reticuloendothelial system (RES), instantly coated by plasma proteins and blood components, and rapidly cleared before reaching the targeted region (Aggarwal, Hall, McLeland, Dobrovolskaia, & McNeil, 2009).

Recently, a novel mechanism of induction heating using a thermosensitive biopolymer coating has been proposed. In this mechanism, biopolymer coatings with a low-melting point within the secure T_H range have been applied to provide SPIONs with 'stealth' characteristics and make them invisible to the immune system.

The aim of these thermosensitive coating shells is to enhance the steric stability, dispersity, and biodistribution and confer excellent stealth characteristics to the SPIONs and minimize RES sensitivity. Although, a number of aliphatic linear polyesters has been applied including polyethylene glycol (PEG) (Sebak, 2018), polyglycolic acid (PLGA) (Ferreira et al., 2019), and polylactic acid (PLA) (Ferreira et al., 2019), several shortcomings such as non-biodegradability and degradation under stress and discourage interaction with the receptors on the targeted cell membranes must be overcome prior their actual application in treatment of human diseases. The application of SPIONs for treatment of brain cancer “glioblastoma” has been approved in Europe since 2011 and some of these thermosensitive magnetic nanoheating agents are currently undergoing clinical trials in different phases to evaluate their efficacy in treatment of other carcinoma cancer types such as prostate, breast and liver.

1.2 Problem Statement

Although SPIONs have been extensively employed for MHT, their low stability in aqueous media hinders their application as effective therapeutic agents. In general, SPIONs are unstable in aerobic conditions derived from their significant vulnerability to air and moisture oxidation, which consequently leads to lose magnetism.

A high tendency to particle agglomeration is another limitation of SPIONs, mainly due to their high surface energy. Therefore, the nanoparticles tend to reach the lowest energy states and diminish such excess energy through clumping together. Moreover, SPIONs possess large amounts of unsaturated and vacant coordination sites owing to their large surface area, which make atoms surface to create bonds with adjacent particles through van der Waals forces and become aggregated. Subsequently, the particle size increases and magnetic behaviour from superparamagnetic changes to ferromagnetic

(Hedayatnasab, Dabbagh, Abnisa, Abu Ksaim, & Wan Daud, 2019; T. K. Nguyen, Duong, Selvanayagam, Boyer, & Barraud, 2015).

Furthermore, in regard to their application as theranostics, the low-size bare SPIONs are easily recognized as foreign bodies by the immune systems and instantly coated by e.g. plasma proteins, resulting in their short half-life and rapid clearance from the body. In particular, when they used as heat generation sources in MHT, the main challenge is to maintain the target temperature within the secure range of 42-47 °C, which not only can result in effective tumour cell apoptosis, but also can avoid overheating of the nearby healthy cells and thus minimize the treatment side effects (Aggarwal et al., 2009; Hedayatnasab et al., 2017).

One of the best approaches to reduce the vulnerability towards air and moisture oxidation is providing the anaerobic condition e.g. nitrogen (N₂), most preferably via administration of inert gases is considered requisite to prevent their activity towards oxygen (O₂) environment (Gupta & Gupta, 2005). In order to increase the SPIONs stability, applying suitable stabilizers such as surfactants or anchoring groups with proper surface charge is offered to reduce the excess surface energy and prevent particle agglomeration (Gan, Lu, Cao, & Chen, 2018). Coating of the particle surfaces is also beneficial in keeping T_H in the secure hyperthermia range. Moreover, applying biopolymers lead to improved cytocompatibility as a considerably important parameter in cancer treatment since the surface of the heating agent is directly in contact with blood and tissue cells without any intermediary (Dabbagh et al., 2019).

In spite of the positive influence of particle coating on their stability, dispersion, in-vivo half-life, and cytocompatibility, excessively decreased heat generation efficacy of the coated particles in the targeted tissue is the remaining challenge. In fact, the coating shield acts as an isolator layer between the nanoparticles and the tumor cells, thus resulting in decreased heat transfer from the SPIONs into the tumor.

One potential solution to overcome the negative effect of nanoparticles coating on their heat transfer efficacy is to provide polymer coatings with melting points in the hyperthermia temperature range (Y. Dai et al., 2019). Therefore, when such nanoparticles reach the affected region and expose to an external AMF, the polymer shell melts, leading to particles transition from their passive to active state and consequently improved heat eradication into the cancer cells.

1.3 Aim and Objectives

This research aims to stabilize and functionalize SPIONs using a cationic surfactant into a controlled micellar conformation, followed by a thermosensitive biopolymer coating to endow a stealth behaviour to SPIONs in order to improve the hyperthermia efficiency under AMF exposure. To best of my knowledge, this research would be the first endeavor in fabrication of thermosensitive biopolymer core-shell SPIONs as magnetic nanoheating agents for in-vitro hyperthermia application.

In order to achieve this aim, the following objectives have been defined:

1. To synthesize and characterize SPIONs under aerobic and anaerobic synthesis environments using two different alkaline reagents in order to determine the best synthesis condition.
2. To synthesize SPIONs using a sole iron precursor through the optimization of the oxidative potency of the synthesis environment, i.e. the O₂:N₂ flow ratio, rather than using both Fe(II) and Fe(III) precursors in a precisely-controlled condition.
3. To stabilize and functionalize SPIONs by using a cationic surfactant in a controlled micellar stability for surface coating with a thermosensitive biopolymer

to enhance the in-vitro magnetic hyperthermia efficiency against human liver carcinoma cells.

1.4 Research Scope

The present research aims to integrate the materials science, chemical as well as biomedical engineering in order to develop magnetic nanoheating agents in a stabilized conformation with high magnetization to evaluate their in-vitro hyperthermia efficiency against human hepatocellular carcinoma (HepG2) cancer cells under the external AMF exposure. Thereby, prior the surface coating of these magnetic nanoheating agents, a thermosensitive biopolymer with specific properties was chosen that not only provide structural stability, but also endows stealth characteristics to the nanoagents due to having a melting point in the secure hyperthermia range; hence, thermal characterizations were performed.

For the first objective, in order to synthesize the magnetic nanoheating agent with desirable properties without using any stabilizing agents, the effects of two alkaline reagents and two synthesis environments were investigated. Through the optimal condition, the nanoheating agents could also be synthesized using only a single iron precursor through alteration of the oxidative potency of the synthesis environment, i.e. the O₂:N₂ flow ratio in the second research objective. Moreover, in order to produce the stabilized and functionalized nanoheating agents with a controlled micellar conformation, zeta potential measurements were performed on varied cationic surfactant quantities. Subsequently, the stabilized sample with optimum surfactant quantity was coated with a thin layer of thermosensitive biopolymer to enhance cytocompatibility and physicochemical properties for performing better in-vitro magnetic hyperthermia efficiency against HepG2 cells. However, in-vitro examination in simulated body fluids, in-vivo studies and determination the kinetic as well as the thermodynamic

behaviour of these magnetic nanoheating agents fall beyond the scope of this project and may be performed in further research.

1.5 Outline and Structure

This report is organized in five chapters concerned with different aspects of the topic and the objectives of the research.

This chapter briefly establishes the scientific framework in which the present work is accomplished. It outlines the application and importance of the SPIONs as magnetic nanoheating agents in hyperthermia cancer treatment and clarifies the remaining challenges which must be addressed to enhance the therapeutic efficacy of this approach. The specific aims and objectives of the research according to the current challenges in this field are also stated.

The chapter 2 provides a comprehensive classification of different types of magnetic nanoparticles, their intrinsic and extrinsic properties, magnetism states and heating mechanisms for hyperthermia application. The effects of SPIONs characterizations as well as AMF parameters such as strengths and frequency on the hyperthermia efficiency are also reviewed. Finally, the latest advancements in nanoparticles coating techniques are highlighted.

The chapter 3 elucidates all the experiments and analytical procedures for the synthesis, characterization, surface modification, induction heating tests and in-vitro cytotoxicity assays of iron oxide samples. The detailed information on materials, equipment, experimental design and instruments used for this study are explained as well.

The chapter 4 presents the results and data analysis obtained from laboratory experiments. In this chapter the results are divided in three main parts. Part 1 investigates the effects of experimental conditions on various chemical, morphological, physical, and

magnetic characteristics of the resulting iron oxide samples and according to the obtained results, an optimal synthesis condition is recommended. Part 2 studies the synthesis possibility of iron oxide particles using a single iron precursor under different oxidative conditions using four varied O₂:N₂ flow ratios and then their physicochemical properties and cytocompatibilities are evaluated in order to determine the optimal sample. The effects of various dose–response characteristics of the optimized SPIONs on the magnetic hyperthermia efficiency upon a wide range of AMF strengths are also investigated. Thereafter, the cytotoxicity assays against HepG2 cells were performed in the presence of varied AMF strengths to evaluate their effectiveness as magnetic nano-heating agents under hyperthermia condition. Part 3 outlines the development of biopolymer-coated SPIONs with structural stability, uniform particle size, improved dispersity, cytocompatibility, and controlled induction heating under hyperthermia condition. Thereby, iron oxide samples were functionalized with a double-layered cationic surfactant to enhance their stability and provide proper functionalized surface for coating modification with a low-melting point biopolymer in order to achieve enhanced cytocompatibility and physicochemical properties for in-vitro magnetic hyperthermia on HepG2 cells. Thereafter, the effects of varied AMF strengths on induction heating capability of these core-shell nanoheating agents were investigated to obtain appropriate T_H profile.

The research report finally closes in chapter five with a summary of the main conclusions from the experimental results and the highlights of the remaining research gaps which could be addressed in further research.

1.6 Workflow of the Thesis

A workflow of the main research activities and the linkage among the research objectives as well as the steps in performing the research based on literature review described in this thesis, are illustrated in Figure 1.1.

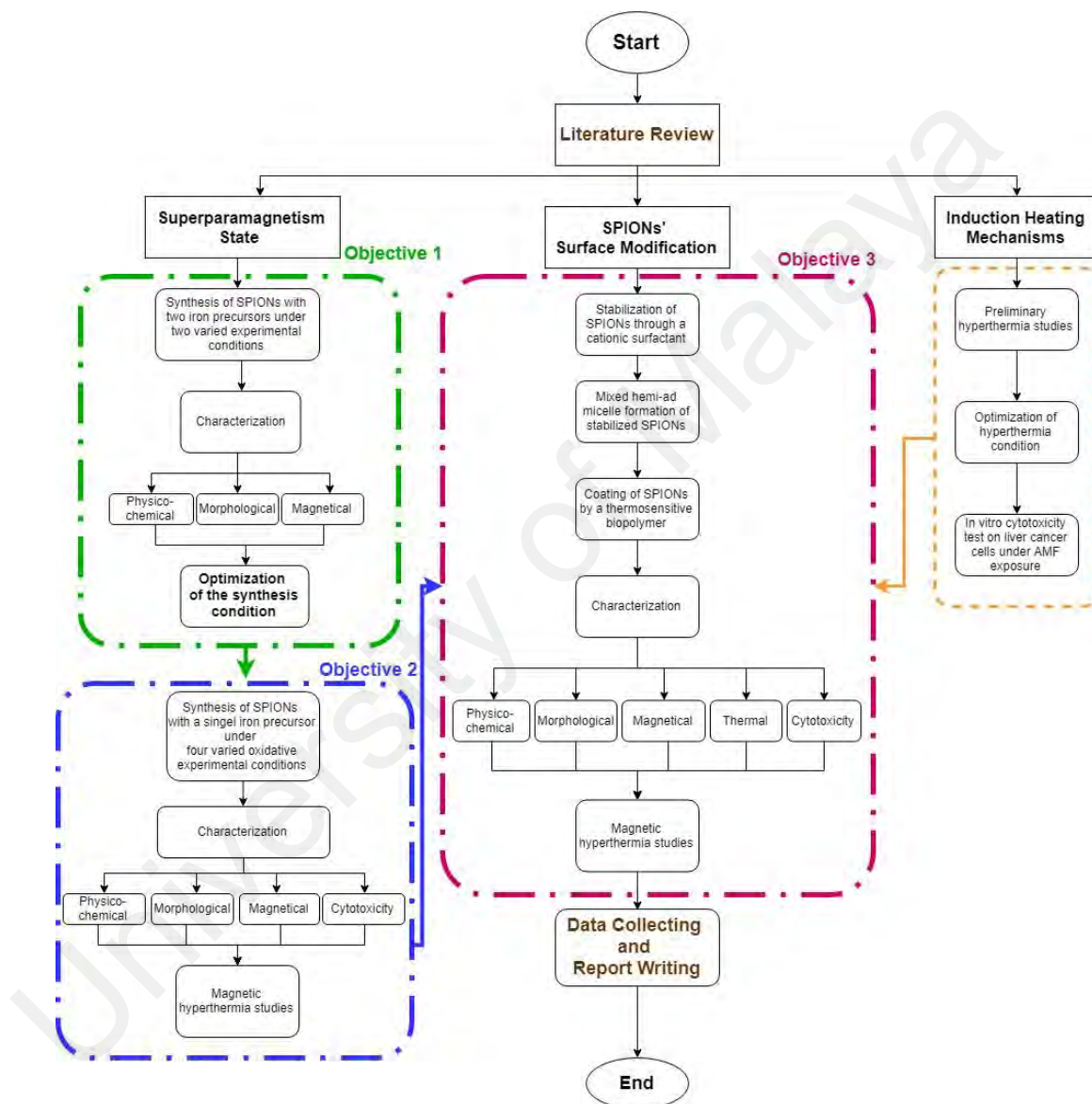


Figure 1.1: Detailed workflow of the main research activities

CHAPTER 2: LITERATURE REVIEW

2.1 Introduction

Nanoparticles are ultrafine particles with at least one dimension in nanometer range (1 to 100). Nanoparticles present high surface-area-to-volume ratio and are extremely reactive, versatile, and strong as compared to bulk ones. These features confer unbounded possibilities to improve their unique mechanical, optical, and magnetic properties. Nanoparticles are mainly classified into either organic group, including carbon nanotubes, liposomes, and fullerenes, or inorganic group, including quantum dots and magnetic nanoparticles (MNPs) (Chen, Roy, Yang, & Prasad, 2016; Doll, Raman, Dey, & Burkhard, 2013; Reza Eslami-Farsani, Reza Khalili, Hedayatnasab, & Soleimani, 2014; Hedayatnasab, Eslami-Farsani, Khalili, & Soleimani, 2013; Khalili, Eslami-Farsani, Soleimani, & Hedayatnasab, 2014; Nath & Banerjee, 2013; Soleimani, Khalili, Farsani, & Hedayatnasab, 2012). MNPs have gained great popularity because of their capability to be functionalized at both cellular and molecular levels (Sun, Lee, & Zhang, 2008).

MNPs are inorganic and zero-dimensional materials with metal-based configuration. These nanoparticles have gained increased importance because they can be easily manipulated using AMF and subsequently employed in various applications. MNPs exhibit intrinsic and unique properties, such as high Ms, biocompatibility, and less toxicity; in this regard, some breakthroughs have been conducted in various fields, such as industrial, environmental, analytical, and biomedical applications. In particular, MNPs have attracted attention for biomedical applications because these particles feature such as easy controllability, biological compatibility, physicochemical properties, and superior magnetic properties.

Biomedical applications depend on the properties of MNPs; such properties, in turn, are affected by the type of applied MNPs, synthesis methods, interaction among particles,

particle size distribution, and particle size and shape. Biomedical applications of MNPs are generally classified into in-vitro (outside the body) and in-vivo (inside the body). In-vitro applications are mainly used in diagnostic processes, such as separation/selection, magnetic relaxometry, and MRI. In-vivo applications include diagnostic processes, such as nuclear magnetic resonance imaging, as well as therapeutic applications (e.g., drug delivery and magnetic hyperthermia) (Reddy, Arias, Nicolas, & Couvreur, 2012).

Hyperthermia is a therapeutic method for cancer treatment; the term “hyperthermia” is derived from two Greek words, “hyper” and “therme,” meaning “rise” and “heat,” respectively (Gas, 2011), because this condition is attributed to increasing body temperature. Busch (Busch, 1867) and Coley (Coley, 1891) observed that a sarcoma disappeared after a very high fever; this finding had been the reaction of immune systems toward a bacterial infection. Based on this study, cancer cells are considered vulnerable to high temperatures; the growth of these cells can be terminated at temperatures ranging from 42 to 47 °C for at least 20 to 60 minutes (min) (varies in the literature) (Chiriac et al., 2015; Moroz, Jones, & Gray, 2002). Although this technique has gained prospects and significant advances, it may also cause several discouragements and frustration because of undesirable effects, such as blister, burns, and pain, increased rapidly in healthy cells. Therefore, hyperthermia method is locally used, instead of exposing the whole body (WB) to high temperatures in order to overcome adverse side effects and increase the treatment efficiency.

Hyperthermia method has not been very effective to cure serious cancers because of basic problems associated with local hyperthermia; such problems include heterogeneous temperature distribution in tumor mass and incapability to prevent overheating at the deep-seated tumor region. Therefore, a novel method must be developed to deal with these critical issues. In this regard, scientists have proposed a safe, easy, and effective treatment approach. The use of MNPs with high Ms indicates that heat is produced to

enhance the hyperthermia efficiency. Technically, MNPs can be injected locally or through the intravascular region within the vicinity of external AMF. This procedure leads to focus-generated heat on the affected cells, and the process is called MHT. In this technique, magnetic nanofluids are used as stable colloidal suspensions of nanoparticles in liquid media, such as water or hydrocarbon fluids (Thorat et al., 2013).

MHT features have broadened new advancements in cancer treatment through several research and usage of varied MNPs with high magnetic properties in different media for in-vitro and in-vivo applications. Experimentally, cancer treatment through MHT was first performed in 1957 by Gilchrist et al. (Gilchrist et al., 1957); in this study, maghemite ($\gamma\text{-Fe}_2\text{O}_3$) nanoparticles, with 20 to 100 nm particle size, were heated by 1.2 MHz AMF at temperature ranging from 43 to 46 °C to cure carcinoma by destroying metastases in lymphatic nodes. The procedure has been well established for application of MNPs in hyperthermia therapy (HT) and has been used to treat various cancers over the past 50 years. To date, MHT has been applied to clinical phase trials for prostatic and esophagus cancers and brain and neck tumors as well as research on other types of cancer under clinical prophase and animal-based experiment stages (Pang, 2015). Therefore, MHT can be considered as a novel alternative therapy with few side effects compared with conventional therapies, such as surgery, chemotherapy, and radiotherapy (Hergt, Dutz, & Roder, 2008).

The proper functionality of MNPs for MHT depends on their intrinsic magnetic properties [Curie temperature (T_c) and M_s] as well as biophysical properties [nontoxicity, colloidal stability, biocompatibility, and specific absorption rate (SAR)] under physiological pH conditions. The surface chemistry of MNPs and their stabilization, are important to achieve the above properties appropriately. Surface chemistry plays an essential role in stabilization of MNPs to prevent particle agglomeration through coating them with different materials, such as polymeric, non-polymeric, organic, and inorganic

surfactants (Reza Eslami-Farsani, Hedayatnasab, Khalili, & Soleimani, 2012; Hedayatnasab et al., 2013). These considerations enhance compatibility and circulation of MNPs in blood as well as reduce toxicity and risk of blood capillary obstruction.

Heat-generation in MHT is a main aspect that should be considered in synthesis procedure of MNPs. Indeed, MNPs with superior magnetic behaviour are necessitated to render remarkable heating power in killing cancer tumors; otherwise, they are disabled to generate sufficient heat. The generated heat by AMF and its quantity from AMF are measured through SAR, which is the amount of electromagnetic energy power absorbed per unit and mass. SAR is described as the ability to produce heat through magnetic connection between the magnetic field and the magnetic moments of nanoparticles. Indeed, SAR is ascribed to three heating mechanisms, namely, hysteresis loss, relaxation loss, and eddy currents. Different types of MNPs demonstrate varied heating mechanisms. The magnetic heat dissipations from such mechanisms are dependent on the intrinsic and extrinsic characteristics of MNPs; such characteristics include particle shape, particle size, and saturation temperature, as well as AMF parameters, such as frequency and strength (Obaidat, Issa, & Haik, 2015).

Over the past decades, various review articles have been published to determine the different features of MNPs, particularly their synthesis methods, functionalization, and magnetic properties, for biomedical applications. Many synthesized MNPs with varied characteristics and magnetizations for in-vivo and in-vitro MHT have been studied. The current review presents a comprehensive classification of different types of MNPs and their magnetization states applied for MHT. An informative explanation is provided regarding the intrinsic and extrinsic properties of MNPs and their effects on hyperthermia application. Recent advancements on the HT procedure through the decades and its features are also discussed. The highlight of this literature review is the investigation on the efficacy of MNPs characterizations and AMF features attributed to the critical

parameters for MHT. Finally, some recommendations are given regarding to types and characterizations of MNPs and also the synthesis experimental conditions that endow MNPs a significant heating capability to enhance the MHT efficiency.

2.2 Classification of MNPs for Hyperthermia Application

Throughout the years, various MNPs with different properties and morphological metallic structures have been applied for MHT. These MNPs are mainly classified into two categories on the basis of their structure; magnetic alloy nanoparticles (MANPs) and magnetic metal oxide nanoparticles (MMONPs). This section explains the main characterization and synthesis of the above nanoparticles. The different types of MNPs discussed in this section are summarized in Table 2.1.

2.2.1 Magnetic Alloy Nanoparticles

Nanoscale metallic magnetic nanoparticles (MMNPs) have attracted increased research attention compared with their bulk counterparts due to monodispersity and narrow size distribution which can be achieved by post-synthesis grading (Edmundson, Capeness, & Horsfall, 2014). Iron (Fe), nickel (Ni), and cobalt (Co) are the most important MMNPs because of high magnetic properties (Lin, Sorensen, Klabunde, & Hajipanayis, 1999; Petit & Pileni, 1999). These nanoparticles demonstrate high ability to control and adjust their size, composition, and shape compared with MMONPs (L.-Y. Lu, Yu, Xu, & Jiang, 2013; McNamara & Tofail, 2015). A good example of soft MMNPs is Fe, which exhibits the highest M_s of about 218 (emu/g), but Fe_3O_4 presents an M_s of 93 (emu/g) at 300 K (Gubin, 2009; Hilger & Kaiser, 2012; Zhang et al., 2006). However, these MMNPs suffer from poor chemical stability and biocompatibility, high reactivity to oxidation, and pyrophoricity at room temperature, leading to loss (partial or complete) of their magnetization which are unsuitable for hyperthermia application (Hergt, Dutz,

Müller, & Zeisberger, 2006). Therefore, a second or more MMNP, added to produce MANPs and enhance their resistance toward oxidation (Leteba & Lang, 2013; Mary et al., 2014; Silke et al., 2006) such as Ni-Cr (Akin, Obaidat, Issa, & Haik, 2009), Fe-Co-Au (Kline, Xu, Jing, & Wang, 2009) and Fe-Cr-Nb-B (Astefanoaei, Stancu, & Chiriac, 2017), while maintaining their magnetic properties.

Wu et al. (Wu, Yang, & Yang, 2013) noted that carbon should be applied as the optimal protector to produce Fe-based alloy nanoparticles from environmental degradation to acquire chemical stability and biocompatibility. This technique can improve the electrical conductivity and mechanical performance of Fe-based alloy nanoparticles (El-Gendy et al., 2009). To attain these remarkable properties, scholars have applied various synthesis methods, including microemulsion coupled with chemical reduction, thermal decomposition in organic or aqueous solvents coupled with chemical reduction of metal ions, pyrolysis of metal-organic polymers as precursors for MANPs, plasma methods, laser ablation, and decomposition of precursors (Azzaza et al., 2006; Berenbaum et al., 2003; Jakobi, Petersen, Menéndez-Manjón, Wagener, & Barcikowski, 2010; Kumar, 2009; Robinson, Zacchini, Tung, Maenosono, & Thanh, 2009; Wen, Liu, Wang, Zhu, & Wu, 2008; T. Zhang, Thomas Gan, Lee, Ramanujan, & Rawat, 2006). Among a wide variety of MANPs, the ordered Fe-Co magnetic alloy has been largely applied because of its significant magnetic properties, such as high M_s 245, (emu/g) with negligible magneto-crystalline anisotropy (MCA) and H_c , high permeability, and high T_C (Carta et al., 2007). These crucial magnetic properties make them a great candidate for high-density magnetic data storage, magnetic recording, drug delivery, and high-performance permanent magnet applications, but they are usually difficult to be produced at the nanoscale level and also present the superparamagnetic (SPM) properties (two main requirements of MHT) (Fukuda, Fujieda, ., Suzuki, & Jeyadevan, 2012; Nguyen et al., 2008; TrinhThang, Shinya, & NguyễnThiKim, 2012; White et al., 2003).

2.2.2 Magnetic Metal Oxide Nanoparticles

MMONPs are oxides belonging to a wide family of smart and functional materials (Niederberger, 2007). These materials comprise two different structural oxidation states: mixed-valence cationic states and anionic deficiencies (vacancies); by altering these characteristics (either or both), the chemical, electrical, and magnetic properties of oxide materials can be tuned (Ali et al., 2014). These characteristics imply that oxides represent various classes of materials with different properties covering almost all material science aspects, including semi-conductivity, superconductivity, and magnetism (Z. R. Dai, Pan, & Wang, 2003). MMONPs are arranged in different metal groups with diverse structures and properties; these nanoparticles include metal oxides (e.g. iron oxides, nickel oxide and even lanthanum strontium manganite) and ferrites. Among oxides, iron oxides have been recognized as a prominent candidate for hyperthermia therapy due to possess varied features such as localized elimination of cancer cells via magnetically induced heating (Hilger & Kaiser, 2012). They are a combination of Fe and O₂, generally comprising 16 pure phases including oxides (Fe₃O₄, γ -Fe₂O₃, hematite and iron oxide beta phase), oxyhydroxides (feroxyhyte, akaganeite, goethite, and lepidocrocite), and hydroxides (iron(II) hydroxide and iron(III) hydroxide) (Cornell & Schwertmann, 2006; Wei, Zhaohui, Taekyung, Changzhong, & Woo-Sik, 2015). Ferrites are comprising iron oxides and at least one metal in their chemical combination with beneficial magnetic and dielectric properties. Ferrites are expressed by M(Fe_xO_y), where M represents any metal cation [such as manganese (Mn), magnesium, copper, aluminum, barium, Ni and Co, or even Fe itself], and the x and y values are variables (Cabanas & Poliakoff, 2001; Lan, Duong, & Hien, 2011). Given the diversity of ferrites, they are largely employed in various applications, such as sensors, MRI, biomedical imaging, catalysts, and electromagnetic and optical devices (Alcantara, Lopez, García-Martin, & Pozo, 2016; Beji et al., 2015; Fu et al., 2005; Jana, Chen, & Peng, 2004; Kim et al., 2011; J. Park et

al., 2005; Santra, Kaittanis, Grimm, & Perez, 2009; Sathe, Agrawal, & Nie, 2006; Sugimoto, 1999; Tailhades, Gillot, & Rousset, 1997). The realization of these purposes depends on the monodispersity of nanoparticles because the majority of MMONPs' applications require that the size and shape of nanoparticles are uniformly oriented. As such, several methods have been applied to synthesize MMONPs; these methods include co-precipitation, hydrothermal, sol-gel, microemulsion, and mechanical ball milling processes (Chin & Yaacob, 2007; Herring et al., 2013; Maity & Agrawal, 2007; Y. Wu, Wang, Luo, & Dai, 2009).

However, synthesized MMONPs have been partly unsuitable and have suffered some difficulties, such as aggregation, hydrolysis, condensation, and non-uniformity in shape and size for the above mentioned applications (Herring et al., 2013). In addition, magnetic hardening, coalescence, and grossing of MNPs are the consequences of high-temperature procedures (Niederberger, 2007). Therefore, MMONPs should be synthesized in non-aqueous media or under N₂ gas to avoid such difficulties (Herring et al., 2013; Jana et al., 2004). Considering the biomedical application, Fe₃O₄, γ -Fe₂O₃, and spinel ferrites [general formula: M_xFe_{3-x}O₄ (M=divalent metallic cations)] with high oxidative stability are extensively studied because of their biological compatibility and superior magnetic properties. However, Fe₃O₄ exhibits magnetic properties superior to those of other iron oxides; thus, Fe₃O₄ is a more suitable candidate for biomedical applications, particularly MHT, because of the presence of Fe²⁺ and Fe³⁺ cations in valence states of the inverse spinel structure (Ali et al., 2014; Beji et al., 2015; Cabanas & Poliakoff, 2001; Tailhades et al., 1997).

Table 2.1: Different types of MNPs

MNPs Classification	Examples	Synthesis Methods	Advantages and Disadvantages	Applications	Ref.
MANPs	Fe-Co	-Thermal decomposition	-Large magnetic	-Ultra high-density	(Azzaza et al., 2006;
	Fe-Ni	coupled with chemical	anisotropy	magnetic recording	Berenbaum et al., 2003;
	Fe-Pt	reduction	-Narrow size	media	Carta et al., 2007;
	Co-Pt	-Microemulsion coupled	distribution	-Magnetic storage	Fukuda et al., 2012;
	Co-Ni	with chemical reduction	-High magnetic	-Magnetic	Jakobi et al., 2010;
		-Pyrolysis of metal-polymers	moment	refrigeration system	Kumar, 2009; Leteba &
		-Reductive decomposition	-Chemical stability	-Ferro-fluids	Lang, 2013; Mary et al.,
		-Hydrogen plasma metal	-Resistance against	-Biomedicine	2014; Nguyen et al.,
		-Polyol	oxidation	-High performance	2008; Robinson et al.,
		-Vapor reduction	-High saturation	permanent magnets	2009; Silke et al., 2006;
		-Electro-deposition	magnetization	-High density data	TrinhThang et al., 2012;
		-Machine-alloying	-High coercivity	storage	Wen et al., 2008; White
		-Laser ablation	-Difficult to control	-Catalysts	et al., 2003; Wu et al.,
		-Liquid phase reduction,	composition size	-Batteries	2013; Zhang et al.,
		-Chemical vapor deposition	and shape		2006)
	-Microwave combustion				
	-Ion-beam				

‘Table 2.1, continued’

MNPs Classification	Examples	Synthesis Methods	Advantages and Disadvantages	Applications	Ref.
MMONPs	Fe ₃ O ₄	-Gas phase methods	-High saturation magnetization	-Labeling cells,	(Alcantara et al., 2016;
	γFe ₂ O ₃	(thermal decomposition,		-Designing ceramic	Ali et al., 2014; Beji et
	NiFe ₂ O ₄	reduction hydrolysis,	-High magnetic	-MRI	al., 2015; Cabanas &
	MnFe ₂ O ₄	disproportionation,	susceptibility	-Drug delivery	Poliakoff, 2001; Chin
	CoFe ₂ O ₄	oxidation)	-Low toxicity	-Gene therapy	& Yaacob, 2007;
	NiO	-Liquid phase methods	-Physicochemical	-Magnetic	Cornell &
	Co ₃ O ₄	(co-precipitation)	-Colloidal stability	hyperthermia	Schwertmann, 2006;
		-Two-phase methods	-High magnetic	-In-vitro diagnostics	Z. R. Dai et al., 2003;
		(Microemulsions,	permeability	-Vaccine and	Fu et al., 2005;
		Water-in-oil	-High electrical resistance	antibody production	Herring et al., 2013;
	microemulsions)	-High oxidative stability	-Gas sensors	Jana et al., 2004; Kim	
	-Sol-gel methods	-High-quality	-Catalysts	et al., 2011; Lan et al.,	
	(hydrolysis	monodisperse	-Electromagnetic	2011; Maity &	
	and condensation)	-Superparamagnetism	and optical devices	Agrawal, 2007;	
	-High pressure	-Light absorbing	-Magnetic data	Niederberger, 2007; J.	
	hydrothermal methods	-Tend to aggregation	storage	Park et al., 2005;	
	-Microwave	-large surface-area-to-	-Biosensing	Santra et al., 2009;	
		volume ratio	-Batteries	Sathe et al., 2006; Y.	
				Wu et al., 2009)	

2.3 Magnetization in Hyperthermia Application

2.3.1 Types of Magnetism

Magnetism originates from the orbital and spin motions of electrons, and its strength is dependent on the intensity of the interaction among them. In some materials, the interactions of atomic magnetic moments are not collective, and the atomic moment interactions of the other materials are sufficiently strong, leading to a significant distinction among all the magnetic materials. Hence, these materials are mainly classified into five categories according to their feedback to AMF: diamagnetic (DM), paramagnetic (PM) and antiferromagnetic (weak magnetic); ferromagnetic (F_{OM}) and ferrimagnetic (F_{IM}) (strong magnetic); though antiferromagnetic determined as a particular case of F_{IM} , it has zero net magnetization and shows weakly magnetization in the both absence and presence of AMF (Kittel, 1976; Spaldin, 2010). In the presence of AMF, these materials exhibit little magnetization and also ignore to follow ordered alignment ascribed to DM and PM; by contrast, the other materials in the two main categories exhibit ordered magnetic moments below the critical temperature (Curie temperature; T_C), even without applying AMF. They differ from their magnetic moment couplings, and their prefixes (ferri-, and ferro-) are truly indicating this matter (Morrish, 2001). This section concentrates on the features of F_{OM} and F_{IM} which are the magnetization states of MNPs applied in hyperthermia therapy, and their magnetic characteristics are listed in Table 2.2.

2.3.1.1 Ferromagnetism

It is regarded as an inherent property that makes some materials naturally magnetic. F_{OM} materials are attracted to magnets in the presence of AMF, but this finding is not significant because the above property makes them capable of attracting other F_{OM} materials. Fe, Ni, Co (transition metals), and their alloys are common F_{OM} materials at room temperature or even above, and their atomic magnetic moments tend to orient

parallel to each other. Generally, F₀M materials can be classified according to their H_c: soft (small H_c) and hard (large H_c) magnetic materials. This classification implies that the hard group presents a wider hysteresis loop in induced flux density-magnetic field curve (B–H); thus, more energy is required to for magnetization. In this state, the materials exhibit two distinct characteristics. The first one is net (spontaneous) magnetization attributed to the internal molecular field even after removal of AMF. The second one refers to temperature-dependent magnetic orders (Cregg, Murphy, & Mardinoglu, 2012). These characteristics indicate that F₀M materials preserve their magnetic properties even after AMF removal. Actually, these characteristics are derived from the strong coupling and interactions among neighboring moments adequately close together. The strong interactions are generated through the electronic exchange forces, which are very large and named as a quantum mechanical phenomenon, given the relative alignment of the two electron spins. These exchange forces among the magnetic moments within the material can bring about to large net magnetizations even when AMF is removed. The positive moment energy indicates that F₀M materials demonstrate a large positive susceptibility (1 to 10⁵, depending on atomic structures, AMF, and temperature) and permeability (Sun et al., 2008).

Below the T_C, magnetic moments of F₀M with long-range order are aligned in one direction, thereby reducing the exchange energy of the material. Above the T_C, the F₀M properties disappear, and the PM properties replace them consequently the magnetic moments become totally disordered. As such, the significant difference between the PM and F₀M materials indicates that the magnetic moments of the latter will maintain their parallel orientation even after AMF removal. This finding implies that F₀M materials still demonstrate spontaneous magnetization with symmetrical and aligned atoms in the same direction, making a permanent magnetic field. Moreover, in DM and PM cases, the combinations of electrons in their orbitals lead to cancel each other out. However, F₀M

material cases vary because no tendency occurs in the electron fields of their atoms to be cancelled out; as a result, these cases display a long-range order. Such order causes the unpaired electron spins, which are aligned parallel in a region known as a domain (Raghunathan, Melikhov, Snyder, & Jiles, 2010). Therefore, these remarkable characteristics of F₀M in nanometer scale with one domain (single-domain) can reach the desirable magnetism known as superparamagnetism (Frey, Peng, Cheng, & Sun, 2009; Thorat et al., 2016), which is determined as an essential requirement of MHT (further explained in detail). Peng et al. (Peng et al., 2016) also observed that graphene oxide can transform from ferromagnetism to superparamagnetism if the magnetic domain of the F₀M graphene oxide decreased through the removal of the functional groups. Liu et al. (Liu et al., 2017) synthesized LSMnO nanoparticles with narrow size distribution and tight phase transition from F₀M to SPM states. Therefore, F₀M can be a promising nanoheating agent for MHT.

2.3.1.2 Ferrimagnetism

This magnetism state can be observed in compounds with more complex structures instead of pure elements. For example, oxides of Fe are combined with at least one transition metal such as Mn, Ni, or zinc to produce F₁M materials, whose magnetic properties depend on the electron interactions and are related to the metal ions. Ferrimagnetism states, such as ferromagnetism, occur in materials when the magnetic moments align spontaneously below the T_C to produce net magnetization. In the absence of a magnetic field, the F₁M lattice is composed of two different sub-lattices with diverse strengths. The magnetic moments of these sub-lattices are oriented randomly with unequal magnitude and antiparallel alignments, implying that the magnetic moments in one direction are stronger than others in the opposite direction, leading to a net magnetization. Therefore, the magnetic behaviour of F₁M similar to F₀M involves net

magnetization, T_C , and hysteresis, but such behaviour is varied in magnetic ordering. The F_{IM} materials show F_{OM} properties below T_C , although they follow PM behaviour above T_C (Sun et al., 2008). F_{IM} as well as F_{OM} display SPM behaviour above block temperature (T_B) (Kolhatkar, Jamison, Litvinov, Willson, & Lee, 2013). This finding indicates that nanomaterials in this type of magnetism demonstrate capabilities of F_{OM} to be used in MHT e.g. $MgFe_2O_4$ (Rashid, Humayun, & Manzoor, 2017), $\gamma-Fe_2O_3$ (Sakellari et al., 2016), $CoFe_2O_4$ and $MnFe_2O_4$ (Cruz et al., 2017).

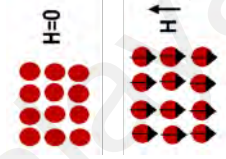
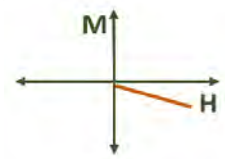
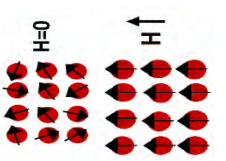
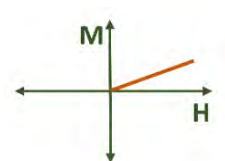
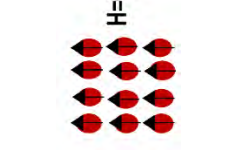
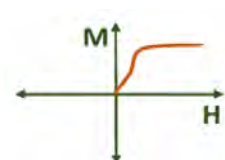
2.3.1.3 Superparamagnetism

A kind of magnetism occurring in very small particles (either F_{IM} or F_{OM}) if the size is around a few nanometers to a couple of tenth of nanometers is called superparamagnetism. For further explanation, the aligned spin orientations of large particles are arranged into domains; thus, these domain walls (multi-domain) are present over the bulk of the material and require relatively little field energy to move them. However, in smaller particles (below 20-30 nm), the number of domain walls per particle decreases to a wall (single-domain), where the superparamagnetism state is observed because of lack of boundaries and minimal energy statement. Nanoparticles in SPM state do make sense if the temperature is below the T_C because their properties are crucially dependent on the net magnetic moment. As such, superparamagnetic nanoparticles (SPMNPs) are aligned in a preferred arrangement, thereby reaching magnetization faster than other states, whereas each atomic magnetic moment retains its ordered state leading to a non-hysteresis curve with zero H_c and M_r (Giustini et al., 2010). Unlike F_{OM} nanoparticles, SPMNPs ignore to maintain any net magnetization when AMF is removed; this finding indicates that these materials show no magnetic memory and no magnetic hysteresis in the B–H curve. Moreover, SPMNPs commonly display two different magnetic structures: either a magnetic particle core (usually iron oxides) that can be

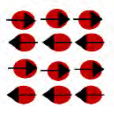
coated by organic materials (peptides, phospholipids, polysaccharides, fatty acids or other surfactants, and varied polymers), as well as inorganic materials (gold, carbon, and silica), or SPMNPs precipitated inside the pores of a porous biocompatible polymer (Mahmoudi, Sant, Wang, Laurent, & Sen, 2011). Therefore, biocompatible SPMNPs are regarded as the optimal candidate to be employed in MHT, as compared with other nanoparticles in different magnetism states.

University of Malaya

Table 2.2: Different types of magnetic behaviour

Magnetism Types	Examples	Net Magnetization	Susceptibility	Permeability	Magnetic Moment Alignment	Magnetic Behaviour	Ref.
Diamagnetism	Ag, Cu	0	Small and Negative $-1 < \chi < 0$	$\mu < 1$			(Pauli, 1967; Simon & Geim, 2000)
Paramagnetism	Mg, Cesium	0	Small and Positive $0 < \chi < \epsilon$	$\mu > 1$			(Getzlaff, 2008; Williams, 1926)
Ferromagnetism	Fe	✓	Large and Positive $\chi \gg 1$	$\mu \gg 1$			(Cregg et al., 2012)

'Table 2.2, continued'

Magnetism Types	Examples	Net Magnetization	Susceptibility	Permeability	Magnetic Moment Alignment	Magnetic Behaviour	Ref.
Ferrimagnetism	Fe_3O_4 , $\text{BaFe}_{12}\text{O}_{19}$	✓	Large and Positive $\chi \gg 1$	$\mu \gg 1$	$H=0$ 		(Sun et al., 2008)
Anti-ferromagnetism	Chromium	0	Small and Positive $0 < \chi < \epsilon$	$\mu > 1$	$H=0$ 		(Julien, Ait-Salah, Mauger, & Gendron, 2006)

2.3.2 Magnetic Properties

The magnetic properties of nanoparticles can be generally classified into intrinsic and extrinsic. Intrinsic properties are those derived from the interactions on an atomic length scale and are mainly determined by chemical composition and crystal structure. These properties include M_s per unit volume, MCA constant per unit volume (K), and T_C , which are all independent of grain size, shape, and microstructure. Extrinsic properties are those that are not as essential as the intrinsic properties and are derived from long-range interactions. These properties include H_c and M_r , which are dependent on the microstructural factors, intermetallic phases, and orientation in a composite (Edelstein & Cammaratra, 1998; Fersi, Mliki, Cabié, & Bessais, 2014; Q. M. Lu et al., 2015). This section presents a detailed explanation of the intrinsic and extrinsic magnetic properties of nanoparticles.

2.3.2.1 Intrinsic magnetic properties

Saturation magnetization: M_s is described as the maximum magnetization quantity (induced magnetic moment) of F₀M and F₁M materials which can be obtained at temperature below T_C when exposed to a sufficiently large AMF. Thus, the magnitude of M_s is considered as a function of temperature, $M_s(T)$. As such, by increasing the AMF magnitude, no further increase occurs in the magnetization leveled off. Additionally, the crystalline size of MNPs affects the M_s reduction, as initially reported by Berkowitz et al. in the late 60s (Berkowitz, Schuele, & Flanders, 1968). Notably, when the particle size of MNPs reduced below the transition point (from multi-domain to single-domain), they actually become appropriate for biomedical applications like MHT. In such magnetic state, the magnitude of M_s decreases due to the increment of the spin disorder effect on the MNPs surface. Thus, the magnitude of M_s is directly proportional to the size of MNPs. The different ways to determine magnetization at room temperature are classified as force

methods (such as Gouy and Faraday balances) and inductive methods (such as extraction magnetometry, alternating current susceptometry, vibrating-sample magnetometry; VSM, and superconducting quantum interference device; SQUID). Among these methods, VSM and SQUID are regarded as the optimum and most sensitive methods to measure M_s (in this research, VSM was just used to measure M_s), considering that high magnetic field can be applied to reach high magnetization; thus, the measurement is not affected by demagnetization effects. Moreover, these methods can perform magnetization measurement from low to high temperature (<2 K to 1000 K) and at the strength of magnetic field beyond 7 Tesla (H. Xu et al., 2013). From the magnetization-magnetic field curve (M-H), the M_s is measured, in which the hysteresis loop typically takes a minimum of 1 hour (h) for completion. Interestingly, M_s is a substantial factor in MHT because of two reasons; the first one, MNPs with high M_s resulted in high SAR value, indicating that MNPs present a great heating power to resist and destroy cancer cells. Secondly, high M_s makes the MNPs movements much more controllable in blood stream using AMF to remain them around tumor cells. As a result, choosing MNPs with high M_s considered as one the extremely influential factor in MHT to dissipate great thermal energy in targeted area. Besides, MNPs in superparamagnetism state is preferable that will be discussed in further section.

Curie temperature: T_C which is derived from the Curie effect (Baaziz, Tozri, Dhahri, & Hlil, 2016), is the temperature at which certain magnetic materials withstand a great change in their magnetic properties, leading to lose the intrinsic magnetization and replace with induced magnetism. This phenomenon is known as the Curie point, at which a transition occurs from magnetic to non-magnetic state (second-order phase transition). In this point, heating of targeted area will be discontinued if AMF is removed; whereas, they will be remained at T_C until AMF is maintained. T_C plays an inevitable role in MHT to

control temperature within the secure hyperthermia range (42 to 47 °C) throughout the entire therapy. Since cancer cells can be destroyed within this range while healthy cells are unaffected, but above 47 °C they may be damaged and subsequently necrosis occurs. Hence, applying MNPs with T_c between 42 to 47 °C crucially consider for self-controlled MHT because measuring the temperature of cells during the therapy is difficult particularly for deep-seated tumors. Self-controlled MHT requires some contrivances to remain T_c of MNPs in the secure range such as reduction in MNPs size and modification of MNPs. The former not only makes them SPM but also gives rise to the decrease in their T_c . In the latter case, combination of MNPs with nonmagnetic materials e.g. zinc and copper or even magnetic ions e.g. chrome resulted in reducing of T_c because the exchange interactions among the magnetic ions in the MNPs decreased (Apostolova & Wesselinowa, 2009). Some studies exhibited that the T_c of MNPs could control properly between 42 to 47°C for instance copper-nickel MNPs (Chatterjee, Bettge, Haik, & Jen Chen, 2005), manganese ferrite with zinc and zinc ferrite with gadolinium (Apostolov, Apostolova, & Wesselinowa, 2011). Therefore, the optimal strategy in performing a successful MHT is selecting MNPs with certain T_c to avoid probable drawbacks. Unfortunately, the measurements of T_c and T_B could not be investigated due to restricted availability to SQUID.

Magnetocrystalline anisotropy: magnetic crystals consist of diverse directions of atoms, which are not equivalent with the direction of their magnetization, indicating the difference between the directions of magnetization and the applied AMF. This dissimilarity is known as magnetic anisotropy, which exerts a strong effect on hysteresis loop shapes and then controls H_c and M_r . MCA for the soft material differs from the hard materials. Soft F₀M materials like iron can be demagnetized at low magnitude of AMF implying, they require low coercive energy for demagnetization. Thus, their coercivities

as well as MCAs are lower as compared to their counterparts, hard F₀M materials. The low H_c and MCA values of soft materials indicate that they have extremely narrow hysteresis loops (very small M_r values) which make them appropriate candidates for MHT. As discussed earlier, there are varied parameters which affect the MHT efficiency such as size and shape of MNPs, the strength of AMF and also MCA through the enhancing of the SAR value. MCA has gained more attention as compared to the others due of the limitation of the MNPs quantity and also the AMF magnitude. Such that, when SPMNPs exposed to AMF, they become magnetized uniformly along with one of their easy axes; thereby, high MCA energy is required to divert the magnetic moment from easy to hard direction in a single crystal, which originated from the magnetic moment interaction. (Evans et al., 2014; Mody, Singh, & Wesley, 2013; Ye et al., 2013). Notably, MCA is one of the parameters that heat dissipation of MNPs are dependent on; hence, by tuning it, the efficiency of MHT can be increased. Lee et al. succeeded to synthesize the core-shell MNPs with the optimal range of MCA. CoFe₂O₄ and MnFe₂O₄ were hard and soft cores of MNPS respectively. MCA tuned through interaction of interfacial coupling exchange between the magnetic phases of core and shell, resulted in remarkable improvement in SAR in comparison with the conventional iron oxide (Lee et al., 2011). However, the investigation of MCA for the iron oxide samples was not the objective of this research study.

2.3.2.2 Extrinsic magnetic properties

Coercivity: A magnetized F₀M material cannot return to zero magnetization in the same direction of its magnetization after AMF removal. Therefore, a field force is required in the opposite direction to return the material to zero magnetization, in which the flux density decreased to zero value, that is, coercivity. This process leads to create a loop known as hysteresis. Hard magnetic materials indicate large H_c (wide hysteresis

loop) in the B–H curve, which require more field force to become demagnetized. Soft magnetic materials show small coercive fields in the range of ~100 Oe; thus, less field force is acquired to reach zero magnetization (Coey, 2011). Hard F₀M nanoparticles with high exchange MCA energy exhibit large H_c that affect the heating efficiency remarkably, indicating high H_c value is in correlation with high SAR value. Applying F₀M with high H_c in MHT contributes to make some difficulties for patients because of that SPMNPs with relatively zero H_c are required to prevent the magnetic memory. Meanwhile, other parameters such as size and shape of MNPs and composition can influence positively on enhancing the heating efficiency of MNPs for MHT. Due to the dependency of coercive field on chemical composition of MNPs, by doping them with ions e.g. Ni–Cu, Fe–Pt doped ferrites, H_c and T_c can be decreased while M_s and SAR increased. Apostolova and Wesselinowa (Apostolova & Wesselinowa, 2009) reported that through the substitution of ferrites with nonmagnetic (Cu, Zn), magnetic ions (Gd), or transition metals (Pt, Pd, Cr), the exchange interaction between magnetic ions in the MNPs can be weakened. This modification led to lower H_c while M_s increased with increasing of ion-substitution content. Furthermore, they realized that H_c in spherical MNPs was smaller in comparison with cylindrical ones due to a coherent rotation of the magnetization.

Remanent magnetization: Mr or residual magnetization is a kind of magnetization left behind the F₀M and also F₁M when the AMF is removed (Yazid, Olsen, & Atkinson, 2016). However, SPMNPs possess large magnetic moments and behaves as PM nanoparticles with instance feedback to become demagnetized with negligible H_c and Mr. This property of F₀M creates the magnetic memory and makes them unsuitable candidates for MHT. Taken in to account that H_c and Mr as the two problematic magnetic properties in MHT which must be avoided by selecting proper SPMNPs with extremely

low value of them because the existence of magnetic memory after AMF removal creates incurable troubles for patients. Notably, synthesized SPMNPs with core-shell structure not only augments the biocompatibility but also assists to demagnetize with zero H_c and M_r , while possessing High M_s (Nguyen & Kim, 2016).

2.4 Hyperthermia Therapy

Hyperthermia is commonly defined as the elevation of abnormal body temperature artificially made by external medical devices; hence, it is completely varied from fever and heatstroke, which can be controlled by the body's temperature set point. Hippocrates of Kos (460 BC to 370 BC), known as the father of western medicine, has made an advisedly influential comment on hyperthermia as follows: "whenever medicines are not a cure, iron (knife) heals; whenever, knife is not a cure, fire (heat) heals. But if heat could not cure, it is an inevitable cureless". (*Quae medicamenta non sanat; ferrum sanat. Quae ferrum non sanat; ignis sanat. Quae vero ignis non sanat; insanabilia reportari oportet*). According to his aphorism, he declared that the ultimate way to cure diseases is by increasing the body temperature of the patients (Streffler & Van Beuningen, 1987). HT is typically used to relieve cysts, inflammation and arthritis pain by increasing the blood flow to provide nutrition to the affected tissues and reduce muscle spasms. Moreover, HT is applied to treat cancer tumors because they are significantly vulnerable to high temperatures as compared to healthy cells. The sensitivity of cancer cells toward high temperature or heat is derived from insufficient O_2 in their own cells because of poor blood flow in the affected region. Notably, healthy cells can organize blood flow systematically and dissipate additional heat in their surrounding vascular network via conduction and convection phenomenon; however, cancer cells demonstrate less capability to promote a vascular network; as a result, blood flow decreases and becomes overheated (above 42 °C). As such, the viability of tumor cells will considerably decrease

in the T_H range, whereas healthy cells are hardly affected (Jordan, Scholz, Wust, Fähling, & Roland, 1999). A wide range of HT methods can be arranged into three groups as follows: (I) WB hyperthermia, (II) hyperthermia by wireless applicators (WA), and (III) hyperthermia by heating source insertion (HIS) (Moroz, Jones, et al., 2002). As shown in Table 2.3, although each technique presents individual benefits and applications (for instance, the WB technique is appropriate for patients whose whole bodies are affected by cancer), HT through WA is much more effective than the two other methods due to concentrating on the affected regions with less damage to healthy cells and avoiding some inconvenience to patients e.g. producing eddy currents. However, WA hyperthermia efficiency was insufficient thus, a novel method is desired to be effective as magnetic-mediated hyperthermia therapy (MMHT), in which either magnetic particles or seeds are localized to the affected region under an external AMF.

Table 2.3: Comparison of three different HT techniques

Methods	Description	Devices	Remarks	Ref.
WB	<p>*The primary hyperthermia method.</p> <p>*It is normally used to treat metastatic cancer (such cancer that involved many parts).</p> <p>*Cover the patient body except the head with one of the instruments.</p>	<p>-Thermal chambers</p> <p>-Hot water blankets</p> <p>-A bath of heated water</p> <p>-Wax</p>	<p>-The simplicity of this method is usually recommended for such patients who are at a high risk of relapse after surgeries of removing a tumor.</p> <p>-Superficial overheating may be caused by heterogeneous of heat distribution in the tissue.</p> <p>-Surface burning leads to thermal lesions and discomfort but a computerized perfusion method recently applied to solve it.</p> <p>-Nevertheless, a sustainable high temperature in the body may influence negatively on the healthy cells like cardiac disorders and changes in intravascular coagulation system, reduction in volume blood plasma volume and capillary leak syndrome.</p>	(Mallory, Gogineni, Jones, Greer, & Simone Ii, 2016; Wust et al., 2002)
HIS	<p>*Heating sources inserted inside or around the affected area through surgery making complication and discomfort for the patients during and after therapy.</p> <p>*It is therefore called invasive method.</p>	<p>Microwave heating</p> <hr/> <p>Radiofrequency (RF) heating</p> <hr/> <p>F₀M seeds</p>	<p>-It is promoted to reduce the heterogeneity of microwave heat distribution in cells by producing heat from electromagnetic waves of inserted devices.</p> <p>-The obvious drawback is that the currents from RF cause a charging effect which leads to an insulator perimeter the electrode formed. This insulation interferes with the emission of waves and also local burning reported.</p> <p>-F₀M seeds (thermo-seeds) produce eddy currents resulted in interstitial hyperthermia. Then without electrical connection between seeds and power device, the heat is transferred to the affected cells.</p>	(Carrafiello et al., 2008; B.-H. Park, Koo, Kim, & Kim, 2002)

‘Table 2.3, continued’

Methods	Description	Devices	Remarks	Ref.
WA	<p>*It is a non-invasive method.</p> <p>*The method is Performed either locally or regionally.</p> <p>*The applicators send waves to the targeted area (tumor), then the wave energy transformed into the heat.</p>	<p>High Intensity Focused Ultrasound (HIFU)</p> <hr/> <p>Electromagnetic applicators: a. RF b. Microwave</p>	<p>-Although HIFU produces enough heat to destroy affected areas, it is unsuitable for areas near bones and lungs since the reflection of sound waves and non-uniform heat distribution cause hot spots.</p> <hr/> <p>a. Capacitive plates and inductive coils are two varied approaches for RF. -When the affected region placed between two charged plates, the fat around that area is heated superficially. -In the deeper area, homogeneity and uniformity of heat distribution reduces rapidly. -Eddy currents are created by induction coils leading to non-uniform temperature distribution.</p> <p>b. High frequency of microwave energy makes the molecular motion to move fast leading to local elevated temperature of targeted area. -Microwave has more efficient temperature distribution than RF due to better convection. -HT through microwave considered as the best method for superficial tumors but it is unable to penetrate and influence on the deep tumors. This matter may cause uneven heat distribution and power absorption around the deep-seated tumors. -Although rotating spiral and multi loop antennas are used to address this issue, in such techniques, lack of temperature homogeneity around the deep-seated tumors are still existed.</p>	<p>(Carrafiello et al., 2008; Cheung, 1982; Stauffer, 2005)</p>

2.4.1 Magnetic-Mediated Hyperthermia Therapy

MMHT modalities can be performed using four different strategies: I) arterial embolization hyperthermia (AEH), II) direct injection hyperthermia (DIH), III) intracellular hyperthermia (IH), and VI) interstitial implant hyperthermia (IIH) (Moroz, Jones, et al., 2002), as presented in Table 2.4. Based on the mediator's scales, they are arranged into three scaled groups: MNPs, micrometer-scaled agents (typically used for AEH purpose), and millimeter-scaled agents (thermo-seed, metallic stents). According to Table 2.4, the intracellular technique based on intravenous injection of MNPs for destroying cancer cells would be the ideal technique to heat and burn cancer cells selectively even in metastatic cases. A controversial issue about the superiority between intracellular and extracellular is still existed. The main difference of extracellular hyperthermia is the sources such as microwave and water bath applied externally to heat up cancer cells. Whereas, in the counterpart, MNPs are localized inside the cancer cells exposed to an external AMF. In extracellular hyperthermia, the heating from the external sources is inadequate to destroy cancer; hence, additional heat is required to reach the T_H . By contrast, the counterpart provides a safe and effective approach through inserting MNPs within affected cells if both chemical effects (cytotoxicity) and mechanical damage are ignored (MNPs rotation). However, clinical applications of IH remain unfeasible because researchers have presented different ideas about the superiority of both techniques during the decades. Gordon et al. (Gordon, Hines, & Gordon, 1979) hypothesized that the destructive effect of IH is much more than the counterpart; however, Rabin (Rabin, 2002) rejected theoretically this hypothesis in terms of thermal sense. He reported that negligible thermal influences are ignored; thus, no logical reasons are available to accept such hypothesis. Overall, IH technique is the optimal strategy to overcome unavoidable problems and appropriately target cells with homogenous heat distribution (nanomediator) (Blanco-Andujar et al., 2016; Espinosa et al., 2016).

Table 2.4: Comparison of four main strategies of MHT

Strategy	Origin of Heat	Administration of magnetic agent	Type of agent	Advantage and disadvantage	Ref.
AEH	Intravascular	Arterially embolizing the blood vessels of the tumors with F ₀ M particles	Therapeutic agent: micro- or nanoparticles (Mono- or multi-domain)	<ul style="list-style-type: none"> -Treatment of local cancers with high temperature, particularly liver cancer. -Capability to determine the thermal dose in cancer cells. -Due to the concentration gradient of agents within cancer cells and their surroundings, distribution of temperature is effective. -This therapy not only can postpone the growth of the tumor but also can inhibit angiogenesis. -It has an adequate ability to interrupt supply to tumor also heat the affected cells locally through hyperthermia upon AMF. -Healthy cells are in the danger of embolization and consequently necrosis of them. -It is not practicable for the cases that the tumor is either out of the liver or without a fine supply. - Temperature Distribution is inhomogeneous within the liver tumor. -The consequence of this therapy can be dire with low hepatic reserve for patients if the affected cells are close to major blood vessels. 	(Moroz, Pardoe, et al., 2002; Xu et al., 2007)
DIH	Extracellular	Injection the suspension into the tumor cells directly	Micro- or nano- F ₀ M particles (Mono- or multi-domain)	<ul style="list-style-type: none"> -Due to the independency on an arterial pathway, it can be used in various tumor types and risk of arterial catheterization prevented. -It can perform percutaneously with radiological guidance or be combined with other traditional therapies. -Heterogeneous distribution and poor conservation of magnetic particles within the tumor cells. -It is required to repeat the injection of suspension for the tumor with either large size or irregular shapes. -Tumor visualization accurately and access adequately are required. -There is a potential risk of implantation of needle track or spread of tumor cells. 	(Moroz, Jones, et al., 2002; Smolkova et al., 2015)

‘Table 2.4, continued’

Strategy	Origin of Heat	Administration of magnetic agent	Type of agent	Advantage and disadvantage	Ref.
IH	Intracellular	Arterial embolization, injection directly or intravenous injection	Nanoparticle (Mono-or sub-domain)	<ul style="list-style-type: none"> -Ability to treat metastases and scattered tumor cells. -Sub-domain particles (i.e. magnetic fluids) which are used in this therapy require moderate and lower magnetic field leading to be safe. -Depending on the delivery pathway, it has all benefits and limitation of both AEH and DIH therapies. -This has adequate potential to focus on the affected cells by the type of particles; hence, its efficiency can be improved. 	(Moroz, Jones, et al., 2002)
IIIH	Interstitial	Directly implanting of F ₀ M seeds	Thermo-seed or stent	<ul style="list-style-type: none"> -This technique can be used with other traditional modalities to improve its efficiency. -Nearly all of the healthy cells are in reserve since the thermo-seeds implanted into the tumor cells. -Due to applying thermally self-controlled F₀M seeds, cell burning is prevented; hence, the safety level improved. -Applying biocompatible thermo-seeds in the affected region makes to repeat the treatment. - This treatment time reduced due to fast-initial heat of such seeds. -High blood flow of tumors or their surrounding may decrease the temperature of affected sites. -The alignment of the F₀M seeds in the direction of magnetic field is vital that in some cases are impossible. -The movement of seeds makes corrosion and other problems but if choose the suitable seeds, the drawbacks avoided. -This therapy is not suitable for tumors with irregular shapes or inaccessible sites. -The difficulty of implantation procedure as well as the risk of infection is probably existed. 	(Smolkov a et al., 2015)

2.4.2 Magnetic Hyperthermia Therapy

This technique is derived from MMHT that applies nanoparticles as magnetic mediators to perform the secure cancer treatment with high efficiency which is known as MHT. In this treatment, nanoscale mediators are injected locally within the affected area in the form of colloidal suspension of SPMNPs under AMF exposure. Thereby, direct destruction of local cancer cells occurs through the heat generated of SPMNPs exposed to AMF without interference to the nearby healthy cells. The superiority of MHT implies that it can boost the local temperature of the affected region through the attachment of MNPs to cancer cells while stimulating the body's active immunity. Moreover, the enhanced homogeneous temperature of MNPs gives rise to increase the MHT efficiency. In addition, MNPs can be administered to achieve relatively low T_C , leading to self-controlled and subsequently avoid overheating within the affected cells (A. B. Salunkhe, Khot, & Pawar, 2014).

In general, magnetic particles produce heat via four different heating loss mechanisms under AMF exposure: I) eddy currents (in magnetic particles with size of $>1 \mu\text{m}$), II) hysteresis losses (in multi-domain magnetic particles with size of $>1 \mu\text{m}$), III) relaxation losses (in single-domain SPMNPs), and VI) frictional losses (in viscous suspension) (Goswami, Dey, Bandyopadhyay, Sarkar, & Ahir, 2016). According to Joule loss, AMF induces eddy currents because their existence depends on how materials are resistant towards the current heating. Majority of magnetic particles indicate higher electrical resistivity, resulted in induction of very low eddy current loss. Additionally, the eddy current loss is mostly shown in bulk (multi-domain) magnetic particles thus, such heating loss in small magnetic particles (nanosized particles) is negligible compared with other heating losses (Khot, Salunkhe, Thorat, Ningthoujam, & Pawar, 2013). Consequently, the prevailing heating loss mechanism in multi-domain state is hysteresis loss (below the T_C) attributed to F₀M particles (above the critical size range, $>20\text{-}30 \text{ nm}$) (Hergt et al., 2006).

However, as the particle size reduced (<20-30 nm), the thermal energy barrier for the magnetization reflux are also reduced, leading to the magnetic transition from multi-domain to single-domain then another heating mechanism occurs known as SPM mechanism or relaxation loss mechanism, which falls into two modes. Following the AMF removal, the magnetic moments can relax either by the motion of the internal magnetic moment spins (Néel relaxation) or by the rotation of individual nanoparticles rotating around their own axes (Brownian relaxation) (Prasad et al., 2013). As such, SPMNPs with Néel and Brownian heating loss mechanisms are the most feasible candidates for MHT; these particles can control nanoscale dimensions and exhibit superior magnetic properties with incapability to maintain any magnetization in the absence of AMF (Amarjargal, Tijing, Park, Im, & Kim, 2013). The theoretical investigations in the kinetics and thermodynamic of SPMNPs are required to understand the various heating mechanisms that could contribute though detailed discussions are beyond the scope of this thesis.

Experimentally, nano-ferrofluids can be placed in a micro-centrifuge tube in the center of a circular coil (with certain diameter), which is exposed to AMF. Temperature changes over time (dT/dt) are measured throughout the process by a thermocouple connected to a data processing system to record the temperature (T_H) (Chiriac et al., 2015; Hilger et al., 2002). As clearly shown in Figure 2.1, after passing a certain time, the temperature becomes leveled off; this finding indicates that with increasing time, no changes occur in the temperature. The desirable case is to achieve saturation temperature between 42 - 47 °C because MNPs within this range are prone to kill cancer cells. As temperature exceeds this secure range, overheating may occur and cause some disorders in healthy cells. Therefore, SPMNPs with certain T_C are essential in MHT to control T_H and avoid painful problems, although some factors affect T_C and subsequently T_H . The second important parameter in MHT is SAR, which actually implies the power of MNPs to destroy cancer

cells under AMF exposure. The high SAR value, the more cancer cells are killed. Indeed, the SAR value is affected by different factors such as M_s , particle size and shape of MNPs, T_H , frequency, and intensity of AMF. The applicability determination of MNPs with adequate SAR for in-vivo application is dependent on their evaluation in the in-vitro studies. In the latter study, the optimization of AMF parameters and MNPs characteristics are required due to if the results are reasonable, the samples with sufficient heating capabilities within physiological tolerable range can be applied for the in-vivo trials. Meanwhile, the latest and important theoretical and experimental studies have examined the effects of MNPs' characteristics, as well as AMF' features on MHT reviewed and then summarized in Table 2.5.

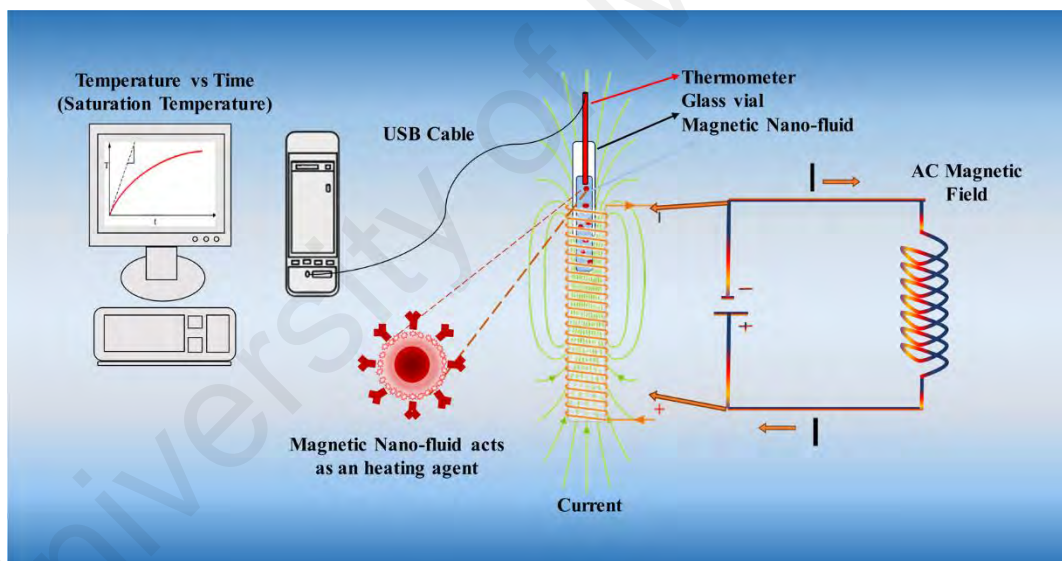


Figure 2.1: Schematic of experimental setup for induction heating test

2.4.2.1 Effect of coating on hyperthermia efficiency

Bare SPMNPs not only are incapable to maintain stability in a colloidal suspension but also make some difficulties during synthesis procedure and subsequently during MHT due to their hydrophobicity and large surface-area-to-volume ratio. These difficulties include the following:

- a) Surface sensitivity to air and moisture.
- b) Self-agglomeration and creation of clusters (dipole–dipole attractions), which cause behaviour similar to that of F₀M particles (Hc and Mr appeared); consequently, the particle size is increased.

Besides the two main problems mentioned above, which must be solved before applying in MHT, SPMNPs with biocompatibility, biodegradability, stability (in an aqueous medium at neutral pH), and nontoxicity are essentially required. Hence, the surface chemistry of SPMNPs plays a critical role which can be acquired by improving the steric and electrostatic repulsive forces to hinder agglomeration formation (through passivate SPMNPs' surface), subsequently prevent oxidation (Figure 2.2). On the basis of the reasons mentioned below, coating is considered as one of the most remarkable requirements to perform successful MHT.

- a) Preservation the physiochemical properties of SPMNPs.
- b) Existence biocompatible and nontoxic shield around SPMNPs because their surface is directly in contact with blood and tissues.
- c) Creation of hydrophilic molecules on the surface to improve the dispersity of SPMNPs (prevent agglomeration then control the particle size and reduce the risk of blood capillary obstruction) and enhance blood circulation (deliver SPMNPs to targeted area).
- d) Reduction the sensitivity of the SPMNPs surface toward air and moisture and making more appropriate surface for further functionalization and absorption of proteins.
- e) Prevention the opsonization of SPMNPs (acting like bacteria) by RES causes their fast clearance from the blood stream before reaching the targeted area (Gupta & Gupta, 2005; Laurent, Dutz, Häfeli, & Mahmoudi, 2011; A. B. Salunkhe et al., 2014).

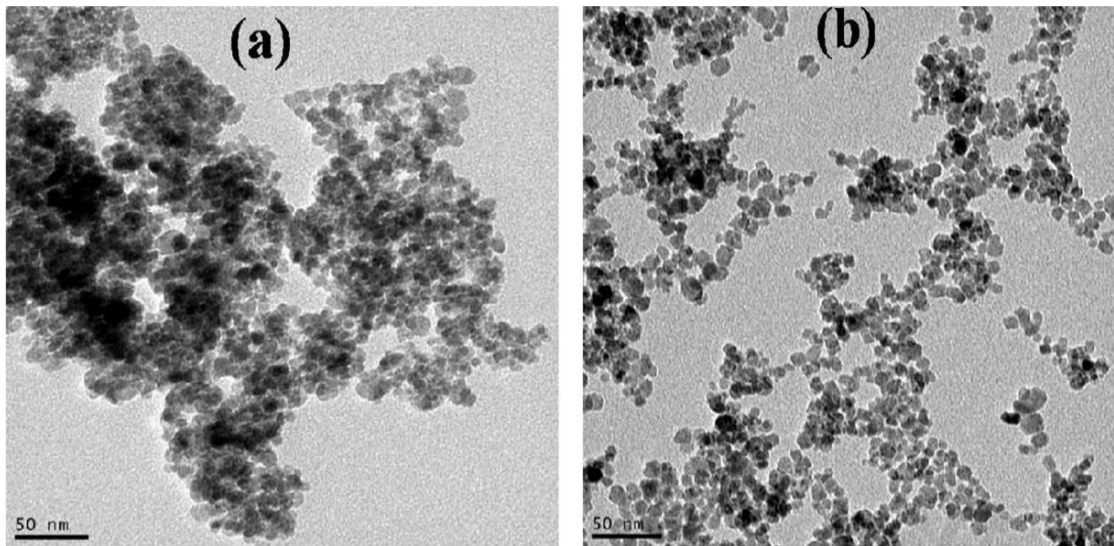


Figure 2.2: TEM images of (a) uncoated CoFe_2O_4 and (b) coated CoFe_2O_4 (Ashwini B. Salunkhe, Khot, Ruso, & Patil, 2016)

Coating the SPMNPs surface can also significantly influence the magnetic properties and may thus form a new material with enhanced properties (combination of both particles and coating layer). The large difference between coated and uncoated SPMNPs is the M_s value. In the latter case, given the large surface-area-to-volume ratio, the attractive force among SPMNPs increases and become aggregated; thereby, facilitating the temperature (T_B) and then reducing their magnetization. The T_B of the former is moved to the lower temperature, leading to boost the magnetization and subsequently the SAR value (Gupta & Gupta, 2005). Clearly, coated SPMNPs (with high SAR) is demonstrated stronger power to kill cancer cells with less treatment time in human body and lower concentration (dosage).

A wide variety of materials have been applied as SPMNPs coating for hyperthermia applications, which can be categorized into two main groups, namely, organic and inorganic (Figure 2.3). For instance, the organic group divided in three subcategories, surfactants, polymers, and biological molecules, and the inorganic group consists of three types of materials; metals/non-metals, metal oxides/sulfides, and silica. The organic compounds are used to functionalize SPMNPs by employing functional reactive groups,

such as hydroxyl, aldehyde, amino, and carboxyl groups for further interactions in order to enhance the properties. These types of coatings are capable of keeping the magnetic properties of such particles simultaneously while maintaining the properties of organic materials, leading to three main supposed structures, core shell (different core shapes such as spherical, hexagonal, multiple, and movable within the hollow shell) (Ghosh Chaudhuri & Paria, 2012), matrix (mosaic, shell-core), and shell_x-core-shell_y (Chomoucka et al., 2010). Figure 2.4 illustrates the various types of coated-MNP structures in two different dimensions. The core-shell structure has attracted more attention by preserving the physical and chemical properties of the core and furnishing SPMNPs surface for functionalization. In some cases, the core-shell has been used for being cost effective (Zhang, Lee, Joo, Zaera, & Yin, 2013). Inorganic coating renders the SPMNPs' surface to bind biological ligands while maintaining the stability of particles to make SPMNPs target-specific (A. B. Salunkhe et al., 2014). In addition, such stabilizers may own distinct properties like high electron density, photoluminescence, and strong optical absorption to enhance the semiconductor efficiency (Wei et al., 2015). Inorganic stabilizers coat MNPs through five types of structures, including core-shell, mosaic, shell-core, shell_x-core-shell_y, and dumbbell. However, among various organic coatings, surfactants and polymers endow the SPIONs remarkable features.

Surfactant: The utilization of surfactants as a type of surface modification is desired to provide them with a higher colloidal stability. However, addition of surfactants to nanoparticles dispersions may induce agglomeration of fine particles through charge neutralization, bridging and formation of surfactant-particle surface or via a combination of these mechanisms. Hence, a highly efficient surfactant with appropriate adsorption is required to make surface saturation. Consequently, surfactant can prevent nanoparticles

from bridging and destabilization by changing their surface properties and also reducing the particle size through better dispersion (Abu-Jdayil et al., 2016; Günister et al., 2006).

Surfactants have capability to make three main varied surface modifications on nanoparticles including hemi-micelle, ad-micelle and mixed hemi-ad micelle which are formed through the adsorption of surfactants on the opposite surface charge of the nanoparticles. In the hemi-micelle arrangement, a monolayer coverage is formed when the adsorbed surfactant spread on the nanoparticles surface related to columbic attraction among the nanoparticles. While the adsorbed surfactants onto the nanoparticles surface increased, the hydrophobic interactions between hydrocarbon chains called surfactant tails lead to the bilayer formation of surfactant known as ad-micelle arrangement. The intermediate array between these formations is named mixed hemi-ad micelle which is combination of two-fold arrangements with superior capability in making columbic as well as hydrophobic interactions (Amiri-Aref, Raoof, Kiekens, & De Wael, 2015; Ranjbari, Hadjmohammadi, Kiekens, & De Wael, 2015).

Surface modification is twofold: on the one hand, surfactants are indeed applied to improve controlled micellar stability by using zeta potential measurements. On the other hand, surfactants are used to provide some functional groups on the surface of nanoparticles for the attachment of polymer shell through hydrophobic/hydrophilic and/or electrostatic interactions.

Polymer coating: If the shell layer is polymer, it can render more benefits like better particles dispersion, high colloidal stability, solubility, and drug loading on the protective shell for further treatments. Polymer coating promotes the blood circulation time and cytocompatibility, but the thickness of the surface layer may be increased (Zhang et al., 2013).

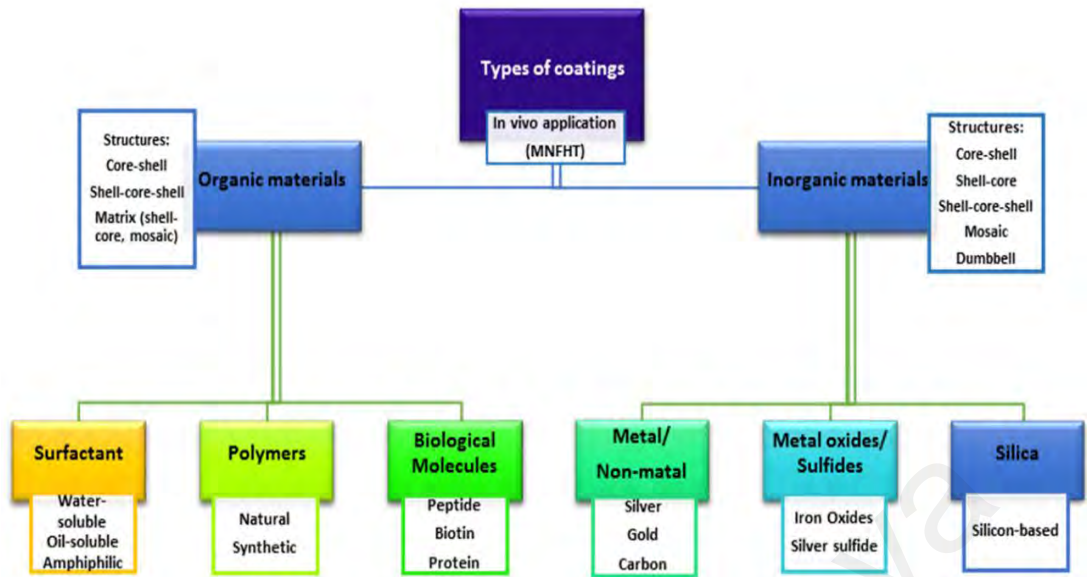


Figure 2.3: Different types of coatings

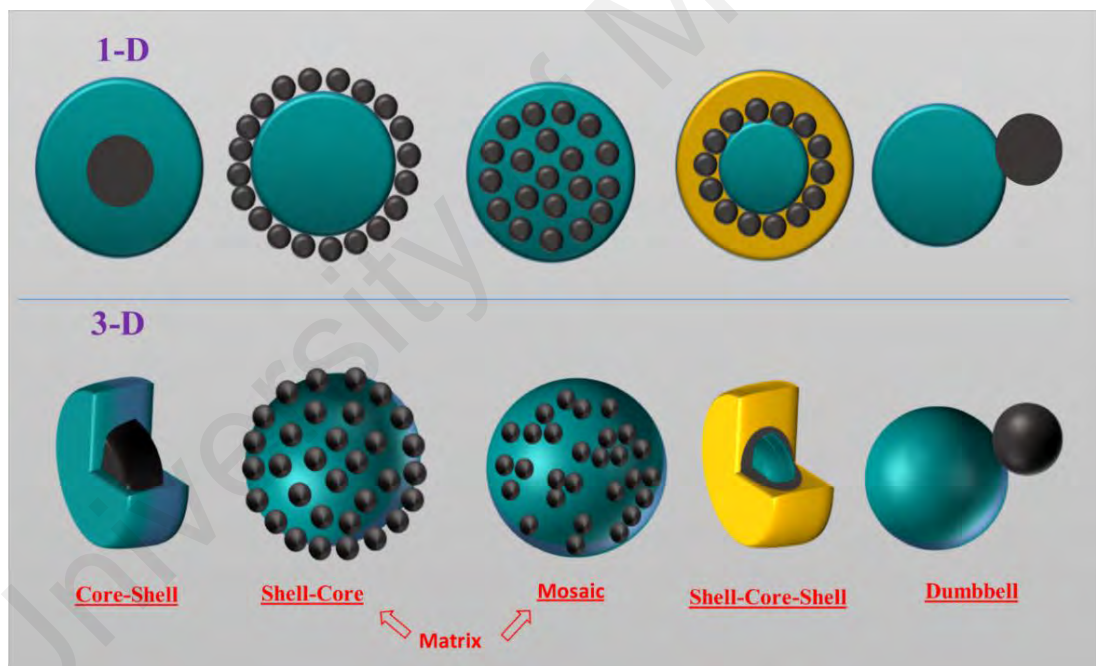


Figure 2.4: Various structures of coated MNPs

Thorat et al. (Thorat et al., 2013) synthesized LSMO MNPs through combustion method, then coated by organic surfactant [oleic acid (OA)] as a hyperthermia agent. OA not only assisted to control particle agglomeration by making a shell around the MNPs core but also raised the affinity for more interaction with biocompatible molecules, such

as betaine HCl. However, after coating the M_s of LSMO decreased from 70 to 35 emu/g because M_s is indeed proportional to the weight of MNPs; thus, by increasing the OA layer, the particle size increased to 25 nm. Notably, H_c and M_r did not change after modification, which were indicative the superparamagnetism state of LSMO nanoparticles. In addition, coating LSMO with OA enhanced the induction heating as compared to the uncoated-LSMO nanoparticles because such coating could prevent agglomeration properly while retaining the SPM nature. Alkaline precipitation method was used to synthesize the nanocrystal Fe_3O_4 MNPs by Shete et al. (Shete et al., 2014), which were coated by natural organic polymer, chitosan (CS), to increase their biocompatibility and then determine the coating effects on MHT. Interestingly, CS coating did not significantly influence the reduction of Fe_3O_4 magnetization (M_s values of coated and uncoated MNPs were 49.96 and 51.68, respectively), as shown in Figure 2.5. This was due to after modification, the particle size decreased from 21.8 ± 5.3 nm to 15.1 ± 5.0 nm. This finding implies well dispersity and less agglomeration degree of MNPs with very thin CS layer coating. Moreover, the SAR value of CS-coated MNPs boosted to 118 W/g at 335.2 Oe and 265 KHz. The coating also strongly affected T_H , and the coated MNPs become saturated in less time as compared to the uncoated ones.

The effects of various biocompatible and hydrophilic synthetic polymer coatings, such as PEG, dextran (DEX), polyvinylpyrrolidone (PVP), and bovine serum albumin (BSA), on the magnetization of spherical-shaped Fe_3O_4 (4 nm to 11 nm in diameter) were determined for in-vitro application (Zavisova et al., 2015). The M_s of bare Fe_3O_4 was 64.35 emu/g. However, after modification, its values decreased to 58.42, 56.59, 55.70, and 58.64 emu/g for PEG, DEX, PVP, and BSA respectively. The M_s values of the coated Fe_3O_4 did not alter significantly with the uncoated Fe_3O_4 , meanwhile biocompatibility was enhanced (Zavisova et al., 2015). Fantechi et al. (Fantechi, Innocenti, Albino, Lottini, & Sangregorio, 2015) improved the magnetic hyperthermia properties of Fe_3O_4 by

substituting Fe^{+2} ions with inorganic metallic ions. Co^{+2} were then evaluated in terms of their properties by increasing the amount of Co content in $\text{Co}_x\text{Fe}_{3-x}\text{O}_4$ ($0 < x < 1$). They observed that the induction heating power increased considerably to 40.4 W/g for the organic Co value of $x=0.6$ and then decreased to 10.8 W/g for $x=1$ at 150.79 Oe and 183 KHz. Similarly, the M_s values reached the maximum of 98 emu/g for $x=0.6$ and then decreased to 87 emu/g. They mentioned that this odd behaviour was attributed to the magnetic anisotropy. Amarjargal et al. (Amarjargal et al., 2013) reported the dispersion of Fe_3O_4 nanoparticles dispersed in electrospun polyurethane (PU) nanofiber matrix by in situ polymerization to investigate the effects of biocompatible PU polymer on M_s and temperature. The M_s of PU nanofiber-decorated Fe_3O_4 decreased from around 70 emu/g (bare MNPs) to 37 emu/g. However, the T_H of decorated Fe_3O_4 with 0.5 and 1.0 mg/mL could maintain their stability in T_H range, indicating two crucial points. First, the compatibility of the magnetic sample could be improved for hyperthermia application. Second, some disorders such as overheating were prevented carefully with less magnetic concentration. Recently, in situ reduction method applied for shape-controlled of Fe_3O_4 with the silver (Ag) coating into the core-shell ($\text{Fe}_3\text{O}_4@\text{Ag}$) or heteromer ($\text{Fe}_3\text{O}_4\text{-Ag}$) structures. Both coated Fe_3O_4 exhibited higher biocompatibility with SMMC-7721 and L02 cells as compared to uncoated one and Ag nanoparticles as well. Moreover, Ag coating could improve in-vitro and in-vivo tumor therapeutic effect significantly. Besides, SPM- $\text{Fe}_3\text{O}_4@\text{Ag}$ (core-shell) and $\text{Fe}_3\text{O}_4\text{-PAA}$ showed M_s values of 75.1 and 82.4 emu/g and SAR values of 76 and 87 W/g, respectively. Indicating, the thin layer of Ag coating had insignificant influence in the reduction of MHT efficiency (Ding et al., 2017).

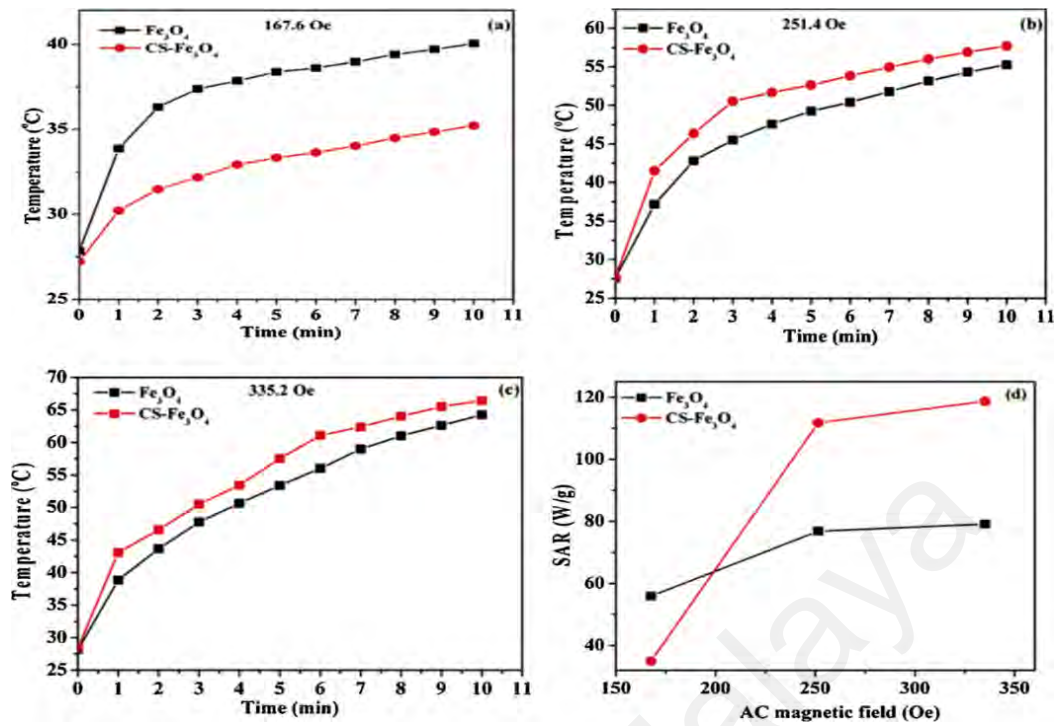


Figure 2.5: Trends of T_H and SAR of coated and uncoated Fe_3O_4 at various strengths (Shete et al., 2014)

2.4.2.2 Effects of particle size and shape of MNPs on hyperthermia efficiency

The magnetic property variations are strongly dependent on the nanoparticle size and shape. Notably, a small particle size leads to high magnetization, as well as high induction heating power, whereas a particle size below 5 nm makes some disorders on the surface spin of nanoparticles consequently magnetization is decreased. Taking the optimal particle size (from (Oh, Lee, Kang, & Oh, 2016)) in to account as a critical tuning parameter for MHT, MNPs with particle size of $5 < d < 20$ nm significantly affect the increase of M_s and SAR values related to the SPM behaviour (Néel and Brownian relaxations). Muller et al. (Müller, Dutz, Neeb, Cato, & Zeisberger, 2013) reported that the hysteresis curve with low M_r indicated that MNPs were in SPM state. They compared the single-domain MNPs with different particle sizes (10.9, 12.6, and 20.9 nm). Although with increasing particle size in single-domain, M_s rose from 64.9 to 79.9 emu/g, and H_c and M_r appeared gradually, implying that magnetic behaviour was changed from SPM to F_0M . Moreover, they realized that wide size distribution could negatively influence the

magnetic properties because of the particles' statistical orientation. Gonzalez-Fernandez et al. (Gonzalez-Fernandez et al., 2009) investigated the effect of particle size (varied from 5 nm to 110 nm) on the SAR value. The maximum and minimum SAR values of 137 and 1 w/g were belonged to 24 and 110 nm, respectively. They reported that the highest SAR value conformed to the SPM behaviour (as proposed by Rosensweig for the first time (Rosensweig, 2002); MNPs were single-domain with narrow size distribution). As the particle size increased moderately, the SAR value decreased until it become null by reaching the multi-domain particle (110 nm). When the dispersity of MNPs changed from mono-dispersity to polydispersity, the SAR value decreased due to the reduction in homogeneous particle distribution, which helped the increase of the total heat generation. Therefore, size distribution played a significant role in induction heating. Sathya et al. (Sathya et al., 2016) determined the M_s , H_c , and SAR values of cubic cobalt ferrite (in the form of core-shell) with the size of 20 and 27 nm. Their experiments showed that by increasing the particle size, the M_s increased from around 50 to 62 emu/g, and the H_c also significantly increased, but the SAR values decreased substantially, indicating the reduction in heating power in destroying cancer cells, as well as maintaining the magnetization after AMF removal. They concluded that cobalt ferrite (20 nm) with 0.5 to 0.7 Co content stoichiometry could be an effective candidate in MHT.

Furthermore, shape anisotropy (spherical, cubic, rod, and facet irregular were illustrated in Figure 2.6) is another important parameter in enhancing magnetic properties. Mohapatra et al. (Mohapatra, Mitra, Tyagi, Bahadur, & Aslam, 2015) synthesized Fe_3O_4 nanoparticles in rod and spherical shapes. Although both of MNPs displayed SPM behaviour (negligible H_c and M_r), spherical-shaped MNPs demonstrated higher magnetization than their counterpart. For instance, the M_s of nanorods measuring 50 nm in size was 58 emu/g, whereas that of spherical nanoparticles with the same material and volume (equal to 16 nm) was 83 emu/g. They mentioned that this difference in

magnetization is related to not only to the surface spin coating but also to the shape anisotropy of nanorods avoiding them to become magnetized in directions apart from magnetization along their easy magnetic axis. Salazar-Alvarez et al. (Salazar-Alvarez et al., 2008) investigated the influence of shape anisotropy on H_c of γ - Fe_2O_3 nanoparticles and mentioned that an increase in particle size was generally followed by the reduction in M_s . As the diameter of MNPs with spherical shape (14.5 nm) was larger than the cubic one (12 nm) and the interface coupling energy of spherical-shaped MNPs was larger, leading to larger anisotropy and lower M_s than those of cubic shaped-MNPs. In addition, they observed that the H_c of the spherical MNPs was higher than the counterpart. Similarly, the M_s of Fe_3O_4 with spherical shape was lower than the cubic MNPs, and the SAR value of the former was smaller than the latter because of different particle morphologies (Gonzalez-Fernandez et al., 2009). The magnetic properties of differently shaped $CoFe_2O_4$ nanoparticles with various sizes are reported by Joshi et al. (Joshi et al., 2009). With increasing particle size in varied shapes, the M_s and SAR values also increased (Figure 2.7). However, these values of spherical-shaped MNPs were significantly smaller than facet irregular (FI). They discovered the partial attachment of magnetic moments and also severity in orientation of FI-shaped MNPs in the direction of AMF, which could be one of the reasons. The presence of M_r might be important in the reduction of M_s and creation of hysteresis loop. Interestingly, they determined that the particle size and shape affect the T_H and optimum particle temperature to prevent overheating in MHT. Hyperthermia temperatures of FI and spherical MNPs increased with increasing particle size. Not only the T_H of FI MNP could not reach T_H range to kill cancer cells but also was lower than that of the spherical counterpart. However, the T_H of spherical MNPs with 15 nm saturated above 55 °C after 4 min and indicated that overheating might occur during in-vivo trials; thus, MNPs with 12 nm diameter were considered as promising candidates to prevent such problem.

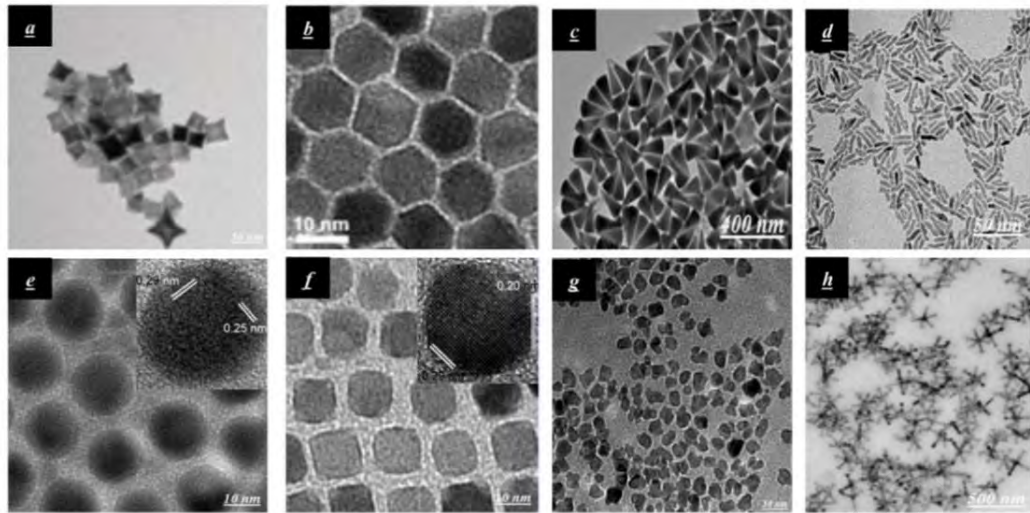


Figure 2.6: TEM images of (a) star-shaped CoFe_2O_4 (L. T. Lu et al., 2015), (b) polyhedron-shaped MnFe_2O_4 (Zeng, Rice, Wang, & Sun, 2004), (c) cone-shaped ZnO nanocrystals and (d) ZnO nanorods (Joo, Kwon, Yu, & Hyeon, 2005), (e) spherical-shaped $\gamma\text{-Fe}_2\text{O}_3$ and cubic-shaped $\gamma\text{-Fe}_2\text{O}_3$ (Salazar-Alvarez et al., 2008), (f) FI-shaped CoFe_2O_4 (Joshi et al., 2009) and (h) MnO multipods (Zitoun, Pinna, Frolet, & Belin, 2005)

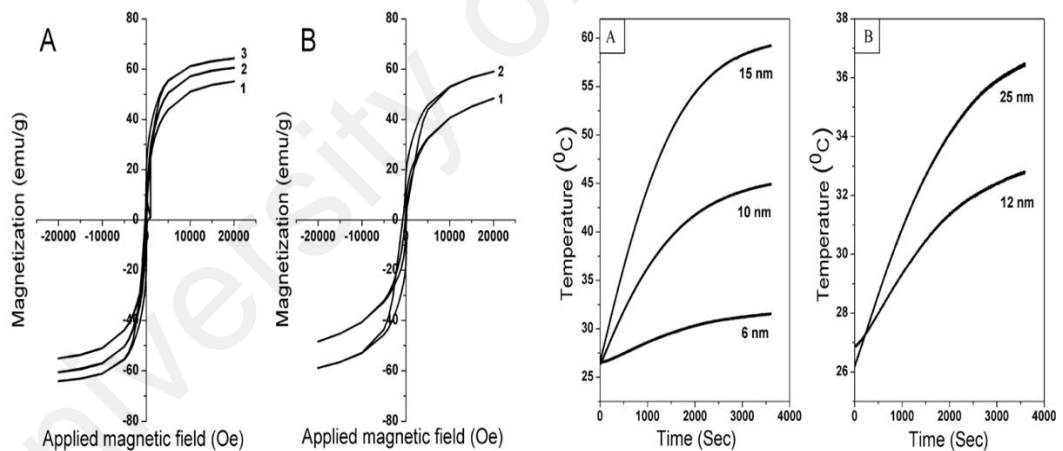


Figure 2.7: The effect of particle size on M_s and T_H . (A) spherical-shaped CoFe_2O_4 : (1) 6 nm; (2) 10 nm, (3) 15 nm, and (B) FI-shaped CoFe_2O_4 : (1) 12 nm, (2) 25 nm (Joshi et al., 2009)

2.4.2.3 Effects of frequency and strength of AMF on hyperthermia efficiency

The variation of the frequency and strength directly influences the induction heating power. Generally, the SAR value is risen by increasing the frequency with considering the limited range. For HT, the ultimate values of the AMF parameters can be effective at

500 kHz and 10 kA/m for frequency and strength, respectively. Thus, in accordance with the induction law, the multiplication of frequency (f) and strength (H) of AMF must not go beyond the accepted value of 5×10^9 A/(ms) to prevent the potential problems that produced by induced eddy currents (Çelik, Can, & Firat, 2014; Hergt et al., 2006). Li et al. (Z. Li, Kawashita, Araki, Mistumori, & Hiraoka, 2011) supposed that the particle size is dependent on the SAR value, but they found that AMF' parameters played inevitable roles, and the optimal results belonged to Fe₃O₄ with 24 nm diameter when exposed to AMF at 100 KHz and 300.33 Oe. Lahiri et al. (Lahiri, Muthukumaran, & Philip, 2016) coated spherical Fe₃O₄ nanoparticles with phosphate through co-precipitation synthesis method and then determined the induction heating power using AMF with 260 KHz frequency and very low strengths of 10.30, 9.17, 8.04, 6.53, and 4.52 Oe. The SAR values decreased from 11.1 W/g to 5.3 W/g. indicating that dipolar interaction and particle agglomeration improved; in contrast, anisotropy barrier height, susceptibility, hysteresis loop, and Néel relaxation time were reduced, which all assisted to diminish the SAR values. The effects of strengths variations (167.6, 251.4, and 335.2 Oe) on the SAR and T_H of uncoated Fe₃O₄ and CS-coated Fe₃O₄ were determined (Shete et al., 2014). At lower strength, the SAR and T_H of uncoated MNPs were higher than those of the coated one; however, by increasing the strengths, these values increased significantly to 118 w/g at 66 °C. The strength exerted both positive and negative effects on T_H. Although the strength improved the induction heating efficiency, it went beyond the T_H range, which resulted in overheating on healthy tissues.

The variation of T_H and SAR values of OA-PEG coated CoFe₂O₄ nanoparticles with 5 and 10 mg/mL was determined in varied strengths by Salunkhe et al. (Ashwini B. Salunkhe et al., 2016). Although the SAR values decreased with increasing MNP concentrations, this growth trend opposed with the T_H values due to the enhancement in exchange coupling energy derived from dipole–dipole interactions, which were

dependent on the density of MNPs. In addition, increasing the intensity of AMF could be beneficial until the temperature became stable in the T_H range; otherwise, overheating occurred. The T_H of coated CoFe_2O_4 nanoparticles went beyond this range when the strength was 378.24 Oe for both of concentrations; thus, 335.52 Oe might be suitable for being saturated within the T_H . The saturation time for such MNPs with 10 mg/mL was less than lower concentration. The SAR value of coated CoFe_2O_4 boosted from around 37 to 58 W/g with increasing concentration from 5 to 10 mg/mL, and the strength was 335.52 Oe. PEG-coated rod-shaped NiFe_2O_4 SPMNPs were synthesized with 16 nm length and 4.5 nm diameter for hyperthermia application by Iqbal et al. (Iqbal, Bae, Rhee, & Hong, 2016a). They realized that the T_H value was strongly influenced by the AMF parameters. The measured T_H values for 8.7 mg/mL were 47, 42, and 35 °C in accordance with 69.11, 49.0, and 28.9 Oe with the frequency of 260 KHz; as a result, PEG-coated NiFe_2O_4 with 49 Oe strength was appropriate as nanoheating agent to prevent the normal cells from burning by displaying SAR of around 18 W/g. Indeed, the T_H values decreased when the concentration of MNPs decreased. Oh et al. (Oh et al., 2016) observed that different strengths exerted strong effects on crucial hyperthermia factors (SAR and T_H) of CS- MnFe_2O_4 (shown in Figure 2.8). They performed hyperthermia test at varied strengths of 251.32, 376.99, 502.65, 628.31, and 753.98 Oe. The SAR values were 57.2, 97.5, 152.21, 209.41, and 278.69 W/g, which were in accordance with the saturation temperatures of 44.10 °C, 48.24 °C, 55.25 °C, 62.81 °C, and 65.38 °C, respectively. The maximum SAR value of 278.69 W/g at 753.98 Oe was not acceptable because at this strength, overheating might be accrued; thus, reasonable values could be 57.2 and 97.5 W/g in order to prevent probable problems.

They also applied 1.5 mg.ml^{-1} of CS- MnFe_2O_4 on MDA-MB 231 cancer cell for in-vitro MHT and noticed the apoptosis of tumor cells occurred at 42 °C. Generally, overheating in MHT can be prevented with optimal induction heating efficiency if the

parameters of AMF are in 250-270 KHz and 300-350 Oe (23-28 KA/m) ; however, the nano-scaled particle size, shape anisotropy and composition of MNPs affect the SAR and T_H as well. As a good example, Simeonidis et al. (Sakellari et al., 2016) compared the SAR values of nanorods magnetite nanoparticles in low (150 Oe and 210 kHz) and high (300 Oe and 765KHz) magnetic field. These values were measured of 10 and 759W/g, respectively. The large values of AMF parameter made nanorod MNPs appropriate candidate for MHT; however, to reach and control T_H within the range of 42–47°C for around 30 min should be considered to enhance the efficiency. Taken particle's concentration into account as an important factor in being stable at T_H range, since low concentration would not be effective to close to this range. They also mentioned that, although the ultimate frequency-strength values of the AMF $\leq 5 \times 10^9$ A/(ms) (the Atkinson-Brezovich (Atkinson, Brezovich, & Chakraborty, 1984) were determined as the safe range for clinical trials, comprehensive successful experiments were performed beyond this threshold between 1.8×10^9 A/(ms) and 18.7×10^9 A/(ms), because of that they performed SAR experiment with such AMF in range of 2.5×10^9 and 18.3×10^9 A/(ms) as low and high field, respectively.

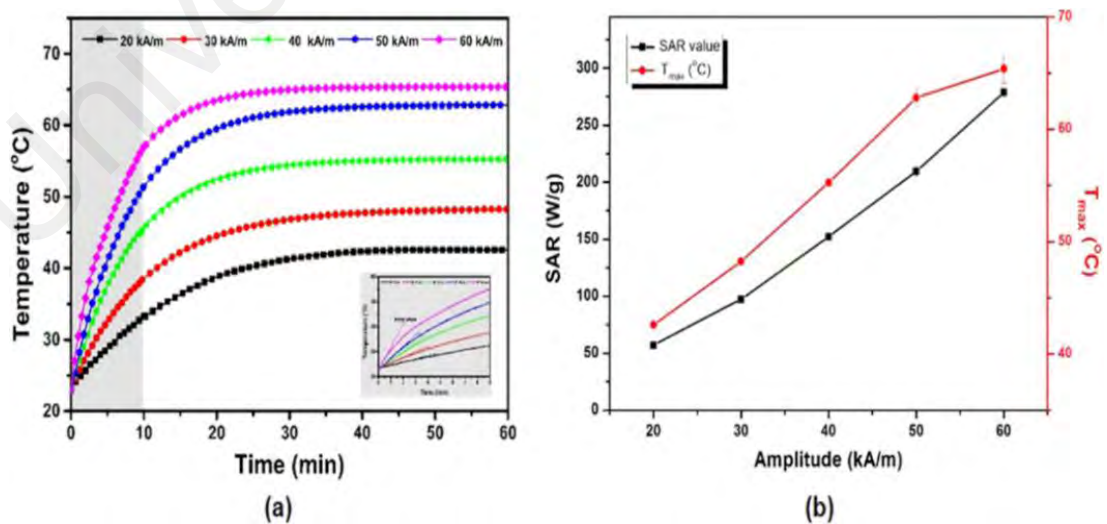


Figure 2.8: The effects of varied strengths (20, 40, 50, 60 KA/m) on T_H and SAR of CS-MnFe₂O₄ (Oh et al., 2016)

Table 2.5: Magnetic and in-vitro hyperthermia characteristics of varied MNPs

Materials		Precursor	Solvent	Method	Material	Coating Method	Size and Shape	Magnetic Properties	Hyperthermia Parameters	Remarks	Ref.									
		Material	Method	Size (nm)	Shape	Ms (emu/g)	Hc (Oe)	Mr (emu/g)				f (KHz)	H (Oe)	SAR (W/g)	T _H (°C)	Concentration (mg/mL)				
CoFe ₂ O ₄	MnFe ₂ O ₄	Cobalt chloride, Ferric chloride	Manganese (II) acetylacetonate, Iron(III) acetylacetonate	Water	1-octadecene	Thermal decomposition	CS	Sonication	18	Cubic	A:71.45, B:58.34	0	0	307	251=I, 377=II, 503=III, 628=IV, 754=V	I: ~50, II: ~95, III: ~150, IV: ~210, V: ~270	I: ~42, II: ~47, III: ~54, IV: ~62, V: ~65, (6min)	1.5	*SPMNP's had zero Hc and Mr. *SAR increased with increasing of AMF intensity. *CS-coated MNPs could be stable in secure hyperthermia range with high SAR specially at 377Oe.	(Oh et al., 2016)
CoFe ₂ O ₄		Cobalt chloride, Ferric chloride		Water		Co-precipitation	OA	Stirring	~ 9.9	Spherical	60.42	0	0	370	251.32=I 378.24 =II	I: ~25, II: ~70	I: ~41, II: ~47	10	*When intensity of AMF increased, SAR and T _H increased significantly with stability in secure hyperthermia range.	(Ashwini B. Salunkhe et al., 2016)

‘Table 2.5, continued’

Materials		Precursor	Solvent	Method	Material	Method	Size (nm)	Shape	Ms (emu/g)	Hc (Oe)	Mr (emu/g)	f (KHz)	H (Oe)	SAR (W/g)	T _H (°C)	Concentration (mg/mL)	Remarks	Ref.
Fe ₃ O ₄ hollow spheres	Zn _{0.9} Fe _{0.1} Fe ₂ O ₄	Ferric chloride hexahydrate, Oleylamine	Tetra thylene glycol	Solvo-thermal	-	-	~ 22	Spherical	81	Low	-	0.7	1156.1	1	-	-	*SAR rose by increasing of frequency. *Increasing temperature reduced Hc and then decreased greatly with increasing of AMF intensity.	(Goswami et al., 2016)
Fe _{68.2} Cr _{11.5} Nb _{0.3} B ₂₀	Fe _{68.2} Cr _{11.5} Nb _{0.3} B ₂₀ amorphous ribbon	-	-	Milling	CS	Ultra-sonication	20-40	-	A: ~42, B: ~34	-	-	153	3500	A:215, B:189	A: ~50, B: ~47 (5min)	10	*Coated and uncoated showed FoM behaviour. Ms of uncoated was higher than coated. SAR of coated was lower than to uncoated. *Coated could properly keep T _H in secure hyperthermia range.	(Chiriac et al., 2015)
		Zinc acetate dihydrate		Polyol	-	-	11	Spherical	12	-	-	700	34.4	36	38.6	6	*MNPs showed SPM state with low magnetization. *T _H was lower than secure range.	(Hanini et al., 2016)

‘Table 2.5, continued’

Materials	Precursor	Solvent	Method	Material	Method	Size (nm)	Shape	Ms (emu/g)	Hc (Oe)	Mr (emu/g)	f (KHz)	H (Oe)	SAR (W/g)	T _H (°C)	Concentration (mg/mL)	Remarks	Ref.
Fe ₃ O ₄	Fe ₃ O ₄	Iron(III) acetylacetonate	Seeded growth	-	-	~13.9	Spherical	III: 81.26	-	-	111	37.69	I:4.6, II:2.7, III:7.3	-	I: 5.84, II: 6.90, III: 7.08	*MNPs dispersed in n-tetracosane showed maximum SAR due to higher T _B during slow cooling procedure; hence, this sample had 11% higher heating ability than others.	(Andreu, Natividad, Solozábal, & Roubeau, 2015)
Co _x Fe _{3-x} O ₄ 0<x<1	Iron(III)acetylacetonate, Cobalt(II) acetylacetonate	Benzyl ether, Phenyl ether	Thermal decomposition	-	-	8-8.5	Spherical	X=0: 72, X=0.2: 79 X=0.4: 81, X=0.6: 88 X=0.8: 73 X=1: 79	low	low	183	150.79	X (0) = 6.5, X (0.2) = 11.2 X (0.4) = 27.7 X (0.6) = 40.4 X (0.8) = 19	X (0.4) = ~25, X (0.6) = ~32	-	*SAR rose with increasing of X until reaching to 0.6. *Particle size were acceptable to be use in clinical trials. *Co _x Fe _{3-x} O ₄ could not reach 42-47 °C.	(Fantechi et al., 2015)
Fe ₃ O ₄	Ferric chloride hexahydrate, Ferrous sulfate heptahydrate	Ammonium hydroxide	Co-precipitation	PEG, DEX, PVP, BSA	-	28-34	Spherical	A:64.35, B (PEG):58.42 B (DEX):56.59, B (PVP):55.70, B (BSA): 58.64	0	0	-	-	-	-	10, 20	*Magnetic measurements confirmed SPM behaviour of coated-MNPs. *Ms decreased with non-magnetic materials.	(Zavisova et al., 2015)

‘Table 2.5, continued’

Hydroxyapatite (HAp)		γ -Fe ₂ O ₃	Fe ₃ O ₄	Materials
Precursor	Solvent	Method	Precursor	Solvent
Material	Method	Size (nm)	Method	Material
Shape	Ms (emu/g)	Hc (Oe)	Mr (emu/g)	f (KHz)
H	H	SAR (W/g)	T _H (°C)	Concentration (mg/mL)
Remarks	Remarks	Remarks	Remarks	Remarks
Calcium nitrate tetrahydrate, Diammonium hydrogen, phosphate Ammonia solution Wet precipitation	Iron (III) salt, Iron (II) salt Water, Nitric acid Aqueous alkaline co-precipitation	Iron (III) salt, Iron (II) salt Water, Nitric acid Aqueous alkaline co-precipitation	Low magnetic moment Fe ₃ O ₄ (LM), Sodium phosphate buffer Precipitation	Fe ₃ O ₄
Iron (III) nitrate nonahydrate, Nickel (II) nitrate hexahydrate Co-substituting	-	-	-	-
17-19 Spherical and multifaceted	32 Quasi-spherical	32 Quasi-spherical	LM: 8, HM:18 Spherical	LM: 8, HM:18 Spherical
1.15 low low	55 - -	55 - -	LM: 41, HM:104 LM: 0, HM: 0 LM: 0, HM: 0	LM: 41, HM:104 LM: 0, HM: 0 LM: 0, HM: 0
265 502.65 - ~ 45, ~ 70, ~ 86 (10min)	394, 785 301.5 193. 472	394, 785 301.5 193. 472	337 276.4 - -	337 276.4 - -
10, 30, 50	33	33	0.01	0.01
*Pure HAp, co-substituted HAp indicated diamagnetic, and F _{0M} behaviour, respectively. *Low magnetization ascribed to lower magnetic phase in a non-magnetic calcium phosphates.	*Frequency variation played essential role in increasing of SAR. *AC measurements were more accurate than calorimetric.	*Frequency variation played essential role in increasing of SAR. *AC measurements were more accurate than calorimetric.	*Magnetic moment of Fe ₃ O ₄ had higher T _c could not perform self-controlled heating as much as LM.	*Magnetic moment of Fe ₃ O ₄ had higher T _c could not perform self-controlled heating as much as LM.
(Karunamoorthi et al., 2014)	(Garaio et al., 2014)	(Garaio et al., 2014)	(Yu et al., 2014)	(Yu et al., 2014)

‘Table 2.5, continued’

Materials	Mn _{0.8} Ca _{0.2} Fe ₂ O ₄	Mg _{0.4} Ca _{0.6} Fe ₂ O ₄	Materials
Fe ₃ O ₄			
Iron(II) chloride	Manganese (II) nitrate, Calcium nitrate,	Magnesium nitrate, Calcium	Precursor
Hydrochloric acid	Ethylene glycol		Solvent
Alkaline precipitation	Sol-gel followed by thermal treatment		Method
CS	-	-	Material
Ultra-sonication	-	-	Method
15.1	11	10	Size (nm)
Spherical	Cubic		Shape
A: 51.68, B: 49.96	39	23.1	Ms (emu/g)
A: 16.85, B: 13.29	61.9	5.7	Hc (Oe)
A: 2.23, B: 1.63			Mr (emu/g)
265	195		f (KHz)
335.2	125.66		H (Oe)
A: 79.32, B: 118.85	-		SAR (W/g)
A: ~ 64, B: ~ 66 (10min)	35 (10 min)	50 (10 min)	T _H (°C)
2	20		Concentration (mg/mL)
*CS is biocompatible, biodegradable, with amine groups offered functionalization. *Fe ₃ O ₄ and CS-Fe ₃ O ₄ showed SPM behaviour. *After coating, hyperthermia efficiency enhanced: 1- CS had capability to retain SPM nature. 2- CS was able to prevent agglomeration and contribute to better suspension.	*Increasing Ms and Hc of Mn _{0.8} Ca _{0.2} Fe ₂ O ₄ related to increment of particle size. *A partial substitution of Fe ²⁺ by Mg ²⁺ and Ca ²⁺ caused deformity and increased Hc. *Mn _{0.8} Ca _{0.2} Fe ₂ O ₄ lost SPM properties.		Remarks
(Shete et al., 2014)	(Saldivar-Ramirez et al., 2014)		Ref.

‘Table 2.5, continued’

MgFe ₂ O ₄		CoFe ₂ O ₄	
Materials	Precursor	Solvent	Method
Iron(III) nitrate, Magnesium nitrate	Fe(acac) ₃ Co(acac) ₂	I. Phenyl ether, II. Benzyl ether, III. Octyl ether	Thermal decomposition
Water			
Combustion			
DEX	-		
Sonication	-		
12.02	I: 5.4, II: 9.3, III: 9.9		
Spherical	Cubic		
A: 33.83, B: 31.56	I: 47, II: 51, III: 63		
A: 53, B: 45	Hc (Oe) 0		
-	Mr (emu/g) 0		
256	f (KHz) 571		
84.1, 335.2	H (Oe) 40.21		
B (84.1/5): 9.5, B (84.1/10): 10, B (335.2/5): 85.57, B (335.2/10): 55.6	SAR (W/g)		
B (84.1/5) = 27, B (84.1/10) = 30, B (335.2/5) = 50, B (335.2/10) = 72 (6min)	T _H (°C)		
5, 10	I: 22, II: 8, III: 1		
	I: 30, II: 40, III: 55 (4 min)		
	Concentration (mg/mL)		
	-		
*Interparticle repulsion of DEX caused reduction of interaction particles that prevented agglomeration. *Non-magnetic polymer reduced exchange coupling energy, particle-particle interaction, and Ms. *Higher AMF with low concentration showed better hyperthermia properties than lower ones.	*CoFe ₂ O ₄ in Phenyl ether had the maximum SAR with Néel relaxation. CoFe ₂ O ₄ in Octyl ether had the maximum value with Néel and Brownian relaxation time.		
(Khot et al., 2013)	(Çelik et al., 2014)		
	Ref.		

'Table 2.5, continued'

Materials	Precursor	Solvent	Method	Material	Method	Size (nm)	Shape	Ms (emu/g)	Hc (Oe)	Mr (emu/g)	f (KHz)	H (Oe)	SAR (W/g)	T _H (°C)	Concentration (mg/mL)	Remarks	Ref.
La _{0.7} St _{0.3} MnO ₃	Iron (II) chloride	Water	Precipitation followed by thermal treatment	PU nanofibers mats	Polyol immersion	30-40	Semi-spherical	A: 66.24, B: 32.12	A: 0, B: 0	A: 0, B: 0	368	12.57	-	B: 55 (10 min)	2	*Improvement in surface chemistry and acting as carriers for particles. *Decreasing value of Ms due to existence of non-magnetic polymer. *Main heating mechanism of PU-Fe ₃ O ₄ was Néel relaxation since MNPs anchored ont PU.	(Amarjargal et al., 2013)
La _{0.7} St _{0.3} MnO ₃	Lanthanum Nitrate, Strontium nitrate, Manganese (II) nitrate	Water	Solution combustion	OA, Betaine hydrochloride	Ultra-sonication	~25	Spherical	A: 35, B: 28 A: 5, B: 5 A: 1, B: 1			265	167.6, 251.4, 335.2		-	20	*La _{0.7} St _{0.3} MnO ₃ with a large magnetic moment and zero Hc determined as a good candidate for MHT among the other series of LSMO. *A high affinity of OA to the MNPs surface and having a long chain fatty acid for controlling agglomeration made them to be used in MHT. *Higher SAR value of coated LSMO might be ascribed to OA functionality that prevented agglomeration.	(Thorat et al., 2013)

‘Table 2.5, continued’

Materials	Precursor	Solvent	Method	Material	Method	Size (nm)	Shape	Ms (emu/g)	Hc (Oe)	Mr (emu/g)	f (KHz)	H (Oe)	SAR (W/g)	T _H (°C)	Concentration (mg/mL)	Remarks	Ref.
Fe ₃ O ₄	Iron (II) sulfate	Water, Ethanol	Precipitation	Tetraethyl orthosilicate	Ultra-sonication	A=I:24, II:30, III:45, IV: 42, B= II: 30+1, III: 45+4.5	Spheroid (only IV), Cubic	A=I: 83, III: 85, IV: 82, B=II: 85, III: 86	A=I: 44, III: 75, IV:79, B=II: 86, III: 93	A=I: 6.64, III: 11.9, IV: 12.3, B=II: 14.45, III:16.34	260	160	A=I: 137.4, III:62.7, IV: 11.7, B=II: 81, III: 45	-	5	<p>*Silica has high resistance against biodegradation by controlling the interactions among dispersed colloidal particles.</p> <p>*The Hc and Mr values decreased with decreasing particle size related to the increased surface-volume ratio and the effect of thermal energy on single-domain particles.</p> <p>*The SAR values of coated MNPs were smaller than uncoated ones due to insulating nature of the silica so the thickness of silica coating should be as low as possible.</p> <p>*SAR of cubic MNPs was larger than the spherical ones with the same size due to different particle morphology.</p>	(Gonzalez-Fernandez et al., 2009)

2.5 Conclusions and Outlook

The application of SPMNPs as nanoheating agents in MHT has made a significant breakthrough in cancer treatments because of their high efficiency for in-vitro application and subsequently in-vivo trials. Intravenous injection of SPMNPs assists to enhance the therapeutic effectiveness through homogenous heat distribution in a secure procedure. Magnetic hyperthermia parameters include SAR and T_H play critical roles in the elimination of cancer cells without significant damage to healthy cells, particularly overheating. Therefore, considering the characteristics and surface chemistry of SPMNPs, as well as the parameters of AMF are remarkably important. The requirements of these factors and parameters are summarized as follows:

- If the T_C of SPMNPs is very high, overheating among the healthy cells might be occurred. Thus, either coating with non-magnetic materials or substituting with less magnetized elements could be applied to reduce T_C and then maintained T_H within the secure hyperthermia range of 42 to 47 °C.
- Although the small size of MNPs brings about some benefits, such as being in SPM state, better dispersion and homogenous distribution of nanoparticles, higher generated heat, and prevention of particle aggregation, MNPs with particle size below 5 nm could not render the high heating capability in killing the cancer cells.
- The cubic shape of MNPs displayed the higher SAR values as compared to other shapes because of the varied shape anisotropies.
- Application of coated MNPs in hyperthermia therapy outweighed the uncoated MNPs due to the improved properties, such as biocompatibility, homogenous dispersion, and moderate T_H . However, coating with a thin layer should be considered to avoid the reduction of M_s and SAR values.

- The frequency and strength of AMF played decisive roles in the induction heating power, the saturation time of MNPs, and the stability within the T_H range. Clearly, very low and very high strengths were directly proportional to the SAR value with unsatisfactory T_H .

The MHT efficiency is indeed depended on the surface chemistry of nanoparticles that by applying biopolymers as coating protective layer to fabricate either core-shell or mesoporous structure would be increased. Meanwhile, the substitution of MNPs with other ferrites possessed photo-thermal property would significantly enhance the cancer cells destruction.

University of Malaya

CHAPTER 3: METHODOLOGY

3.1 Introduction

This chapter provides information about the materials, the chemical methods and the procedures that were used to synthesize the promising magnetic nanoheating agent for in-vitro magnetic hyperthermia therapy of cancer. Details of synthesis experimental conditions, surface modifications, characterization, induction heating tests and in-vitro cytotoxicity of magnetic nanoheating agents on liver cancer cells under hyperthermia conditions are also presented. The following descriptions are divided into three main parts based on the presented objectives in the Chapter 1. Part 1 describes the synthesis and characterization of iron oxide nanoparticles (IONPs) by using two alkaline reagents under two different experimental environments. Part 2 studies the synthesis possibility of SPIONs using a sole iron precursor through optimization of the oxidative potency of the synthesis environment, i.e. the O₂:N₂ flow ratio. The final part reports the stabilization and functionalization of the optimized SPIONs sample from part 2 with a controlled micellar conformation and then coating with a thin layer of low-melting point biopolymer to achieve enhanced cytocompatibility and hyperthermia efficiency under AMF exposure.

3.2 Synthesis of Highly Stable Superparamagnetic Iron Oxide Nanoparticles under Mild Alkaline Reagents and Anaerobic Condition

3.2.1 Materials

Ferric chloride hexahydrate ($\text{FeCl}_3 \cdot 6\text{H}_2\text{O}$; >99%), ferrous chloride tetrahydrate ($\text{FeCl}_2 \cdot 4\text{H}_2\text{O}$; >99%), sodium hydroxide pellets (NaOH ; 99%), ammonium hydroxide (NH_4OH ; 28%w/w) and absolute ethanol were purchased from R&M Chemicals. All the chemicals were in analytical grades and used without further modification or purification.

3.2.2 Synthesis Procedure

The synthesis procedure was performed under anaerobic condition using NH_4OH as a mild alkaline reagent ($\text{NH}_4\text{OH.N}_2$, IO_4). Besides, the procedure was also followed by the common methods; aerobic condition with NH_4OH ($\text{NH}_4\text{OH.Air}$, IO_2), anaerobic condition with NaOH (NaOH.N_2 , IO_3), and aerobic condition with NaOH (NaOH.Air , IO_1), in order to distinguish the superiority of the resultant IO_4 sample. In a typical procedure; 2.33 g of $\text{FeCl}_3 \cdot 6\text{H}_2\text{O}$ was dissolved in 8 mL of distilled water and 0.85 g of $\text{FeCl}_2 \cdot 4\text{H}_2\text{O}$ was dissolved in 2 mL of distilled water. The volume of the solutions was then set up to 50 mL using distilled water. The solution was put under vigorous stirring for 15 min, followed by dropwise addition of 50 mL of the alkaline reagent. After an hour, the synthesized nanoparticles were separated using a strong magnet, washed once with absolute ethanol and rinsed five times with distilled water to remove impurities. The magnetic nanoparticles were dried at 80 °C for 24 hours, for further analyses.

3.2.3 Characterization

The surface charge for the synthesized iron oxide samples was investigated through zeta potential (ζ) measurement using a Zetasizer instrument (Malvern Instruments, Worcestershire, UK) with three times repeats for each sample. The phase composition and crystallographic state of the samples were determined by powder X-ray diffraction (XRD; Philips PW1840, Amsterdam, the Netherlands) equipped with Cu-K α radiation ($\lambda=1.542 \text{ \AA}$) at scanning rate of $2^\circ/\text{min}$ in 2θ angle from 10° to 80° . The full width at half maximum (B) as an indicator of the crystallinity degree was measured using Origin Pro software (version 9.4, Origin Lab, Hampton, MA). The average crystallite size (D) of all iron oxides was then calculated from the diffraction line-width of XRD pattern, according to the Debye Scherer's formula (Kingsley, Desai, & Srivastava, 2015):

$$D = \frac{K\lambda}{B\cos(\theta)} \quad (3-1)$$

where K_S is a dimensionless shape factor of Scherrer (0.94). The structural morphologies of iron oxide samples were observed using transmission electron microscopy (TEM; LEO Libra 120 kV, Carl Zeiss AG, Germany) while the mean particle size for each group was examined as the standard deviation (SD) from the size measurements of at least 100 randomly selected nanoparticles using ImageJ software. The magnetic characteristics of the samples were only measured using VSM (model 7400 series, Lakeshore, Chicago, IL) at ambient temperature in the field range of 0 to $\pm 8 \text{ kG}$ (0.8 Tesla). The Zero-field-Cooled and Field-Cooled measurements were limited due to availability restrictions for SQUID.

3.2.4 Data Analysis

The experiments were performed at least thrice, and the obtained results were presented as the means \pm SD.

3.3 Synthesis and In-Vitro Characterization of Superparamagnetic Iron Oxide Nanoparticles Using a Sole Precursor for Hyperthermia Therapy

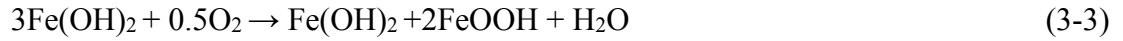
3.3.1 Materials

FeCl₂.4H₂O and NH₄OH were applied respectively as the single iron precursor and precipitator to synthesize iron oxide samples under four varied oxidative conditions. The chemicals were in analytical grades and used without further modification.

3.3.2 Synthesis Procedure

Bare iron oxide nanoparticles are usually produced in an aqueous medium through precipitation of ferrous and ferric chlorides with the stoichiometry of [Fe³⁺]/[Fe²⁺]=2:1; however, it is arduous to maintain such molar ratio in oxidative air environment due to a high tendency of ferrous cation to partial oxidization. Hence, the synthesis process is often performed under non-oxidative environments, preferably N₂, to avoid the uncontrollable oxidation of the ferrous ions (Gupta & Gupta, 2005). Iron oxide may also be synthesized in oxidative environments with lower initial molar ratios of iron cations e.g. [Fe³⁺]:[Fe²⁺]=3:2 (Jiang et al., 2011; S. Wu et al., 2011), where partial oxidation (approximately 17%) of the ferrous ions to ferric eventually endows a molar ratio of [2:1].

Based on the great oxidation vulnerability of Fe²⁺, formation of iron oxide may be independent of using ferric precursor. In this route, iron oxide can be produced using a Fe²⁺ salt as the single precursor. With provision of a highly-controlled oxidative environment, a partial oxidation of around 67% of ferrous ions to ferric (Hedayatnasab, Dabbagh, Abnisa, & Wan Daud, 2020b), could result in formation of Fe₃O₄ according to the following formula:



For the synthesis of Fe_3O_4 using a sole Fe^{2+} precursor, the oxidative potential of the synthesis environment must be approximately fourfold of the ambient air, which results in 17% oxidation of ferrous ions when two iron precursors with molar ratio of $[\text{Fe}^{3+}]:[\text{Fe}^{2+}]=3:2$ are used. Accordingly, a rule of thumb calculation indicates that the partial pressure of O_2 in the air with value of 21% must increase fourfold to nearly 80% and the O_2 solubility in the aqueous medium must rise around quadruple as well. Based on the Henry's law, the O_2 solubility in water is directly proportionate to the partial pressure of O_2 over the solution and it is expressed as the following (Gómez Ruiz, Roux, Courtois, & Bonazzi, 2018):

$$P = K_H C_{\text{do}} \quad (3-5)$$

where P , C_{do} , and K_H are the partial pressure of O_2 , concentration of the dissolved O_2 in the solution, and the Henry's law constant, respectively. Therefore as presented in Table 3.1, the synthesis procedure in the present study was carried out using four varied $\text{O}_2:\text{N}_2$ flow ratios of 3:7, 4:6, 5:5, and 6:4 in the synthesis reactor in order to determine the optimal oxidative condition for iron oxide production.

In a typical synthesis procedure, 0.85 g of $\text{FeCl}_2 \cdot 4\text{H}_2\text{O}$ dissolved in 2 mL of distilled water and then volume up to 50 mL using distilled water, followed by dropwise incorporation of 50 mL of NH_4OH under 600 rpm stirring at 80 °C is shown in Figure 3.1. After an hour, product was magnetically separated, washed once with absolute ethanol and rinsed five times with distilled water to remove impurities, then dried at 80

°C in an oven for 24 h. Finally, the samples were dispersed and kept in distilled water for further characterization. The detailed parameters of the four conditions are mentioned in Table 3.1.

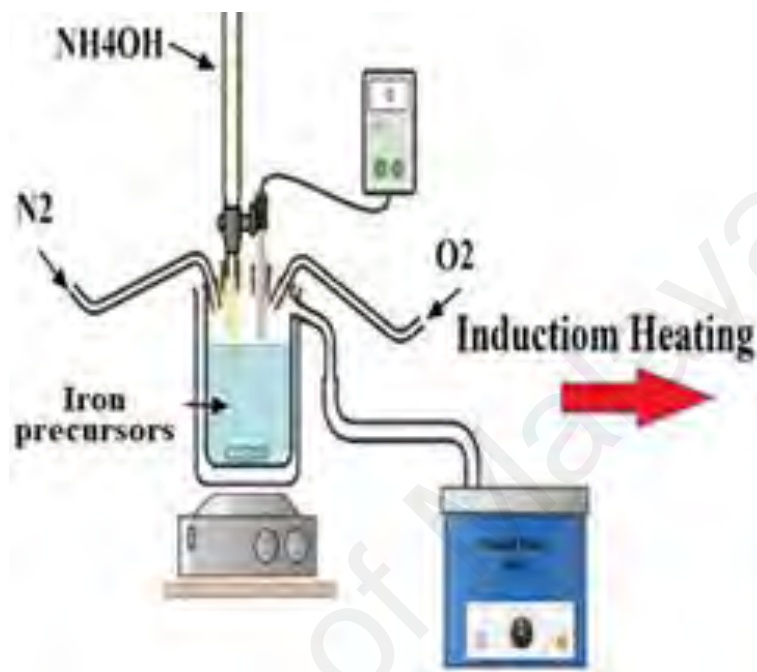


Figure 3.1: Experimental setup to synthesize iron oxide under oxidative condition

Table 3.1: The experimental conditions applied for the synthesis of iron oxide samples

Sample	FeCl ₂ .4H ₂ O (g)	Water (ml)	Alkaline (ml)	O ₂ (Pa)	N ₂ (Pa)
S ₃	0.85	50	50	0.30	0.70
S ₄	0.85	50	50	0.40	0.60
S ₅	0.85	50	50	0.50	0.50
S ₆	0.85	50	50	0.60	0.40

3.3.3 Characterization

Determination of surface charge, structural and phase analysis, morphological and magnetic behaviour of iron oxide samples were respectively carried out using ζ measurement, XRD, TEM and VSM analyses which followed by the 3.2.3 subsection.

3.3.4 Cell Viability Assay

The HepG2 cells were resuscitated according to the standardized method in Dulbecco's Modified Eagle Medium (DMEM; Sigma Aldrich, USA) high glucose containing 4500 mg/L D-glucose, L-glutamine, 110 mg.L⁻¹ sodium pyruvate, supplemented with 10% v/v fetal bovine serum (FBS; Sigma Aldrich, USA), 1% v/v penicillin/streptomycin (Gibco by Life Technologies) at 37 °C in a 5% CO₂ humidified incubator and monitored daily. The growth media were changed in every three days and the cells were subcultured at 80% confluence through trypsinizing and were resuspended in culture medium in a new flask or seeded in 96-well plates; hereupon, they were never encountered with the crowded conditions. When the density of the cells reached to 1×10⁵ per well then incubated overnight to adhere prior to the cell viability assay (Hurrell, Lilley, & Cromarty, 2019).

Cell viability and proliferation were observed by a dye-reduction assay known as the MTT (3-[4,5-dimethylthiazol-2-yl]-2,5-diphenyltetrazolium bromide) assay for the biomaterial toxicity detection. Briefly, the cells with a density of 1×10⁵ cultured in a 96-well plate for 24 h for adhering to the plate surface then the cells were rinsed with phosphate-buffered saline (PBS; pH 7.4) in order to remove the disjointed cells and replace by fresh media with varied concentrations of iron oxide samples (100, 50, 25, 12.5, 6.25, 3.125, 1.5 µg.ml⁻¹), followed by adding PBS to each group (triplicate wells) and incubated at 37 °C in a 5% CO₂ atmosphere for 24 h (Mondal et al., 2017). Control plates (the media with only cells) were also remained to monitor the potential changes in the culture media. The media were thereafter removed, and the cells were washed with PBS to remove supernatant particles, followed by adding 10 µl of MTT dye solution to each well including control wells followed by 4 h incubation for metabolization of MTT with the samples and cell media. Meanwhile, the non-contamination of the cells was checked through an inverted microscope observation. The media were then removed

through flicking the plates; thereby, only the anchored cells stayed in the wells. The water-insoluble formazan product extracted in 100 μl pure dimethyl sulfoxide (DMSO) was added to each well and incubated 2 h in the dark, followed by adding 25 μL Sorensen's glycine buffer as MTT stopper reactions and finally the absorbance was read with an iMarkTM Microplate Absorbance Reader (Bio-Rad laboratories, Inc. USA) at 570 nm and reference filter at 630 nm. The cell viability was calculated using the following equation (Mondal et al., 2017):

$$\text{Cell Viability} = \frac{I_s}{I_c} \times 100 \quad (3-6)$$

where I_s and I_c indicate the optical values of cells which incubated with sample and control group, respectively.

3.3.5 Magnetic Induction Heating

The induction heating efficiency of the optimized iron oxide sample was determined by subjecting its colloidal dispersion (dispersed in distilled water owing to approximately 70% of human body is made up of water) with five different concentrations (1, 2, 3, 4, and 5 $\text{mg}\cdot\text{ml}^{-1}$) to an external AMF with five varied electric currents of 50, 100, 150, 200, and 250 A, which respectively corresponded to frequencies of 326, 318, 313, 312, and 311 KHz. For this purpose, magnetic hyperthermia experiments were carried out in plastic micro centrifuge tubes (2 ml) placed in the center of the helical coil (inner diameter of 2.54 cm and 8 turns) of an induction heating instrument (Easy Heat 8310, Ambrell, UK) cooled with water circulation. The schematic of the experimental setup utilized for this research is illustrated in Figure 3.2. The applied field strengths (H) during the MHT tests were calculated from the following equation (Singh, Singh, Singh, & Srivastava, 2018);

$$H = \frac{ni}{L} \quad (3-7)$$

where n, i, and L indicate the number of turns, applied current (A), the diameter of the turn (m) for the helical coil, respectively. The calculated magnetic field values at five varied applied currents were 15.74, 31.49, 47.24, 62.99, and 78.74 kA.m⁻¹. The temperatures profiles were obtained through the iron oxides exposure to external AMF over 5400 seconds (s). The heating efficiency of samples was quantified through SAR measurement using following formula (Chiriac et al., 2015):

$$SAR = \left(\frac{\sum_i C_i m_i}{m_{Fe}} \right) \left(\frac{dT}{dt} \right) \quad (3-8)$$

where C is the specific heat capacity of the colloidal dispersion which is the combination of medium and iron oxide with values of 4.18 and 0.65 J.g⁻¹.K⁻¹, respectively. The m_{cd} and m_{Fe} are the mass of colloidal dispersion and iron in the fluid respectively, and dT/dt represents the initial slope of the temperature profile over 120 s.

3.3.6 In-Vitro Magnetic Hyperthermia on the HepG2 Cells

To evaluate the in-vitro anticancer hyperthermia efficiency of optimized iron oxide sample, HepG2 cells with the density of 1×10⁵ per well were seeded in a 96-well plate and incubated over night for cell attachment. Thenceforward, the culture media were wiped out and the cells were treated with the particles at 100 µg.ml⁻¹ followed by 4 h incubation (Mondal et al., 2017; Quinto, Mohindra, Tong, & Bao, 2015). Based on the obtained results from induction heating section, both untreated and treated groups with nanoparticles were exposed to different AMF strengths of 31.49 and 47.24 kA.m⁻¹. After the heating exposure, the cells were incubated for another 24 h as demonstrated in Figure 3.2. The MTT assay was then performed to evaluate and compared the cell viability of the samples with the control groups.

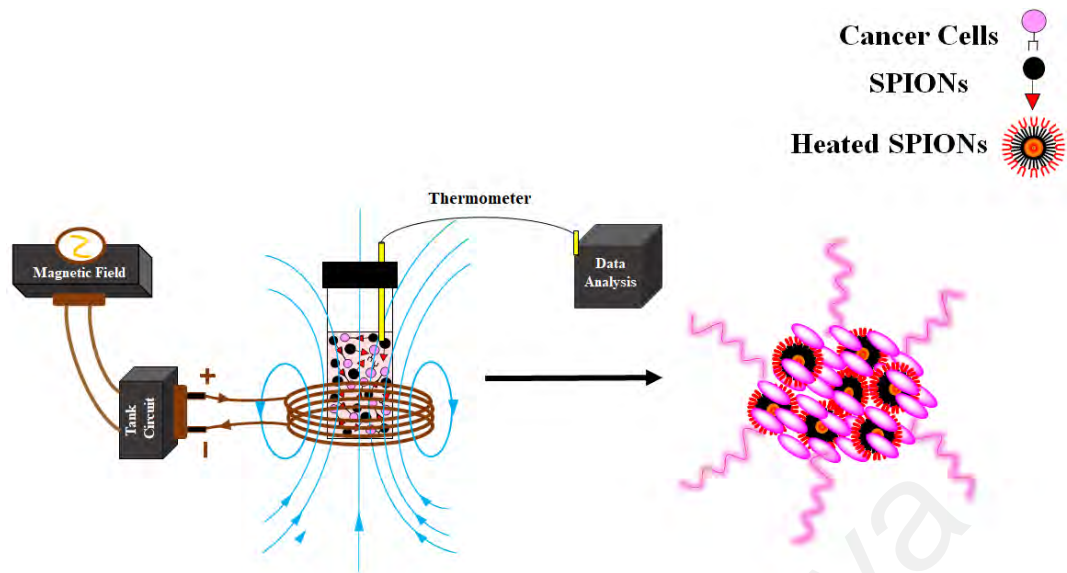


Figure 3.2: The schematic of the in-vitro hyperthermia test

3.3.7 Data Analysis

All the experiments were performed at least three times presented as the means \pm SD. The statistical analyses were performed using one-way ANOVA followed by Turkey's test as the pos-hoc using Statistical Package for Social Sciences software (SPSS; version 25, SPSS Inc., Chicago, IL, USA).

3.4 Polycaprolactone-Coated Superparamagnetic Iron Oxide Nanoparticles Micelles for In-Vitro Magnetic Hyperthermia Therapy of Cancer

3.4.1 Materials

The iron oxides were synthesized using $\text{FeCl}_2 \cdot 4\text{H}_2\text{O}$ as the sole iron precursor, NH_4OH , as well as cetyltrimethylammonium bromide CTAB (Sigma-Aldrich) as cationic surfactant. Polycaprolactone (PCL) with diol terminal groups (PCL-d, 2000 Da) and tetrahydrofuran (THF) solvent were purchased from Sigma-Aldrich. All the chemicals were in analytical grades and used without further modification or purification.

3.4.2 Synthesis Procedure

As a rule of thumb, iron oxides may be produced independent of using ferric precursor when 67% of the applied Fe^{2+} ions are oxidized to Fe^{3+} . This synthesis approach has adequate potential to produce iron oxides with lower costs and waste materials. Besides, reduced usages of chemical reagents incorporated in the synthesis reaction may lead to decreased synthesis complexity and enhanced physicochemical properties.

In order to synthesize iron oxides with the ferrous precursor, varied oxidative environments were preliminarily examined through alteration of the $\text{O}_2:\text{N}_2$ flow ratios in the synthesis reactor (i.e. 0.3 to 0.6) and the $\text{O}_2:\text{N}_2$ ratio of 0.5 was chosen as the optimal oxidative environment for production of iron oxides with desirable physicochemical and magnetic properties. Briefly, in a typical experiment, 0.85 g of $\text{FeCl}_2 \cdot 4\text{H}_2\text{O}$ was dissolved in 2 mL of distilled water and volumed up by 50 ml of distilled water. Thereinafter, NH_4OH was dropwise added to the mixture for further 30 min to obtain the black precipitates. At the end, product was harvested with a strong magnet, washed with ethanol

3.4.4 Preparation of Coated Particles

Water-in-oil (W/O) emulsion was used for coating the particles with PCL-d biopolymer, where the oil phase comprised of THF solvent and PCL-d. Noticeably, coating the particles with amphiphilic or charged polymers gives rise to the reduction the oil-water interfacial tension and improve the stability of the emulsion in high-salinity environments, even at very low concentrations of nanoparticles (Qi et al., 2018). In addition, the CTAB cationic surfactant acted as an emulsifier that formed the great stability of emulsions and created electrostatic interactions with the diol terminal groups of PCL-d, as shown in Figure 3.4.

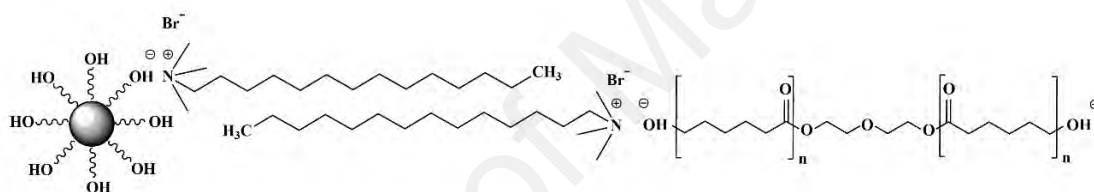


Figure 3.4: A schematic of the attachment mechanism of PCL-d on CTAB-modified iron oxide

Briefly, 1 g of PCL-d was poured into 20 ml of THF and stirred for 30 min, meanwhile, 300 mg of modified-particles dissolved separately in 10 ml of distilled water using ultrasonication for 30 min. Thereafter, the oil and aqueous were mixed and vigorously stirred using a high-speed homogenizer at 10000 rpm for 2 hours to ensure that the PCL biopolymer was precipitated on the particles surface and produced the core-shell nanostructure. The obtained product was washed with THF, THF/distilled water (50:50), and trice with distilled water until complete disappearance of impurities, followed by drying in oven at 80 °C for 24 h. A typical representation of the PCL-coated iron oxides preparation is illustrated in Figure 3.5.

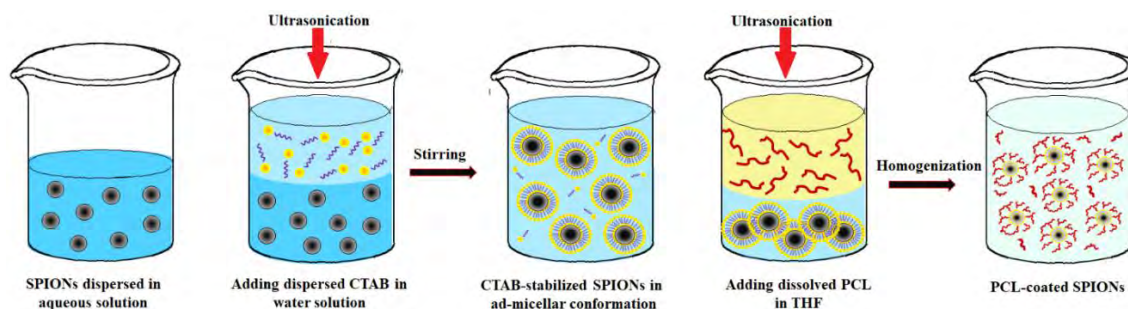


Figure 3.5: A schematic of the functionalization and coating of CTAB-modified iron oxides

3.4.5 Characterization

Determination of surface charge, structural and phase analysis, morphological and magnetic behaviour of iron oxide samples were respectively carried out using ζ measurement, XRD, TEM and VSM analyses which followed by the 3.2.3 subsection.

The high magnification surface morphologies were ascertained by high-resolution transmission electron microscopy (HRTEM, field emission of 200 kV, Tecnai™ G2 20 S-TWIN FEI). The chemical functional groups of the iron oxide samples were monitored using a Fourier transform infrared spectroscopy spectrometer (FTIR; Nicolet 6700, ThermoScientific, Madison, WI) through advanced direct surface contact technique in the range from 500–4000 cm^{-1} . The X-ray photoelectron spectroscopy (XPS) analysis was performed with a fully automated microprobe (PHI Quantera II, Ulvac-PHI, INC.) using Al-K α radiation with $\lambda = 1486.6$ eV operated at 25.6 W (beam diameter of 100 μm). Low-resolution analysis was carried out through passing an energy of 280 eV with 1 eV per step to detect the chemical state of the elemental composition while high-resolution analysis performed over the binding energy range of 112 eV with 0.1 eV per step. The samples were prepared on a carbon tape supported by a stub holder. The charge correction was conducted at C 1s before the deconvolution through the setting binding energy of C-C to 284.8 eV using MultiPak Spectrum software. The onset and peak phase transition temperatures were calculated through differential Scanning Calorimetry (DSC; Q1000

Perkin Elmer TA Instrument) at a heating rate of 20 °C/min using nitrogen air flow of 50 ml/min. In addition, thermogravimetric analysis (TGA; Q500 Perkin Elmer Instrument) of the dried samples were also performed by a NETZSCH STA 409 PC/PG (Selb, Germany) at a heating rate of 20 °C from 20 to 1000 °C using a nitrogen air flow 50 ml/min to monitor the weight percentage of polymer-coated particles.

3.4.6 Cell Viability Assay

The cell viability assay was followed by the 3.3.4 subsections; however, the cell viability profiles of polymer-coated particles against HepG2 cells was evaluated after 24 and 48 h incubations.

3.4.7 Magnetic Induction Heating

The induction heating test of polymer-coated particles was performed under four varied AMF strengths of 15.74, 31.49, 47.24, and 62.99 kA.m⁻¹ and followed by the pervious part, 3.3.5 subsection.

3.4.8 In-Vitro Magnetic Hyperthermia on the HepG2 Cells

This part followed the 3.3.6 subsection. The in-vitro hyperthermia of polymer-coated particles on the HepG2 cells was performed under the exposure of 31.49 and 47. kA.m⁻¹, and the media was replaced after 24 h.

3.4.9 Data Analysis

This part followed the 3.3.6 subsection.

CHAPTER 4: RESULTS AND DISCUSSION

4.1 Introduction

Superparamagnetic iron oxide nanoparticles are at the forefront of nanotechnology research due to their unparalleled and exceptional properties, including magnetophoretic, biocompatibility, a facile low-cost synthesis, and easy surface modification, making them the most prominent magnetic nanoheating agents for hyperthermia therapy of cancer under the external AMF exposure as compared to other transition metallic compounds (Hedayatnasab, Abnisa, & Wan Daud, 2018; Iacovita et al., 2016). However, SPIONs are comparatively unstable in aerobic condition, owing to their significant oxidation susceptibility in oxidative environments, leading to deteriorated dispersibility and magnetism (Elfeky et al., 2017). Therefore, elimination of oxidative atmosphere through vacuum or introduction of inert gases e.g. N_2 to the reaction system can prevent SPIONs' activity towards environmental oxygen. The pH for synthesis medium is the second decisive factor which plays a pivotal role in the particles dispersibility (Xie et al., 2019). The stability of SPIONs in aqueous media can be controlled by altering the pH values through dilution of alkaline reagents or incorporation of varied alkaline solutions in the synthesis medium. NH_4OH and $NaOH$ are the most widely used as precipitating agents for synthesis of SPIONs, which could provide maximum pH values of 10-11 and 12-13, respectively (Hedayatnasab et al., 2019). The different pH values obtained by these alkalis could potentially affect various physicochemical, morphological, and magnetic characteristics of the resulting particles, as well as their aggregation susceptibility. Owing to the crucial impacts of synthesis environment and precipitating reagent, the determination of the main governing parameters for various properties requires

quantitative investigations and comparative analyses of these properties at different experimental conditions.

In this way, the coprecipitation of iron(II) and iron(III) in the aqueous medium is considered as the appropriate synthesis approach to produce SPIONs with the surfaces rich in -OH functional groups which are indispensable for cancer treatment purposes (Ibrahim et al., 2018); however, reducing the amount of applied chemicals could lessen toxicity risks for these treatments and conversion of iron(II) to iron(III) in a partial oxidative environment considered as the main challenge of this approach which requires incorporation of higher amounts of iron(II) precursor than stoichiometric ratio (Refait & Génin, 1993). SPIONs can also be synthesized using a sole iron(III) precursor through either hydrothermal or thermal decomposition methods with various base solutions and reducing agents. However, toxicity of the applied chemicals, water-insolubility and water-indispersibility of products, energy-intensiveness, and tedious high temperature procedures (Rivas Rojas, Tancredi, Moscoso Londoño, Knobel, & Socolovsky, 2018) may render these approaches inappropriate for MHT. Moreover, these methods may produce nonmagnetic wüstite phase and/or a mixed magnetite-maghemite phase with descended magnetic properties (Unni et al., 2017). Interestingly, the precipitation technique has adequate potential to produce SPIONs through the sluggish oxygenation of iron(II) hydroxide in the partial oxidative condition then followed by hydrolysis reaction. Synthesis of SPIONs with a sole iron(II) precursor is desirably preferred to prevent iron(II) and iron(III) cations from re-oxidizing, save expenses, and eschew in wasting materials.

However, agglomeration vulnerability of these magnetic nanoheating agents in biological media, low control over the heat generation and dissipation at the target region, and eschewed clearance by the RES remain as the main challenges for clinical translation of this approach. One potential approach to provide higher colloidal stability is surfactant-

based surface modification of nanoparticles (Hedayatnasab et al., 2017). Thereby, precise adjustment of the surfactant quantity is essential to prevent bridging and destabilization of nanoparticles, leading to controlled particle size and improved dispersion. As SPIONs often possess a negative surface charge, surfactants with high cationic surface charges such as CTAB are necessary for their stabilization. CTAB is determined of a cationic organoamine with a 19-carbon tail and hydrophile-lipophile balance value of 10, presenting a substantial capability to separate precipitates in water medium (Yalcinkaya et al., 2017). CTAB may experimentally produce smaller particle size, which in turn gives rise to increased surface area, facilitating attachment of varied therapeutic adjuvants through surface functionalization strategies (Gan et al., 2018).

Another challenge of SPIONs for in-vivo purposes is a rapid opsonization and subsequent segregation by the immune system. These nanoheating agents are easily recognized as foreign bodies by the RES, instantly coated by plasma proteins and blood components, and rapidly cleared before reaching the targeted region (Aggarwal et al., 2009). Although a number of polymers are used, PEG is the most widely applied polymer in surface coating of SPIONs, which not only endows excellent stealth characteristics to the SPIONs and minimize RES sensitivity, but also improves their steric stability, dispersity, and biodistribution. However, non-biodegradability and degradation under stress remain as the main drawbacks of PEG coatings (Knop, Hoogenboom, Fischer, & Schubert, 2010). PEG may also discourage interaction with the receptors on the targeted cell membranes and cause hypersensitivity through generation of antibodies which neutralize the nanoparticles efficacy upon repeated administration (S. Zhang, Tang, & Yin, 2015).

More recently, PCL has received increasing interests as a novel carrier of varied therapeutics due its biodegradability, structural stability, partial crystallinity, non-toxicity, and amphiphilic feature. PCL is also of particular interest due to its stealth and

protein repellent characteristics, rendering minimized opsonization and RES sequestration (Espinoza, Patil, San Martin Martinez, Casañas Pimentel, & Ige, 2019). When PCL is applied as surface coating on SPIONs, its partial crystallinity may confer it with potential to enhance the magnetic behaviour due to ordered arrangement of magnetic moment in a single crystal (Hedayatnasab et al., 2020a).

In this study, a novel approach was applied for precipitation of SPIONs from a single iron precursor in a highly-controlled oxidative environment. SPIONs were further functionalized with a double-layered cationic CTAB surfactant to enhance their stability and provide proper surface functionality for biopolymer attachment through electrostatic interactions. Thereupon, the CTAB-coated SPIONs were applied as a core and coated with a thin layer of PCL biopolymer through “graft-to” approach to achieve enhanced cytocompatibility and physicochemical properties for in-vitro MHT against HepG2 cell lines. To the best of our knowledge, ad-micellar stabilized PCL-coated SPIONs have not yet been reported as a magnetic nanoheating agent for in-vitro hyperthermia application. Thanks to desirable melting temperature of PCL, it was also assumed that the polymeric coating may exhibit a thermosensitive performance through dissociation at the T_H range, resulting in exposed SPIONs and enhanced induction heating efficiency in MHT through maintaining the treatment temperature within the secure T_H range.

In this chapter the results are rendered in three main parts based on the presented objectives in the Chapter 1. Part 1 concentrates on the optimization of the synthesis condition via investigating the effects of two alkaline reagents (NH_4OH and NaOH) and synthesis experimental environments (aerobic and anaerobic) on various characteristics of iron oxide particles. Part 2 investigates the effect of varied oxidative conditions through optimization of the oxidative potency of the synthesis environment, i.e. the $\text{O}_2:\text{N}_2$ flow ratio on the physicochemical and magnetic properties as well as cytocompatibility of

synthesized iron oxide particles by using a sole iron(II) precursor and a single alkaline reagent. Thereafter, heating efficiency of the sample with optimum properties under AMF exposure with varying strengths is evaluated. Additionally, the cytotoxicity assays against HepG2 cells is performed on the optimized sample at varied AMF strengths to evaluate their effectiveness as magnetic nanoheating agent under hyperthermia condition. Part 3 reports the development of PCL-coated iron oxide particles with structural stability, uniform particle size, improved dispersity, cytocompatibility, and controlled heating under hyperthermia condition. In this regard, the effects of varied AMF strengths on induction heating capability of these core-shell nanoheating agents are investigated to obtain appropriate T_H profile. The core-shell nanoheating agents are further studied to quantify the cytocompatibility and in-vitro cytotoxicity against HepG2 cells under hyperthermia condition.

4.2 Synthesis of Highly Stable Superparamagnetic Iron Oxide Nanoparticles under Mild Alkaline Reagents and Anaerobic Condition

4.2.1 Physicochemical Characterization

The rates of pH rise during dropwise addition of the alkaline solution into the reaction chamber containing iron precursors are shown in Figure 4.1. Addition of the iron precursors to the aqueous solution resulted in a drastic pH reduction from around 7 to near zero due to their strong acidic nature. The dropwise addition of NH_4OH and NaOH into the reaction mixtures respectively led to moderate pH rise while further injection of 5ml gave rise to rapid pH increase to approximately 10 and 13, and then no significant increase in the solution pH was observed by increasing the volumetric ratios for the alkalis. However, continuous dropwise addition of the alkaline reagent till 50 mL was necessary to maintain sufficient OH^- ions and subsequently pH value above 9 for precipitation of entire Fe^{2+} and Fe^{3+} ions until the color of the solution changed to the black that confirmed the Fe_3O_4 formation (Ahn, Kim, Yang, Lee, & Kim, 2012).

The lower rates of pH rise observed during addition of NH_4OH may have contributed to decreased rates of particles formation compared to NaOH reagent and thus producing iron oxide with smaller particle sizes. The flow of N_2 gas also assisted this effect of NH_4OH and prevented oxidation that might lead to sufficient surface stability against agglomeration (Ali et al., 2016). However, higher pH values obtained when a stronger alkali was used as the precipitating reagent resulted in higher negative surface charges in the synthesized iron oxide particles and thus providing particles with relatively high stability and low aggregation in aqueous media. The ζ values measured for IO_3 and IO_1 were respectively -32 ± 3 and -26 ± 4 mV, which were higher than those of IO_4 and IO_2 (-19 ± 5 and -15 ± 4 mV). Moreover, the lower negative ζ values obtained in the aerobic

environment compared to the anaerobic environment may probably be due to oxidation of iron oxide in the presence of environmental O₂ and CO₂, which potentially leads to increased acidity and lower negative ζ values (Yin et al., 2017).

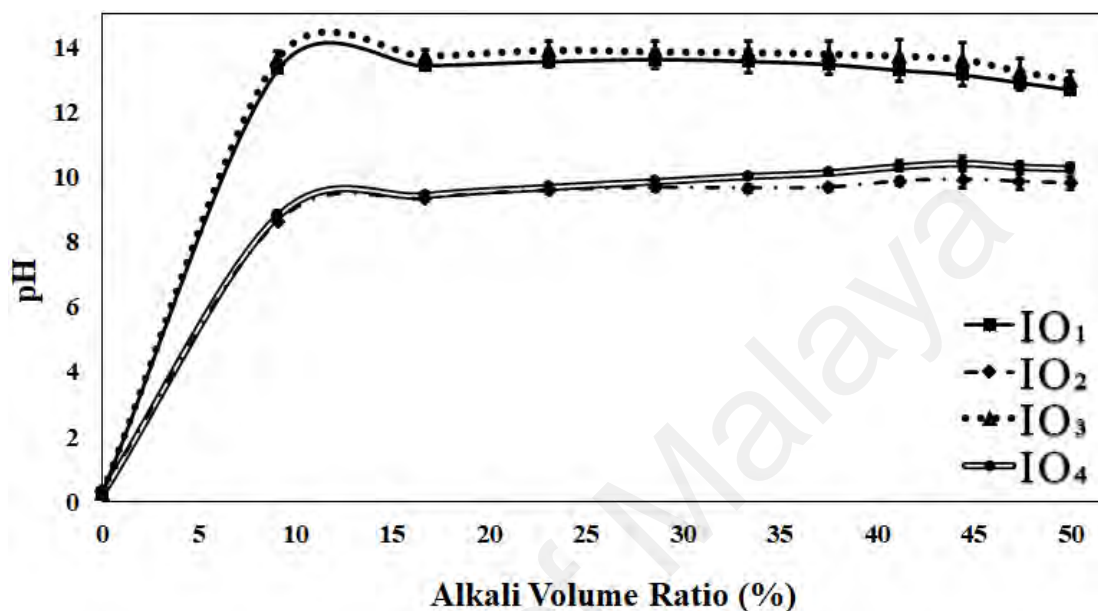


Figure 4.1: The rates of pH rise during dropwise addition of alkaline reagent under four varied synthesis conditions

4.2.2 Structural and Phase Analysis

The XRD spectra for the iron oxide particles synthesized using NH₄OH and NaOH in either aerobic or anaerobic environments (Figure 4.2) confirmed formation of magnetite phase with cubic structure and space group of Fd3̄m (JCPDS 00-001-1111), where the peaks observed at 2 θ values of 18°, 30°, 35°, 43°, 54°, 57°, 63°, and 74° respectively, corresponded to (111), (220), (311), (400), (422), (511), (440), and (533) planes in the magnetite crystalline structure (Unterweger et al., 2018). The interplanar spacings ' d_{hkl} ' (Table 4.1) represents all samples had inverse cubic spinel structure of magnetite. The highest intensity peak at 35° in all the four iron oxide samples corresponded to (311) plane from magnetite, implying that the Fe₃O₄ was considered as the major phase.

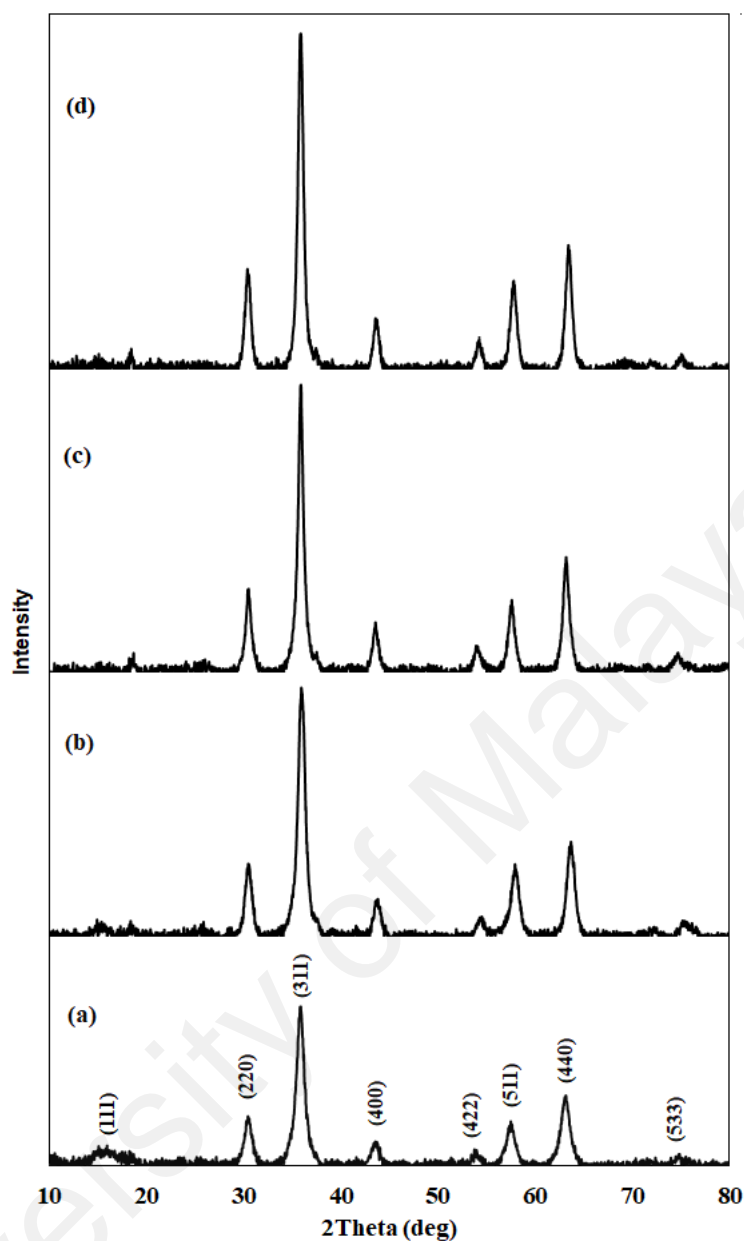


Figure 4.2: The XRD spectra of a) IO₁, b) IO₂, c) IO₃, and d) IO₄

The D values of all samples, calculated by eq. (3-1) using the B value of the (311) peak at 35° as the representative plane of magnetite phase, are given in Table 4.1. The crystallinity for the synthesized the samples was significantly governed by both the experimental variables, although the effect of synthesis environment overweighed the influence of alkaline reagent. The IO₄ sample synthesized by NH₄OH under the N₂ environment provided the narrowest peaks with highest crystallinity, endowing for maximum D value (14 nm), as compared to 13 nm, 10 nm, and 9 nm for IO₃, IO₂, and

IO₁, respectively. The obtained results were consistent with previous studies, which showed that the magnetic nanoparticles synthesized through electron beam irradiation displayed smaller crystallite size of 15.29 nm for the samples that were precipitated by NaOH as compared with NH₄OH (X. Zhang, Zhou, Rao, & Shanghai, 2006).

Table 4.1: The phase structural characteristics of the iron oxide particles synthesized in varied synthesis conditions

Characteristics	IO ₄	IO ₃	IO ₂	IO ₁
2θ (°)	35.69	35.77	35.60	35.77
B (°)	0.64	0.69	0.84	0.95
Intensity (cts)	6991.25	6871.41	5025.86	4409.26
D (nm)	14	13	10	9
d(311) (Å)	2.51	2.51	2.52	2.51

4.2.3 Morphological Analysis

Figure 4.3 shows a comparison between the particle morphology and dispersibility of the as-synthesized iron oxide particles in varied experimental conditions. It was clearly seen that the presence of N₂ environment was significantly effective in reducing the agglomeration tendency in the IO₂ and IO₄ samples (Figure 4.3 b and d). In regards to the effect of alkaline solution, a slightly lower susceptibility to agglomeration was observed in the particles synthesized using NaOH reagent, probably owing the higher negative ζ values produced by this alkaline, which consequently contributed to higher repulsive interparticle forces and enhanced dispersibility. In fact, a swift solution attained by this strong alkaline reagent, the condensational growing process through the Ostwald ripening process could be overcome (Bui, Ton, Duong, & Tran, 2018; Cao & Wang, 2011).

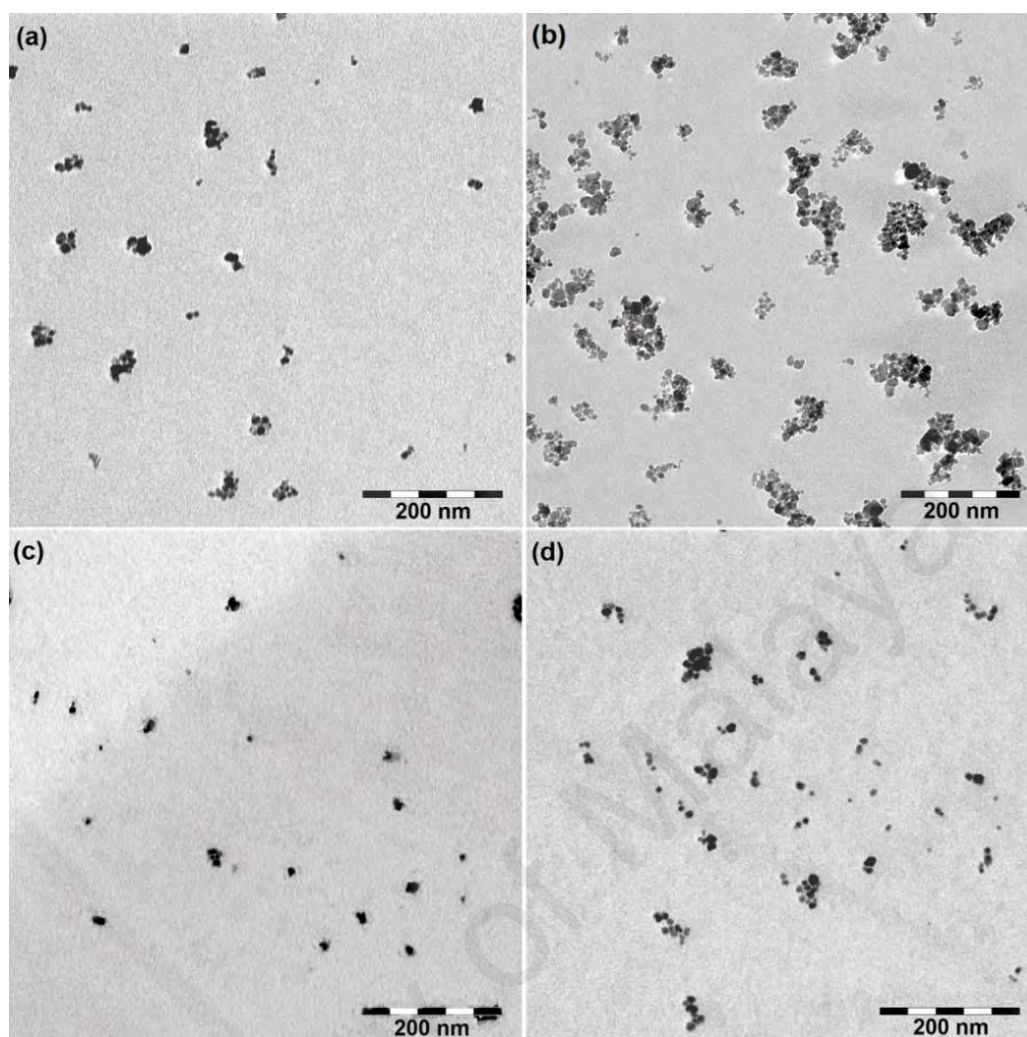


Figure 4.3: TEM images of a) IO₁, b) IO₂, c) IO₃, and d) IO₄

Moreover, although utilization of NH₄OH as a mild precipitating reagent induces lower rates of particle formation and thus smaller particle sizes (17 ± 5 nm) compared to NaOH (20 ± 4 nm), the cohesive forces generated in the smaller particles prevail the interparticle forces and consequently stimulate agglomeration tendency (Hayden, Park, & Curtis, 2003). These average particle size of the samples indicate they are within the single-domain region (<20-30 nm), implying SPM behaviour which is in line with the findings from XRD analysis.

4.2.4 Magnetic Analysis

The magnetization of IONPs produced in varied experimental conditions at room temperature are illustrated in Figure 4.4. The VSM graphs clearly showed that all the synthesized IONPs presented SPM behaviour with nearly zero M_r and extremely low H_c values (Patsula, Moskvin, Dutz, & Horák, 2016). However, the M_s values of all the IONPs were lower than that of bulk iron oxide with value of 92 emu.g^{-1} , probably due to increased thermal fluctuations as well as disordered magnetic spins at nanoparticles surfaces, which intrinsically express reduced M_s at higher magnetic field strengths (Boyer, Whittaker, Bulmus, Liu, & Davis, 2010; L. Liu, He, Zhao, Sun, & Tong, 2018).

The comparative investigations on the magnetic characteristics of the IONPs synthesized in varied experimental conditions indicated that the IO_4 sample could offer the highest M_s ($59.62 \pm 4.2 \text{ emu.g}^{-1}$) as well as lowest H_c ($4.99 \pm 0.8 \text{ G}$) and M_r ($0.46 \pm 0.1 \text{ emu.g}^{-1}$) values followed by IO_3 ($M_s = 54.79 \pm 3.5 \text{ emu.g}^{-1}$, $H_c = 6.07 \pm 0.9 \text{ G}$, $M_r = 0.64 \pm 0.2 \text{ emu.g}^{-1}$), IO_2 ($M_s = 45.05 \pm 4.8 \text{ emu.g}^{-1}$, $H_c = 7.70 \pm 1.2 \text{ G}$, $M_r = 0.48 \pm 0.3 \text{ emu.g}^{-1}$), and IO_4 ($M_s = 43.42 \pm 2.8 \text{ emu.g}^{-1}$, $H_c = 8.80 \pm 1.5 \text{ G}$, $M_r = 0.48 \pm 0.2 \text{ emu.g}^{-1}$). Moreover, a higher crystallinity of IO_4 sample implied facile alignment of the magnetic moments in the magnetic field direction. In addition, a single-domain nature endowed by small particle size (<20-30 nm) as well as the presence of noncollinear surface spins could result in improved magnetic characteristics in the IO_4 (Deraz, 2010; Guo, Chen, He, & Deng, 2018; Wenger et al., 2008). These obtained results concluded that the provision of an anaerobic environment with the use of NH_4OH as a precipitating agent brought the optimal synthesis condition to produce nanoparticles with maximum crystallinity and SPM behaviour as well as sufficient dispersibility.

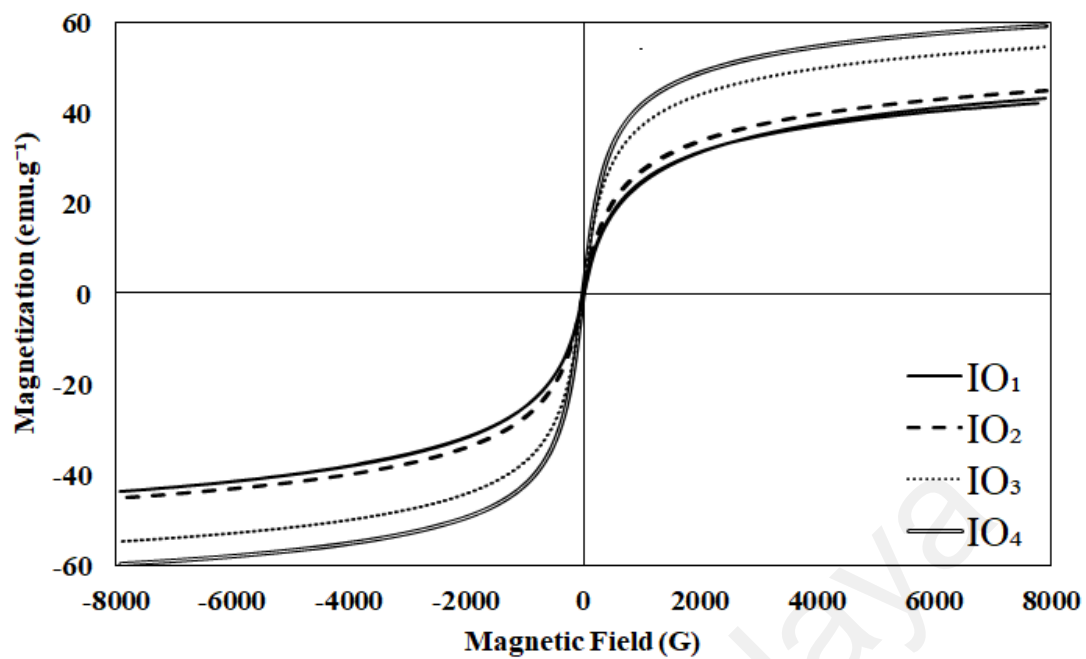


Figure 4.4: The magnetization graph of IO₁, IO₂, IO₃, and IO₄

University of Malaysia

4.3 Synthesis and In-Vitro Characterization of Superparamagnetic Iron Oxide Nanoparticles Using a Sole Precursor for Hyperthermia Therapy

4.3.1 Physicochemical Characterization

The rates of pH rise during dropwise addition of the alkaline reagent into the glass cylinder reactor are illustrated in Figure 4.5 for S₃, S₄, S₅ and S₆. The addition of iron precursor to the aqueous medium led to an abrupt pH reduction from around 7 to a range of 2-3, due to the strong acidic nature of iron salt, implying a great H⁺ donor with high acidic capability which situated on the central ions (Yin et al., 2017). Thereafter, the dropwise addition of the alkaline solution to the reactors brought about a gradual rise in the pH of iron mixtures, whilst further addition of 5 ml made a prompt pH rise to around 10 and then no remarkable pH changes were beheld with further increase of the alkaline reagent. However, persistent addition of alkaline reagent until 50 mL was crucial to retain adequate OH⁻ ions and pH rate above 9. to completely precipitate the Fe²⁺ and Fe³⁺ ions.

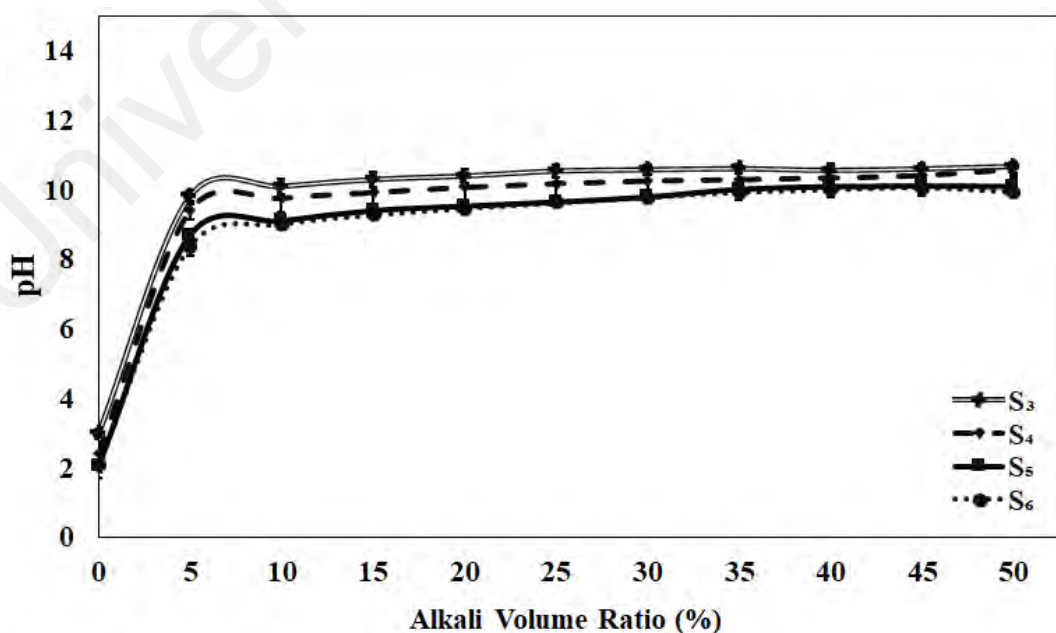


Figure 4.5: The rates of pH rise during dropwise addition of alkaline reagent under four varied oxidative conditions

Table 4.2 presents the initial and final pH values in varied oxidative environments as well as the ζ values of the obtained products. In overall, the higher oxidative environments led to lower initial and final pH values due to production of higher OH^- ions via more intensified oxidation of ferrous ions according to the following reaction:



The increased oxidative potency of the synthesis environment also resulted in higher ζ values through giving rise to the OH^- concentration and thus the particles negative surface charge (Hedayatnasab et al., 2020b; C. Lu, Chiu, & Liu, 2006). Consequently, the S₆ sample presented the highest ζ value (-31.94 ± 2.8 mV), although this value was not significantly higher than that of S₅ (-30.62 ± 2.3 mV). The increased ζ values in S₅ and S₆ could possibly render higher colloidal stabilities and lower agglomeration tendencies compared to the other two counterparts.

Table 4.2: The initial and final pH values of the synthesis solutions as well as the ζ values of the particles produced in synthesis environments with varied oxidative potencies

Sample	Initial pH	Final pH	ζ (mV)
S ₃	3.05 ± 0.07	10.81 ± 0.16	-27.31 ± 2.2
S ₄	2.66 ± 0.03	10.74 ± 0.18	-28.68 ± 2.7
S ₅	2.35 ± 0.15	9.97 ± 0.19	-30.62 ± 2.3
S ₆	2.15 ± 0.14	9.85 ± 0.16	-31.94 ± 2.8

4.3.2 Structural and Phase Analysis

The XRD spectra of all samples synthesized under varied oxidative conditions are illustrated in Figure 4.6. The obtained patterns showed an agreement with magnetite phase with inverse cubic spinel structure containing the space group of $\text{Fd}\bar{3}m$ (JCPDS

00-001-1111), where the peaks observed at 2θ values of 18° , 30° , 35° , 43° , 54° , 57° , 63° , and 74° respectively corresponded to (111), (220), (311), (400), (422), (511), (440), and 533) family planes (PDF 89–4319) (Unterweger et al., 2018).

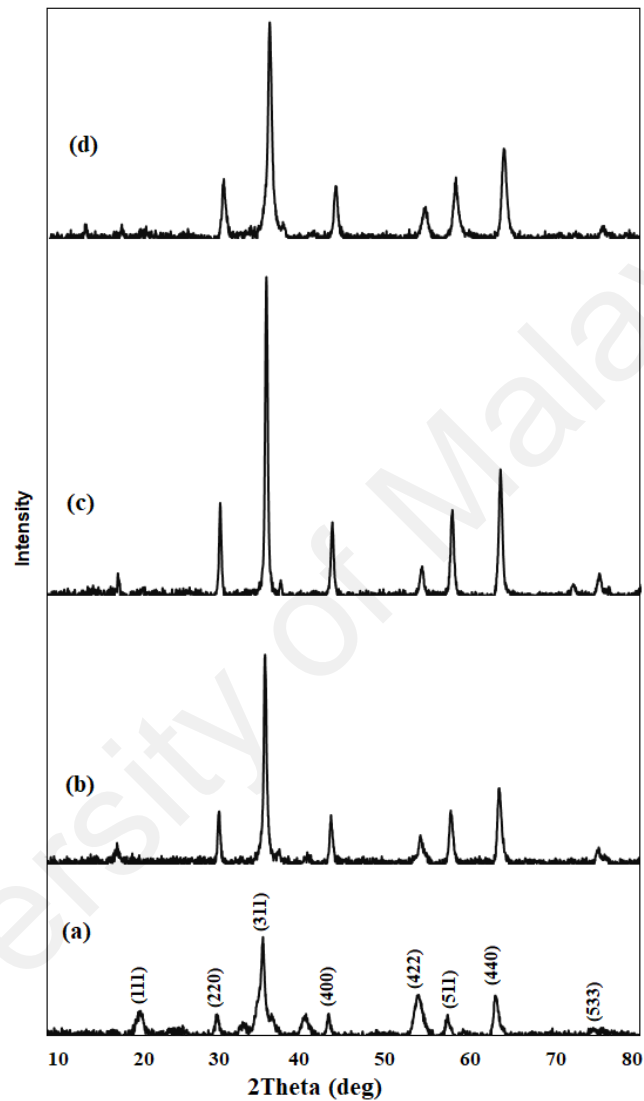


Figure 4.6: The XRD spectra of a) S₃, b) S₄, c) S₅, and d) S₆

The B and D values of the corresponding highest peak at 35° as the representative plane (311) of magnetite phase for the all samples are given in Table 4.3. Insignificant alterations were observed in 2θ positions of the representative peak in all the samples. Moreover, the interplanar spacings ' d_{hkl} ' were almost unaffected and consonant with reference value of 2.53 (Unterweger et al., 2018). However, the peak intensity, as well as

the B and D values as indicators of the particles crystallinity were significantly influenced by the oxidative potency of the synthesis environment. A significant enhancement in particles crystallinity was observed with increase of the O₂:N₂ ratio up to 5:5, probably due to reaching a stoichiometric balance Fe²⁺ and Fe³⁺ ions. However unexpectedly, a further increment of O₂:N₂ ratio to 6:4 led to the imbalanced ionic stoichiometry and thus reduced crystallinity. This could be probably due to a partial oxidation of ferrous ions by the water molecules and dissolved O₂, which may contribute to reaching the maximum crystallinity in an environment with lower oxidative potency than the expected value (S. Wu et al., 2011). In fact, the Fe²⁺ ions are intrinsically oxidised to Fe³⁺ ions through taking up the dissolved O₂ in water. In addition, vigorous stirring of the solution gives rise to the Fe²⁺ oxidation due to the dissolution of O₂ in the aqueous medium and the exposure of Fe²⁺ ions to the O₂ in air. Besides, water molecules have adequate potential to oxidize the Fe²⁺ ions to the Fe³⁺ ions even though the medium properly deoxygenated. The slow dropwise addition of alkaline reagent in the solution with the excess of the Fe²⁺ ions leads to the Fe³⁺ ions formation as well. Furthermore, when the particle size is in the nanoscale dimension, the Fe²⁺ ions may readily be oxidized in the solution with pH above 3 under the atmospheric condition as following the oxidation reaction (Gotić, Jurkin, & Musić, 2009; Hedayatnasab et al., 2020b):



Thereby, S₅ sample possessed the highest crystallinity with the narrowest peaks, followed by S₆, S₄, and S₃ as listed in Table 4.3. Such oxidation rate in S₅ possibly rendered particles with enhanced stability and highly ordered arrangements.

Table 4.3: The phase structural characteristics of the iron oxide particles synthesized in varied oxidative environment

Characteristics	S ₃	S ₄	S ₅	S ₆
2θ (°)	35.69	35.73	35.74	35.69
B (°)	0.91	0.62	0.45	0.56
Intensity (cts)	3088.22	5597.92	9197.18	6153.96
D (nm)	12.56	13.92	17.22	15.68
d(311) (Å)	2.51	2.51	2.51	2.51

4.3.3 Morphological Analysis

The TEM observations of the particles produced in varied oxidative environments (Figure 4.7) revealed formation of particles with mean diameters below 20-30 nm. This range of particle size was comparable to the crystallite size values obtained in XRD analyses, depicting formation of single-domain iron oxides.

However despite the presence of spherical morphology in all the samples, considerable differences were observed between varied samples in terms of particles agglomeration and particle size distribution. The bare IONPs often show a great tendency to agglomerate and clump together through the interparticle van der Waals forces due to their high surface energy (T. K. Nguyen et al., 2015). Beside this intrinsic feature, the low oxidation rates during the synthesis procedure result in nanoparticles with bigger particle sizes and higher agglomeration vulnerability. However, the increased oxidative potential of the synthesis environment, not only result in faster nucleation of the nanoparticles, but also enhance the repulsive interparticle forces due to increment of the ζ values, resulting in higher particle dispersity. Accordingly, with increase of the O₂:N₂ flow ratio from 3:7 to 5:5, nanoparticles with narrower particle sizes and higher dispersity were formed. As shown in Figure 4.7 c, S₅ comprised of uniformly dispersed particles with the mean diameter of 18 nm, smooth distribution, and negligible agglomeration. Whereas, dense clumps of

IONPs were observed in both S₃ and S₄ samples, probably due to their relatively lower ζ values. However with further increase of the O₂:N₂ ratio from 5:5 to 6:4, the particle size distribution became significantly broader again, possibly due to the excessively rapid nucleation of the nanoparticles and decreased controllability over the synthesis process.

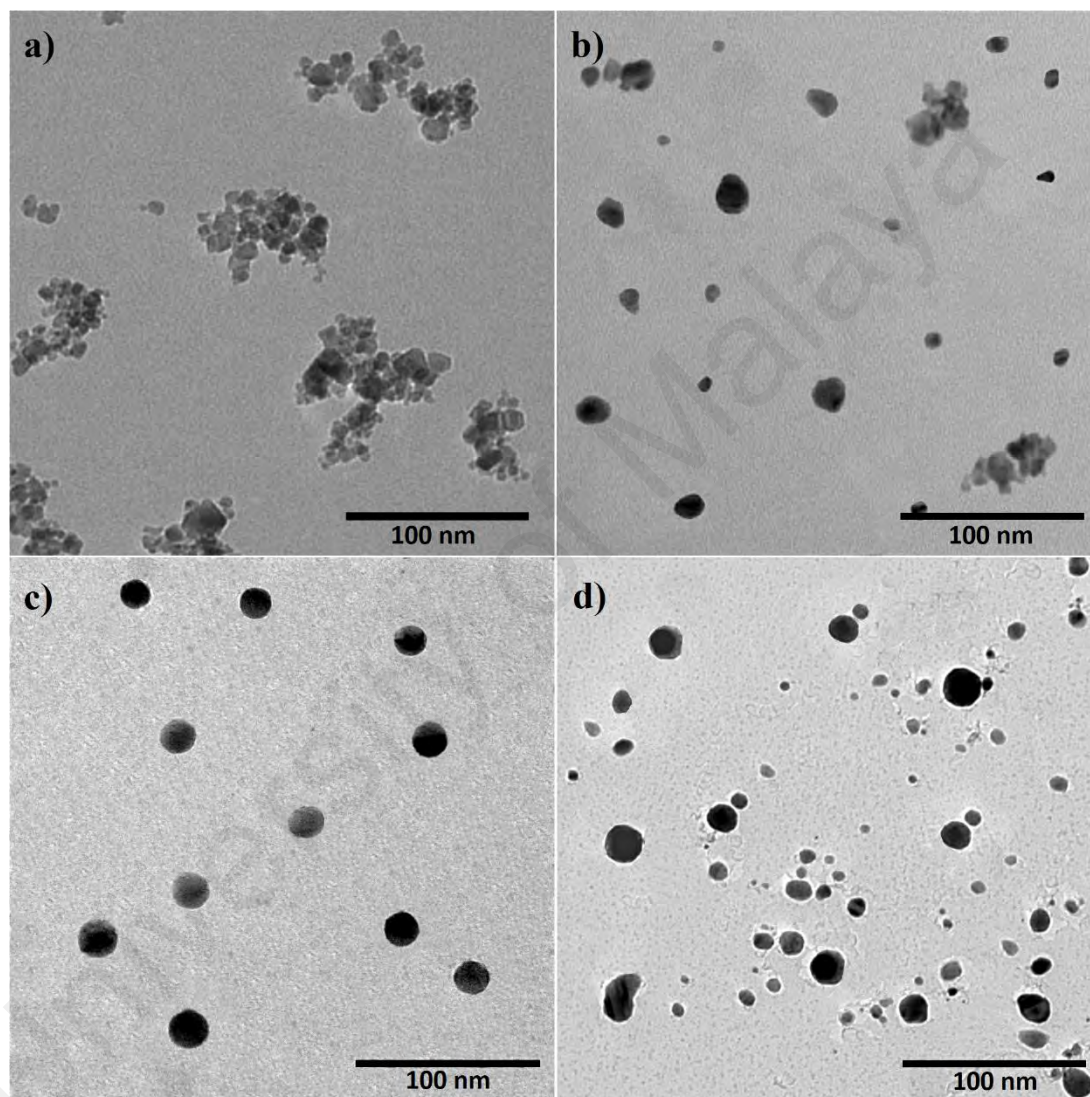


Figure 4.7: The TEM images of a) S₃, b) S₄, c) S₅, and d) S₆. The narrowest particle size distribution with minimal agglomeration tendency is observed in S₅ possibly due to the optimal oxidative potency of synthesis environment with O₂:N₂ flow ratio of 5:5

4.3.4 Magnetic Analysis

The room-temperature magnetic behaviour of all four samples were characterized through VSM measurement. Figure 4.8 illustrates the symmetry as well as reversibility of four magnetization curves in the form of sigmoidal shape, which are indicative of the SPM behaviour of all samples with nearly zero M_r and relative remanence (M_r/M_s) (Schweiger et al., 2012), which are in line with the single-domain particles observed in TEM analyses. The comparative investigation on obtained magnetic properties from all SPIONs samples tabulated in Table 4.4, demonstrated that S_5 could offer the highest M_s of $72 \pm 3 \text{ emu.g}^{-1}$ which was significantly higher compared to the counterparts probably attributed to its more uniform single-domain morphology and higher crystallinity, followed by S_6 ($66 \pm 2 \text{ emu.g}^{-1}$), S_4 ($64 \pm 2 \text{ emu.g}^{-1}$), and S_3 ($60 \pm 3 \text{ emu.g}^{-1}$). It is noteworthy that the M_s values above 50 emu.g^{-1} are considered as a pivotal characteristic of nanoheating agents for provision of sufficient induction heating power in MHT application to kill cancer cells (Kandasamy, Sudame, Luthra, Saini, & Maity, 2018). However, the lower M_s value of SPIONs as compared to the corresponding bulk phase resulted in nanoparticles incapability to overcome the anisotropy energy barrier, leading subsequently to reduced susceptibility towards magnetic field strength (Iida, Takayanagi, Nakanishi, & Osaka, 2007; Jiang et al., 2011).

Table 4.4: The magnetic properties of SPIONs synthesized in four varied oxidative environments

Samples	M_s (emu.g^{-1})	M_r (emu.g^{-1})	H_c (G)	M_r/M_s
S_3	60 ± 4	0.8 ± 0.1	2 ± 0.2	0.013
S_4	64 ± 2	0.9 ± 0.3	3 ± 0.3	0.014
S_5	72 ± 3	1.8 ± 0.3	10 ± 0.6	0.013
S_6	66 ± 2	1.7 ± 0.2	9 ± 0.5	0.026

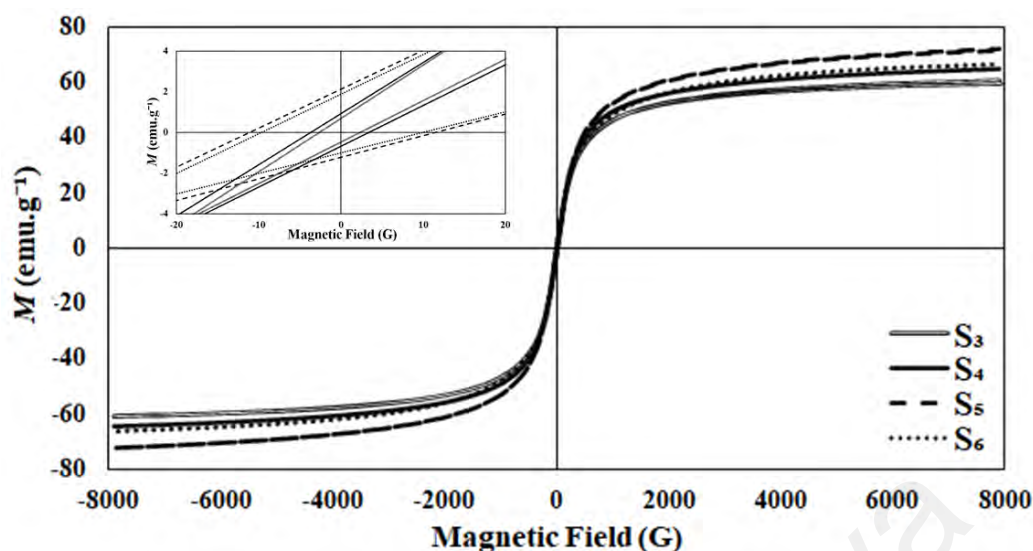


Figure 4.8: The magnetization graph of S₃, S₄, S₅, and S₆. The inset indicates the magnified view of the graph

4.3.5 Cytotoxicity Assay

In-vitro cytotoxicity assays are necessitated to ascertain the safety of magnetic nanoheating agents for in-vivo purposes. The cytotoxic activities of four varied SPIONs (inhibitors) were quantified on HepG2 carcinoma cells at a series of various concentrations from 1.5 to 100 $\mu\text{g}\cdot\text{ml}^{-1}$ using an MTT assay. The viability of HepG2 cells treated with four SPIONs samples are demonstrated in Figure 4.9, indicating the negligible cytotoxicity profiles of all samples on HepG2 cells as compared to the controls over the concentration range after 24 h incubation. These results offer that the SPIONs were cytocompatible on HepG2 cell line over the range of various concentrations, which was in line with previous reports on negligible cytotoxicity effect of Fe_3O_4 nanoparticles against various cancer cell lines (Kandasamy et al., 2019; X. Peng et al., 2019; Tudisco et al., 2018). In particular, S₅ expressed cell viabilities above $90.37\pm 3\%$ at its maximum concentration, which was significantly higher than the other counterparts. Noteworthy, owing to the great cytocompatibility of S₅ even in high concentrations, along with its paramount crystallinity, uniform morphology, and SPM properties, this sample was selected as the optimal nanoheating agent for further hyperthermia investigations.

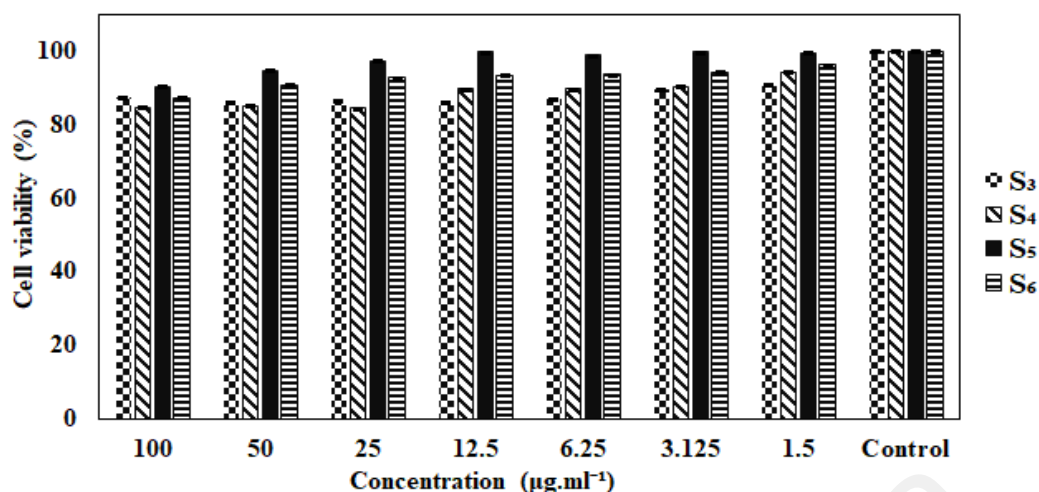


Figure 4.9: Cell viability profiles of HepG2 cells treated with different SPIONs for 24 h

4.3.6 Magnetic Hyperthermia Studies

To perform a successful MHT, a minimal dosage of magnetic nanoagents with remarkable heating power is desired; meanwhile, the AMF strength must be limited to a clinically safe range to prevent disorders in the human body (Hergt & Dutz, 2007). In addition, the hyperthermia treatments are recommended to be carried out in time intervals of below 900 s to minimize potential disorders on the human body. This is due to the inner temperature of SPIONs is approximately twice that of the aqueous medium, hence longer residence of stealth SPIONs may enhance protein absorption on the SPIONs surfaces, leading to higher agglomeration and reduced colloidal stability. Moreover, longer time exposure to AMF may incur irreversible damage to the surrounding tissues (Dutz & Hergt, 2013). Therefore, treatment repetition in shorter time intervals is not only avoid the side effects but even boost the hyperthermia efficiency by completing tumour regression (Hedayatnasab et al., 2020b; Laurent et al., 2011).

In this research, the hyperthermia efficiency of ferrofluids was assessed using five S₅ concentrations from 1 to 5 mg.ml⁻¹, as well as the AMF strengths of 15.74, 31.49, 47.24, 62.99, and 78.74 kA.m⁻¹ over exposure interval of 5400 s to understand the minimal particle concentration and AMF strength that generate sufficient thermal energy in the

recommended interval of 900 s for raising the medium temperature into the hyperthermia range, while preserving the maximum temperature in the secure T_H range. The temperature-time profiles of ferrofluids containing 1 to 5 $\text{mg}\cdot\text{ml}^{-1}$ of S_5 at varied AMF strengths are illustrated in Figure 4.10. As expected, a faster temperature rise could be obtained with increase of the particles concentrations. In all the graphs, a considerable temperature rise was observed in the initial 120 s, followed by a moderate increase till around 900 s. The medium temperature continued to raise until reaching a steady state at approximately 1500 s and then, no statistically significant temperature rise was perceived over time in all applied AMF strengths.

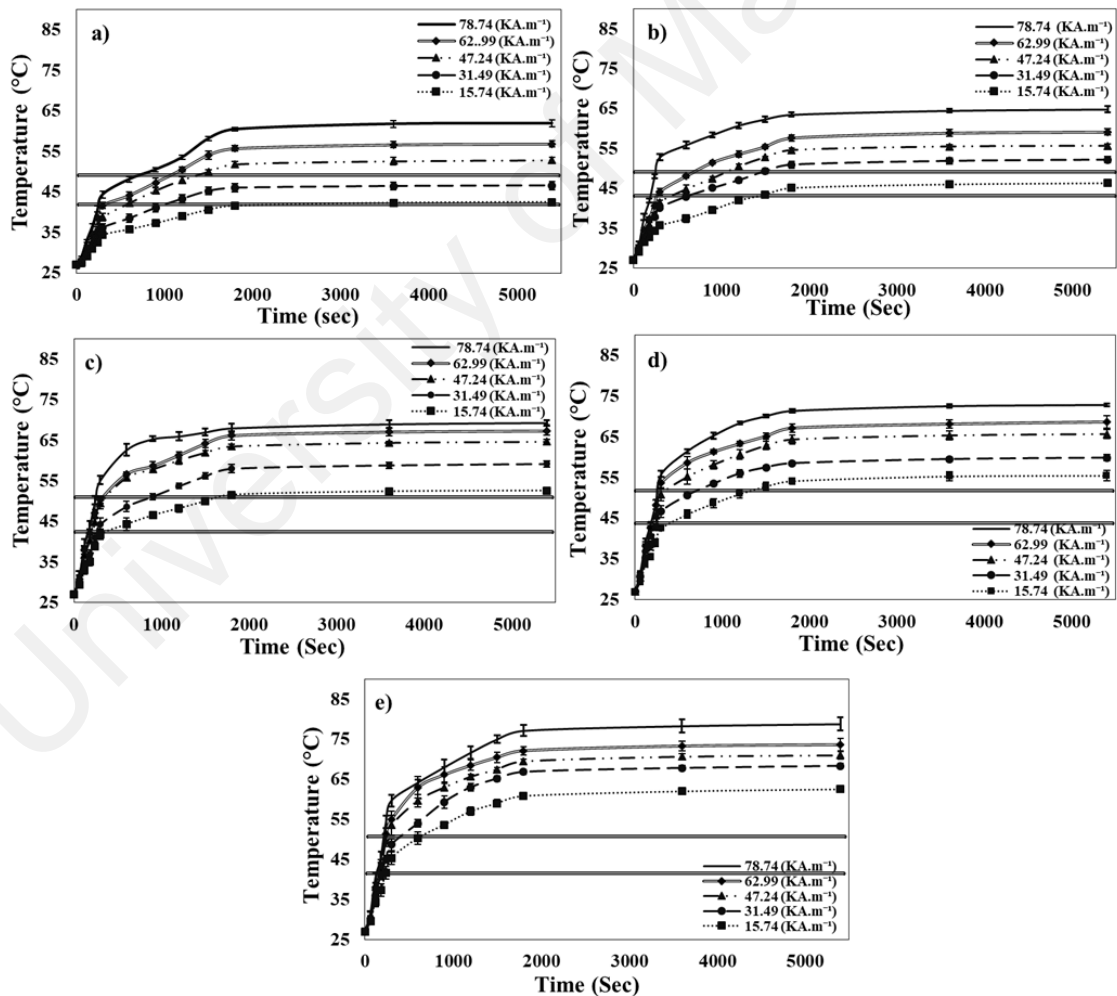


Figure 4.10: The thermal profiles of S_5 with various concentrations a) 1 $\text{mg}\cdot\text{ml}^{-1}$, b) 2 $\text{mg}\cdot\text{ml}^{-1}$, c) 3 $\text{mg}\cdot\text{ml}^{-1}$, d) 4 $\text{mg}\cdot\text{ml}^{-1}$, and e) 5 $\text{mg}\cdot\text{ml}^{-1}$ exposed to five varied AMF strengths. The band illustrates the hyperthermia range

Table 4.5 presents the achieved temperatures after 900 and 5400 s using varied concentrations and AMF strengths. The data presented in this table can clearly highlight that the SPION concentration of 1 mg.ml^{-1} and AMF strength of 31.49 kA.m^{-1} are the only hyperthermia parameters that not only provide a temperature rise in the T_H range within 900 s, but also maintain the maximum temperature of the fluid within the safe range after exposure for 5400 s.

The SAR values of S_5 sample with five varied concentrations exposed to various magnetic strengths are demonstrated in Figure 4.11. The SAR values increased with increment of the AMF strength from 15.74 to 78.74 kA.m^{-1} due to the heating loss mechanisms; while the SAR values reduced with increasing the concentrations, probably due to the dipole-dipole interactions among nanoparticles (Dabbagh et al., 2019), which led to faster relaxation of SPIONs and diminished heating power (Iqbal et al., 2016b). Hence, the lowest and highest SAR values for 1 mg.ml^{-1} were $92.89 \pm 2 \text{ W.g}^{-1}$ and $301.22 \pm 3 \text{ W.g}^{-1}$ and for 5 mg.ml^{-1} were $38.33 \pm 3 \text{ W.g}^{-1}$ and $116.17 \pm 4 \text{ W.g}^{-1}$ at 15.47 kA.m^{-1} and 78.74 kA.m^{-1} , respectively. However, the minimal concentration that S_5 could produce the remarkable heating value of 145.15 ± 4 under hyperthermia condition was 1 mg.ml^{-1} at 31.49 kA.m^{-1} . In fact, the heating efficiency of SPIONs is mainly governed through Néel and Brownian heating loss mechanisms. The former is favored for particles that are smaller than 20-30 nm, while the latter is prevalent in larger nanoparticles. Therefore according to the mean particle size of 18 nm observed in TEM studies, the Néel relaxation is probably the dominant heating mechanism of the single-domain spherical S_5 particles developed in this study.

Table 4.5: The achieved temperatures (°C) in the nanofluids containing varied SPIONs concentrations exposed to different AMF strengths for 900 and 5400 s

Concentration (mg.ml ⁻¹)	Time (s)	AMF strength (kA.m ⁻¹)				
		15.74	31.49	47.24	62.99	78.74
1	900	37.2±0.7	43.1±0.6*	46.5±0.8	48.5±0.7	50.5±0.5
	5400	42.3±0.5	45.7±0.4*	50.4±0.8	57.5±0.8	62.4±0.9
2	900	39.5±0.4	44.8±0.4	47.5±0.5	52.5±0.5	57.8±0.6
	5400	45.6±0.5	52.4±0.8	56.6±0.6	60.3±0.8	64.5±0.8
3	900	40.5±0.5	47.5±0.9	51.4±0.8	58.3±0.7	59.5±0.9
	5400	48.6±0.5	55.5±0.5	59.7±0.8	65.6±0.6	68.8±1.2
4	900	41.5±0.4	50.5±1	55±0.5	62±0.6	66±1.6
	5400	50.1±0.3	57.5±1.3	65.4±0.8	69.1±1.2	72.3±1.1
5	900	43.2±0.8	54.3±0.6	61.5±1.4	64.4±1.2	68.2±1.1
	5400	52.2±0.5	63.1±0.5	69.4±0.6	71.5±0.9	75.3±1.3

*The hyperthermia parameters, which led to a temperature profile within the secure T_H range over the treatment time of 900-5400s.

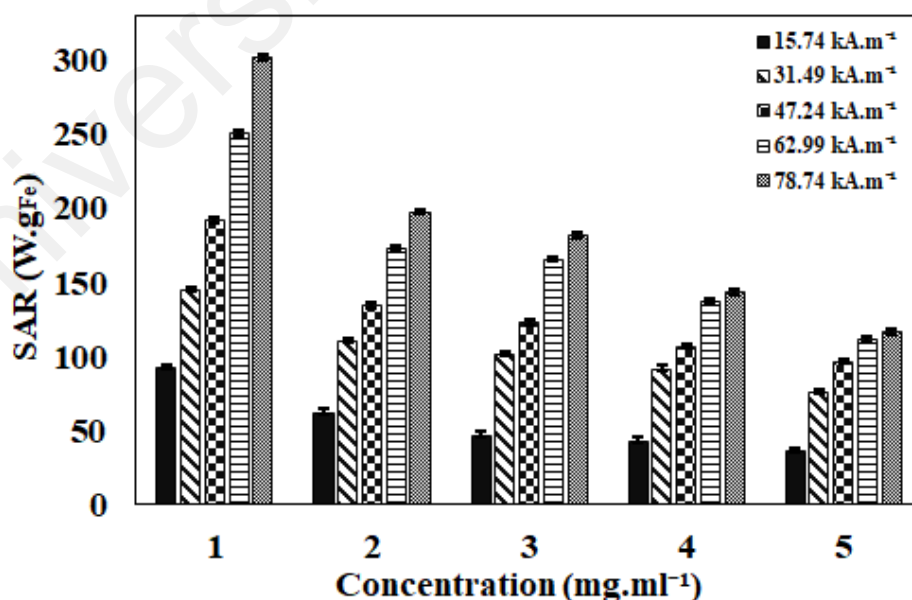


Figure 4.11: The SAR comparison of different S₅ concentrations under exposure to five varied AMF strengths. The stronger AMF strengths and lower particles concentrations result in higher SAR values

4.3.7 In-Vitro Hyperthermia Test on HepG2 Cells

The temperature profiles of the cell media containing $100 \mu\text{g}\cdot\text{ml}^{-1}$ S_5 and the control groups under the exposure of different AMF strengths are illustrated in Figure 4.12. The initial temperatures were set at $36\pm 1^\circ\text{C}$ corresponded to the physiological temperature. The medium temperature raised to $42.1\pm 0.3^\circ\text{C}$ and $44.5\pm 0.5^\circ\text{C}$ within the T_H range during the AMF exposure of 31.49 and $47.24 \text{ kA}\cdot\text{m}^{-1}$ over 900 s. However, the minimal magnetic strength that could not only reach to T_H range but also retain the temperature in the T_H range over 5400 s was $31.49 \text{ kA}\cdot\text{m}^{-1}$.

The inhibitory effect of S_5 against HepG2 cell lines was investigated through MTT assay under hyperthermia condition. As hyperthermia tests were run, the MTT assay was instantaneously performed on the control groups and S_5 samples in order to avoid the external factors effects. The viability HepG2 cells 24 h after treatment with S_5 are compared with the control groups in Figure 4.13. Despite the magnetic strength variation, the control group exposed to AMF presented cell viabilities similar to the untreated control group, implying the safety of the AMF strengths applied in this study. Thereby, the cell viability of HepG2 was unaffected by S_5 alone and/or AMF exposure alone, which was in line with previous reports (W. Li, Liu, Qian, & Yang, 2017). However, the cell viability of HepG2 cells treated by S_5 was reduced significantly to $67\pm 0.5\%$ and then $49\pm 0.3\%$ under the AMF exposure with strengths of 31.49 and $47.24 \text{ kA}\cdot\text{m}^{-1}$ respectively, after the incubation interval of 24 h. Hence, the cytotoxic effect exerted by the heating effect of SPIONs under hyperthermia condition was considered as the principal mechanism for the cell growth inhibition. Therefore, the S_5 samples comprised of SPIONs with particle sizes of below 20 nm could endow sufficient cytotoxic effect for hyperthermia treatment of cancer when the particles concentration and field strength are adjusted to $100 \mu\text{g}\cdot\text{ml}^{-1}$ and $47.24 \text{ kA}\cdot\text{m}^{-1}$, respectively.

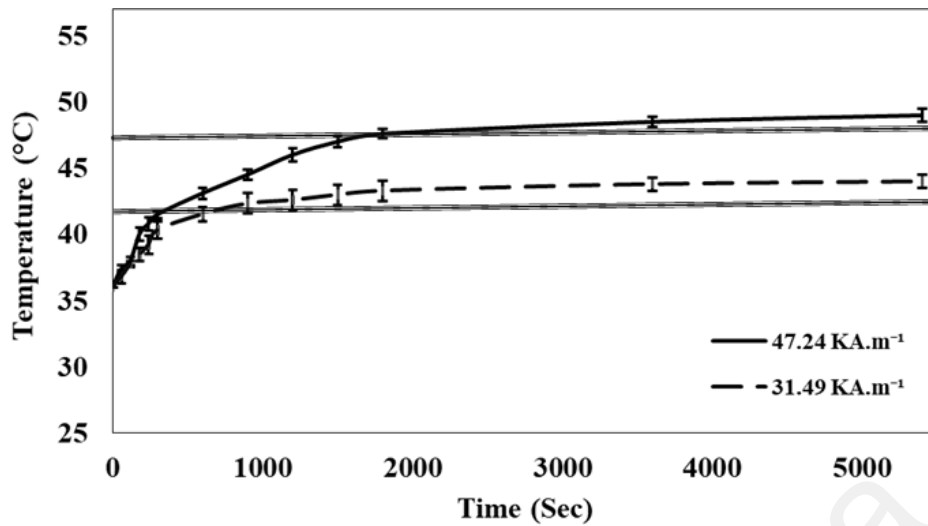


Figure 4.12: The temperature profile of the HepG2 medium with S₅ during exposure to varied AMF strengths. The minimal magnetic field of 31.47 kA.m⁻¹ could only render S₅ with adequate heating capability to retain the desirable T_H (the band area)

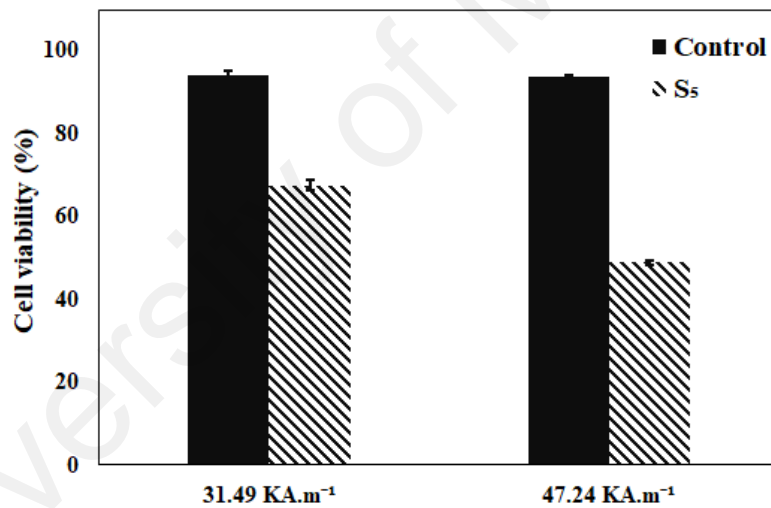


Figure 4.13: Cytotoxicity profiles of HepG2 cells treated with S₅ exposed to varied AMF strengths, as quantified by MTT assay

4.4 Polycaprolactone-Coated Superparamagnetic Iron Oxide Nanoparticles Micelles for In-Vitro Magnetic Hyperthermia Therapy of Cancer

4.4.1 Conformational Characteristics and Micellar Solution Properties

Based on the concentrations, surfactant molecules often arrange in three main micellar configurations on the nanoparticles surface including hemi, ad, and mixed hemi-ad micelles (Figure 4.14). In the hemi micellar arrangement, a surfactant monolayer is formed on the nanoparticles surface via columbic attraction. With increase of the absorbed surfactant, the hydrophobic interactions between the hydrocarbon chains of the surfactant molecules lead to their bilayer arrangement on the nanoparticles surface and formation of the ad-micellar configuration. A mixed hemi-ad micelle array is also formed at intermediate surfactant concentrations, with both columbic and hydrophobic interactions (Amiri-Aref et al., 2015; Ranjbari et al., 2015). The formation of each configuration could be determined via ζ measurements, where the low and high ζ values indicate the presence of hemi and ad micelles, respectively.

Figure 4.14 illustrates the ζ changes of iron oxide samples with addition of varied surfactant quantities. When CTAB was added into the synthesis solution, the positively-charged hydrophilic heads electrostatically bonded to the hydroxyl groups of iron oxide, resulting in neutral charges. Therefore, the ζ value progressively raised from -30.62 ± 2.3 mV (for bare iron oxide at pH ~ 9 , Table 4.2) to zero at CTAB quantity of 5 ml, confirming formation of hemi micelles around particles through electrostatic interaction. Notably, the hydrophobic interactions among the tail groups of the surfactant molecules is the primary driving force for their ad-micellar configuration in the aqueous medium. Therefore with increase of the CTAB quantity, free hydrophobic polar tails assemble together via chain-to-chain reactions and the polar heads become exposed, leading to

positive ζ values (Amiri-Aref et al., 2015; Ranjbari et al., 2015). This trend continued to reach the maximum ζ value of $+16\pm 2$ mV in CTAB concentration of 15 mg, indicating formation of ad-micellar configuration of the CTAB molecules on the particles surface. Thereby, this surfactant quantity (SPC_{15}) was considered as the critical concentration for ad-micellar configuration (CaMC) and the optimal amount for surface modification of iron oxides for further attachment of the PCL-d chains (Hedayatnasab et al., 2020a).

When PCL-d was added into the solution, the ζ value significantly reduced to around -8 ± 2 mV, implying PCL-d coating layer was formed around particles surface through electrostatic interactions. The presence of unreacted diol groups on the polymer changes probably contributed in generation of negative charges on the coated iron oxide particles.

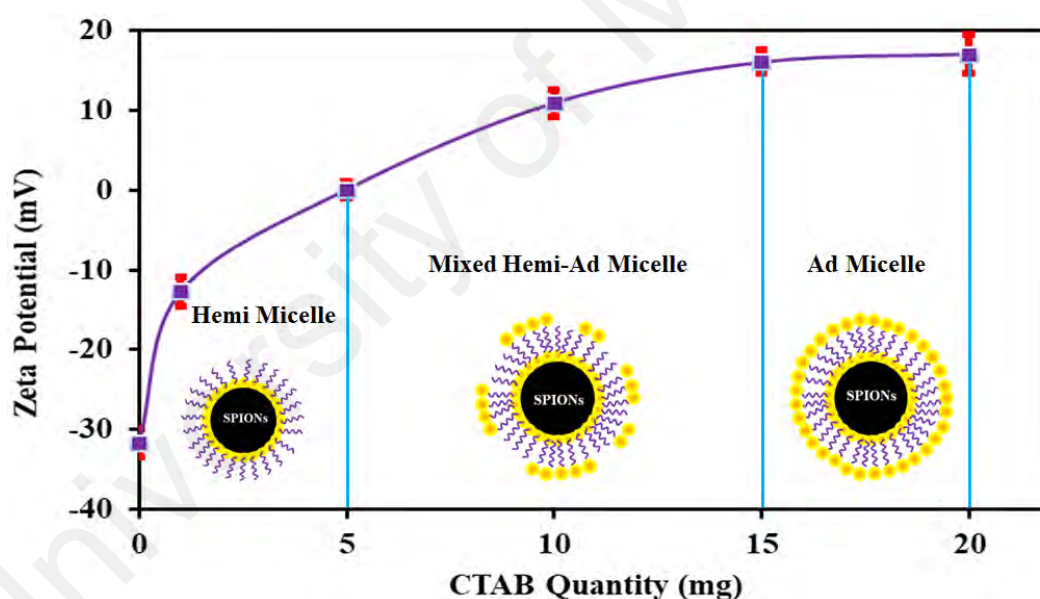


Figure 4.14: Different configurations of surfactant molecules around the iron oxide particles at varied CTAB quantities. Three main micellar structures are determined based on alteration of the ζ values of samples

4.4.2 Morphological Analysis

The morphological characteristics of bare iron oxides, SPC_{15} , and $PCL-SPC_{15}$ are illustrated in Figure 4.15 a-d. The TEM micrographs clearly showed uniform particle size distributions with remarkable dispersibility in all the synthesized nanoparticles. However,

surface modification by the cationic surfactant could slightly improve the particle dispersity in the aqueous medium, probably due to particle–particle interactions (Elfeky et al., 2017). According to Figure 4.15 c, no significant alteration in nanoparticles dispersity and agglomeration was observed by further coating of the SPC₁₅ particles with PCL biopolymer. A typical TEM image from an individual nanoparticle with higher magnification is also illustrated in Figure 4.15 d, which obviously confirms formation of a core–shell structure comprised of iron oxide core and PCL shell. As a result of polymer coating, the mean diameter of nanoparticles was increased from 18 ± 2 to 21 ± 3 nm, indicating formation of a 3 nm polymer coating on the bare IONPs.

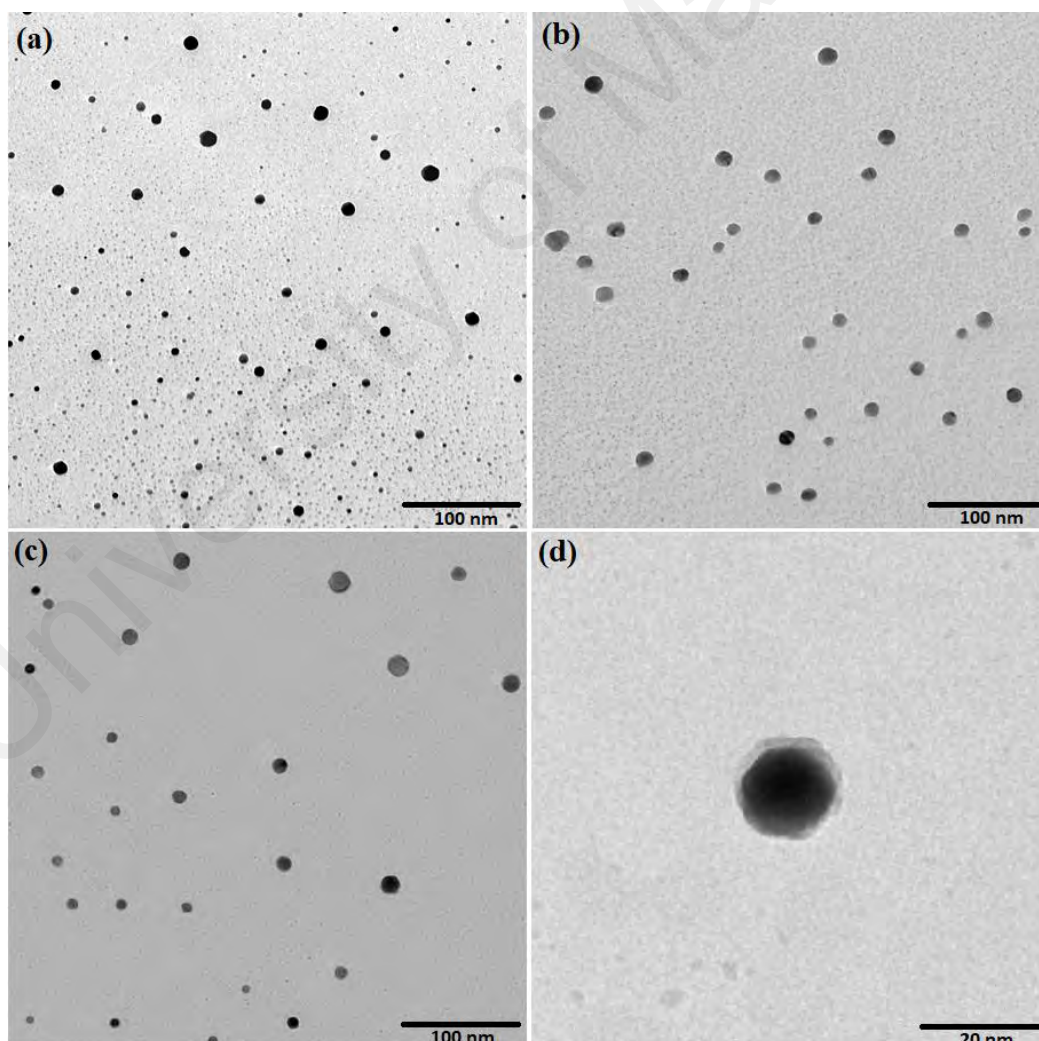


Figure 4.15: The TEM images of a) bare iron oxide, b) SPC₁₅, and c, d) PCL-SPC₁₅ with different magnifications. The core-shell structure of PCL-SPC₁₅ is obviously observed

4.4.3 Structural and Phase Analysis

The obtained XRD patterns on bare IONPs, SPC₁₅, and PCL-SPC₁₅ are illustrated in Figure 4.16 a-c. The XRD patterns confirmed formation of a single magnetite phase (JCPDS 00-001-1111) with cubic spinel and Fd3̄m space group in all samples, implying the negligible effects of CTAB and PCL on the crystalline phase of iron oxides. The XRD diffraction peaks of all samples observed at 2θ values of 18°, 30°, 35°, 43°, 54°, 57°, 63°, and 74° respectively corresponded to (111), (220), (311), (400), (422), (511), (440), and 533) family planes of magnetite (PDF 89–4319).

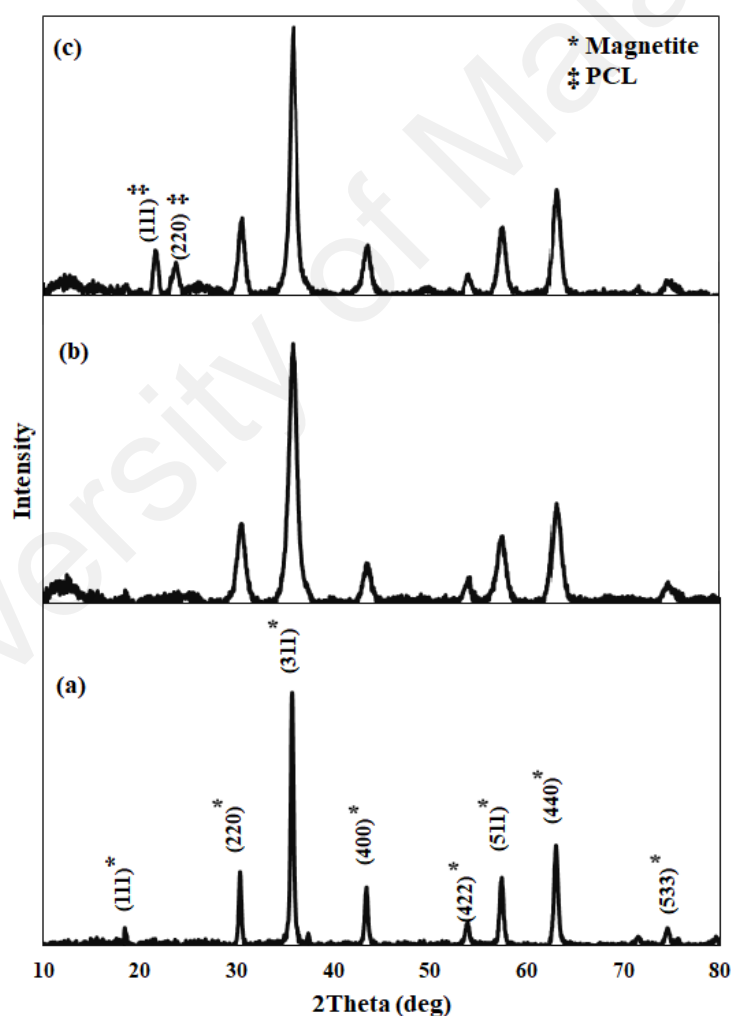


Figure 4.16: The XRD patterns of a) bare iron oxide, b) SPC₁₅, and c) PCL-SPC₁₅. The peaks at 21.4° and 23.7°, which represent the crystallographic planes of PCL, indicated the formation of biopolymer coating on the nanoparticles surface

The XRD Patterns of PCL-SPC₁₅ illustrates the presence of two crystalline polymeric and metallic phases. The added peaks at 2θ of 21.4 and 23.7 (Figure 4.16 c) are represented the crystallographic planes of (111) and (220), respectively (Ravi, Song, Wang, Nadimicherla, & Zhang, 2016).

The HRTEM image in Figure 4.17 also depicts an interlayer spacing of 0.254 nm for Fe₃O₄ cores in PCL-SPC₁₅, which is well-matched with the (311) planes of magnetite (PDF 89–4319) possessing an interlayer spacing of 0.251 nm.

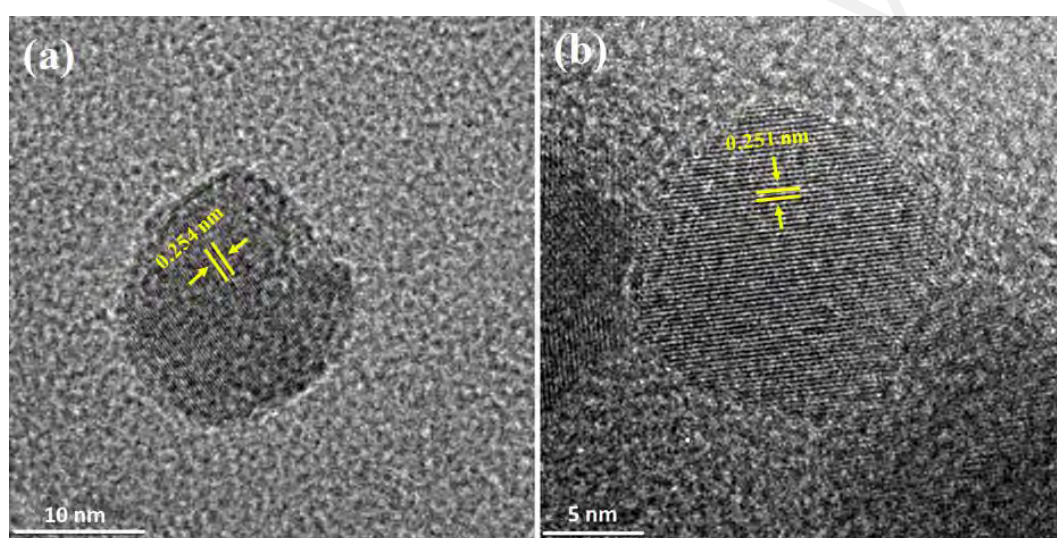


Figure 4.17: HRTEM images of a) bare iron oxide and b) PCL-SPC₁₅

4.4.4 Chemical Structure Analysis

The FTIR spectra of bare Fe₃O₄, SPC₁₅, pure CTAB, pure PCL biopolymer, and PCL-SPC₁₅ are shown in Figure 4.18 a-e. FT-IR spectra of bare Fe₃O₄ clearly displays absorption peaks of 3401.22 and 1627.56 cm⁻¹, which were respectively characteristics of stretching and bending vibrations of hydroxyl functional group (H-O-H), required for electrostatic assembly of CTAB molecules (Cai & Wan, 2007). The peaks in the low-frequency region from 500–800 cm⁻¹, particularly at 583.83 cm⁻¹ were attributed to Fe–O absorption bands which confirmed the presence of the magnetite. The presence of 3017.13 cm⁻¹ band could be attributed to the vibrations of the ammonium moiety in

CTAB. Additionally, the peaks at around 2848.39 and 2916.37 cm^{-1} were related to symmetric and antisymmetric C-H vibration bands of the $-\text{CH}_2$ group which derived from the long aliphatic tail of CTAB. The peaks at 1461.31 and 959.90 cm^{-1} were associated with asymmetric stretching vibration of N^+-CH_3 , besides the peak 718.36 cm^{-1} might be corresponded to Br^- (Elfeky et al., 2017).

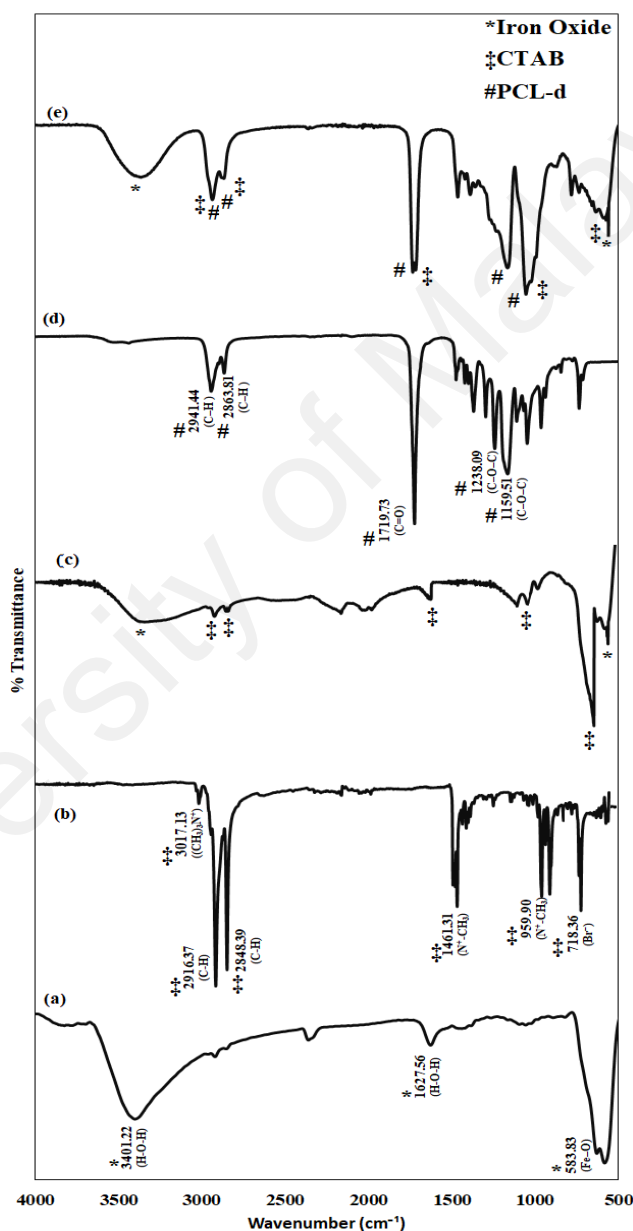


Figure 4.18: FTIR spectra of a) bare iron oxide, b) pure CTAB, c) SPC₁₅, d) PCL-d, and e) PCL-SPC₁₅. The *, ‡, and # symbols represent the specific bonds of iron oxide, CTAB, and PCL-d respectively, indicated the formation of their functional groups on the PCL-SPC₁₅ surface.

FTIR spectrum of PCL biopolymer possessed a strong band at 1719.73 cm^{-1} that could be assigned to carbonyl stretching (C=O groups). In addition, the bands at 2941.44 and 2863.81 cm^{-1} were related to asymmetric and symmetric stretching vibration of aliphatic C–H groups, while absorption bands at 1238.09 and 1159.51 cm^{-1} were belonged to asymmetric and symmetric stretching of C–O–C group in PCL, respectively (Khoee, Bagheri, & Hashemi, 2015). The recorded spectra for PCL-SPC₁₅ (Figure 4.18 e) was identical to that of pure PCL and exhibited the same characteristic vibration bands of Fe₃O₄ with slightly lower intensities owing to the presence of active components.

Figure 4.19 a depicts the low-resolution XPS survey spectra of PCL-SPC₁₅ while high-resolution C 1s, O 1s, and Fe 2p XPS spectra of the PCL-SPC₁₅ are shown in Figure 4.19 b-d. The Fe 2p spectrum (Figure 4.19 d) comprised the doublet Fe 2p_{1/2} and Fe 2p_{3/2} possessed the binding energy values of 723.72 eV and 710.44 eV , respectively which were considered as the common peaks for magnetite. The peaks from such spectra were probably deconvoluted into two components correlated with Fe³⁺ and Fe²⁺ ions. These results implied that the composition of the Fe₃O₄ core was unaffected by surfactant and polymer modifications. The O 1s spectrum (Figure 4.19 c) could be also deconvoluted into four peaks ascribed to the oxygen atoms from Fe-O, OH (Fe₂O₃), C-O/C=O, and COOH located at 529.82 , 530.29 , 531.46 and 532.38 eV , respectively (Wilson & Langell, 2014). The C 1s spectrum (Figure 4.19 b) included the contribution of four components peaks situated at 284.58 , 285.49 , 286.65 and 288.53 eV were respectively corresponded to carbon atoms of C-C, C-O, C=O and COOH from PCL which were well-matched to previous other report (Manakhov et al., 2019). Both XRD and XPS studies confirmed that PCL biopolymer was successfully coated on the surface of SPC₁₅.

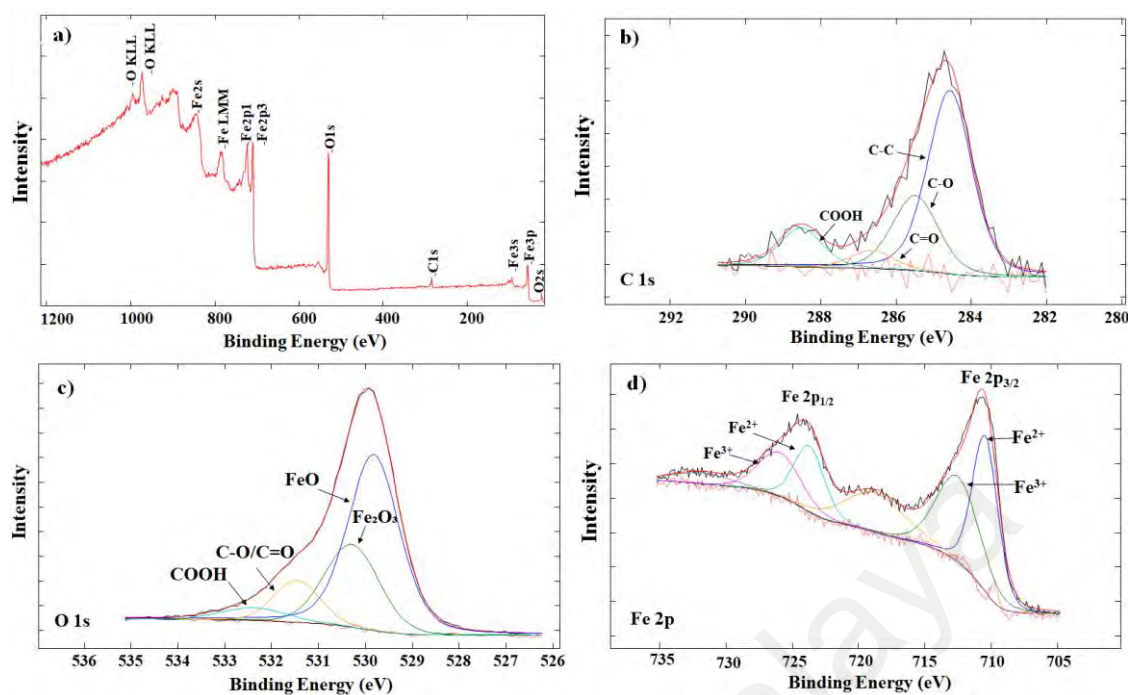


Figure 4.19: The XPS spectra of PCL-SPC₁₅. a) Low-resolution survey spectrum, b) High-resolution C 1s XPS spectrum c) High-resolution O 1s XPS spectrum, and d) High-resolution Fe 2p XPS spectrum

4.4.5 Thermal Analysis

DSC technique was performed to evaluate the phase transition behaviour of pure PCL and PCL-SPC₁₅ samples. As shown in Figure 4.20 a, the peak temperature of endothermic phase transition for pure PCL is observed at 52.1 ± 2 °C (Correlo et al., 2005). However, the onset temperature of this phase transition was initiated at 45.4 ± 2 °C, implying that the melting point of PCL biopolymer with molecular weight of 2000 Da was within the upper hyperthermia range (45 to 52 °C). The DSC thermograms of the PCL-SPC₁₅ is also elucidated insignificant alterations of the onset and peak temperatures of endothermic phase transition of PCL after coating on the metallic core. This range of phase transition temperature in the PCL-SPC₁₅ particles confirmed their appropriacy for cancer therapy under hyperthermia condition.

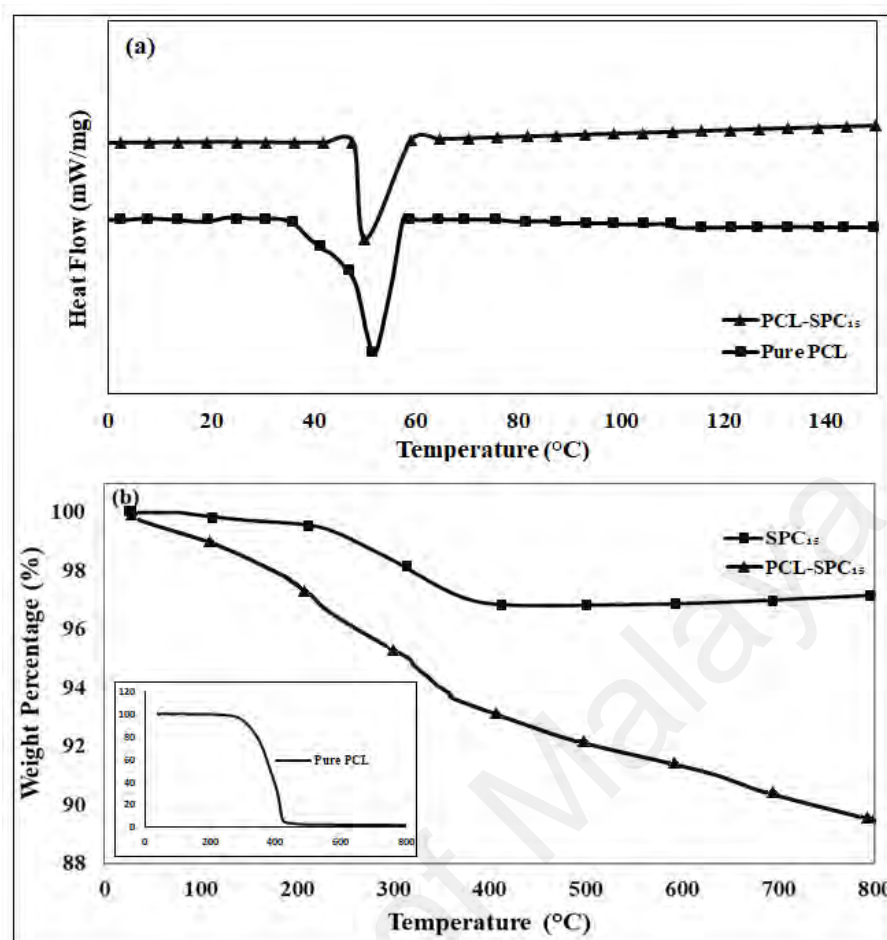


Figure 4.20: The thermal behaviour of (a) DSC thermograms of pure PCL and PCL-SPC15, and (b) TGA curves of pure PCL, SPC15 and PCL-SPC15

TGA analysis was also carried out to determine the quantities of CTAB and PCL in the core-shell nanostructure. As shown in Figure 4.20 b, the curve of SPC₁₅ depicts a small weight loss of around 3%, which could be attributed to the evaporation of CTAB. On the contrary, the TGA measurement of PCL-SPC₁₅ exhibited a mass loss of approximately 12% in two phases. The first phase of weight loss correlated with CTAB evaporation at temperatures below 300 °C, while an additional weight loss of approximately 9% at 300-400 °C in the second phase attributed to degradation of PCL to CO₂, CO, and H₂O (Zhong et al., 2015). The obtained PCL quantity was comparable with the value obtainable from the TEM images (9%), based on the theoretical densities of Fe₃O₄ and PCL.

4.4.6 Magnetic Analysis

The obtained magnetic properties of bare Fe₃O₄, SPC₁₅, and PCL-SPC₁₅ are tabulated in Table 4.6. The symmetry and reversibility of the hysteresis curves are depicted in Figure 4.21 which are indicative their SPM behaviour with extremely low H_c, nearly zero Mr, and Mr/Ms. These findings were consistent with the TEM results, which indicated the potential SPM behaviour of these particles due to their average particle sizes of below 20-30 nm and single-domain large magnetic moments (Weidner et al., 2015).

Table 4.6: The comparison of the magnetic properties among bare SPIONs, CTAB-stabilized SPIONs and PCL-SPC₁₅

Samples	Ms (emu.g ⁻¹)	Mr (emu.g ⁻¹)	Hc (G)	Mr/Ms
Bare SPIONs	72±3	2±0.2	10±0.3	0.0248
SPC ₁₅	69±5	1±0.1	5±0.2	0.0278
PCL-SPC ₁₅	64±4	1±0.2	5±0.2	0.0135

Further, two distinct features were perceived from the magnetic properties. Firstly, the Ms value descended after both stabilization and polymer coating, probably due to the nonmagnetic natures of both CTAB and PCL. Due to a low amount of surfactant, an insignificantly reduction in the Ms value from 72±3 emu.g⁻¹ to 69±5 emu.g⁻¹ was observed after surface modification of SPIONs. The Ms value was further decreased to 64±4 emu.g⁻¹ when PCL was coated on the SPC₁₅ cores. However, this alteration was also statistically negligible, possibly due to the semi-crystalline structure of PCL biopolymer which may lead to more oriented magnetic moments.

Secondly, the H_c of bare SPIONs was almost twice of SPC₁₅ and PCL-SPC₁₅ because of relatively higher particle agglomeration and friction relaxation loss. Besides, the interparticle interactions could also elucidate this effect through high surface-area-to-volume of bare SPIONs that increase the exchange interactions between individual particles and consequently enhanced surface energy, effective magnetic volume, and H_c

(Von der Lü e, Weidner, Dutz, & Schacher, 2017). Meanwhile, surface modification could weaken the interparticle interactions by increasing the distance among the individual particles, giving rise to the coercivity reduction.

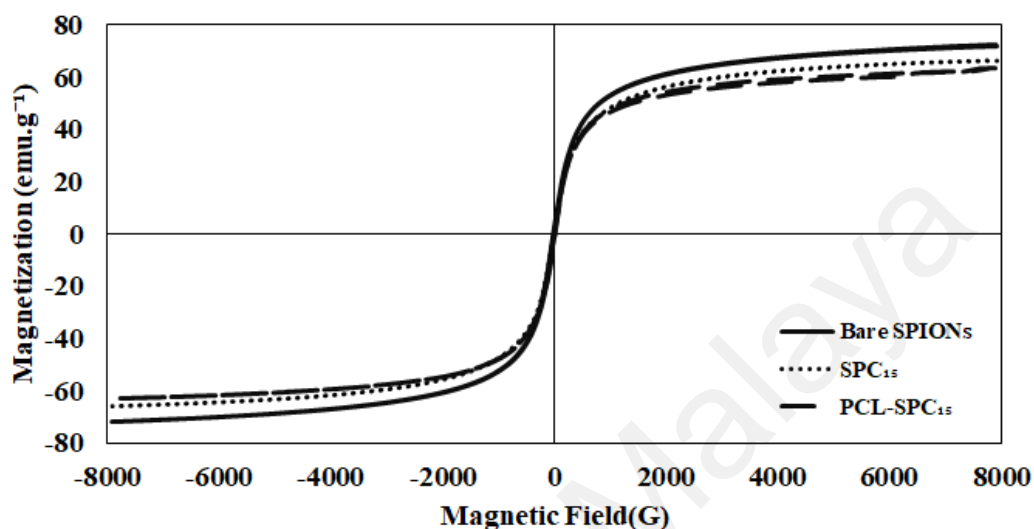


Figure 4.21: The magnetization graphs of bare SPIONs, SPC₁₅, and PCL-SPC₁₅

4.4.7 Cytotoxicity Assay

The cell metabolic activity of PCL-SPC₁₅ at a series of varied concentrations up to 100 $\mu\text{g}\cdot\text{ml}^{-1}$ were assessed against HepG2 carcinoma cells through an MTT assay. The observation of morphological changes in cells indicated that PCL-SPC₁₅ concentrations of up to 100 $\mu\text{g}\cdot\text{ml}^{-1}$ dispossessed antiproliferative activity against HepG2 cells in incubation intervals of 24 and 48 h. Therefore, PCL-SPC₁₅ induced no distinct cytotoxicity towards HepG2 cells with possessing a cell viability above $95\pm 0.01\%$ at the highest concentration (shown in Figure 4.22). Moreover, this value was significantly greater as compared to that of bare SPIONs ($90.37\pm 0.03\%$) observed in previous part (section 4.3.5) with a similar concentration, conforming the positive influence of PCL biopolymer coating on the cytocompatibility of SPIONs. This finding was also in consonance a previous study which reported an enhanced cytocompatibility when chitosan cores were coated by PCL biopolymer shells (Alemi et al., 2019).

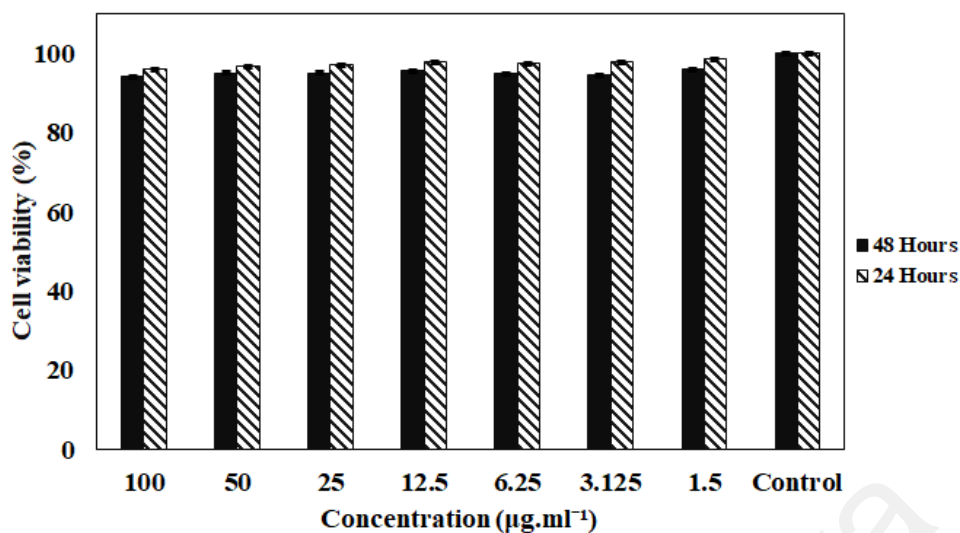


Figure 4.22: Cell viability profiles of HepG2 cells treated with different concentrations of PCL-SPC₁₅ for 24 and 48 h

4.4.8 Magnetic Hyperthermia Studies

In an attempt to correlate the magnetic and structural properties of PCL-SPC₁₅ with the hyperthermia performance, the heating capability of these nanoparticles was examined through measuring the temperature rise upon applying external AMF with different strengths. The temperature profiles of the aqueous solutions containing 1 mg.ml⁻¹ of PCL-SPC₁₅ exposed to varied AMF strengths are presented in Figure 4.23. Analogous heating behaviours at varied magnetic strengths were observed, where an abrupt temperature rise till heating intervals of approximately 120 s (stage I), followed by moderate temperature rise till heating intervals of approximately 900 s (stage II). The medium temperature continued to increase till approximately 1500 s (stage III) and then, no significant temperature rise was observed in the aqueous medium (stage IV). The most influential effect of field strength was in the stage I, where the slopes of temperature rise (dt/dt) at this stage was almost doubled with increase of the AMF strength from 15.47 kA.m⁻¹ to 62.99 kA.m⁻¹. Therefore, the dT/dt values at stage I were determined for SAR values measurement at each magnetic strength. Accordingly, the calculated SAR values

were respectively 99.17 ± 1.1 , 152.65 ± 1.2 , 201.21 ± 0.7 , and 255.12 ± 0.8 $\text{W}\cdot\text{g}^{-1}$ for AMF strengths of 15.74, 31.49, 47.24, and 62.99 $\text{kA}\cdot\text{m}^{-1}$.

The hyperthermia treatment is recommended to be carried out in time intervals of below 900 s to minimize potential disorders on the human body. This is due to the inner temperature of SPIONs is approximately twice that of the aqueous medium, hence longer residence of stealth SPIONs may enhance protein absorption on the SPIONs surfaces, leading to higher agglomeration and reduced colloidal stability (Pérido et al., 2015). Moreover, longer time exposure to AMF may incur irreversible damage to the surrounding tissues (Hedayatnasab et al., 2020a). Therefore, treatment repetition in shorter time intervals is not only avoid the side effects but even boost the hyperthermia efficiency by completing tumour regression (Laurent et al., 2011). The obtained temperatures after exposure to AMF strengths of 15.74, 31.49, 47.2, and 62.99 $\text{kA}\cdot\text{m}^{-1}$ over 900 s were 39.5 ± 0.8 , 44.5 ± 0.5 , 48.1 ± 0.9 °C, and 53.5 ± 0.6 °C, respectively. Therefore, the strength value of 31.49 $\text{kA}\cdot\text{m}^{-1}$ and a heating interval of 900 s were determined as the minimum AMF parameters for generation of sufficient heat within the secure T_H range (the band area in Figure 4.23). This strength could also initiate phase transition of the PCL shell (Figure 4.20) and sustain the medium temperature within T_H range throughout the treatment time. Although the magnetic strength of 31.49 $\text{kA}\cdot\text{m}^{-1}$ exceeded the recommended threshold value ($H\times f < 5\times 10^9$ $\text{A}\cdot\text{m}^{-1}\cdot\text{s}^{-1}$) for the secure clinical purposes, (Hergt & Dutz, 2007), lower magnetic strength e.g. 15.74 $\text{kA}\cdot\text{m}^{-1}$ might require a higher concentration of ferrofluid to produce adequate heat in killing cancer cells within the secure T_H . In addition, higher concentrations may give rise to smaller SAR values due to the possibility of nanoparticles aggregation. Therefore, minimized concentration of magnetic nanoheating agent with remarkable SAR value are necessitated to perform successful hyperthermia treatment and also prevent eddy currents that cause unpredictable disorders in patients during the clinical trials. It is also noteworthy that the

synthesized PCL-SPC₁₅ presented a superior SAR value (255.12 W.g⁻¹) in comparison with other reported SPION coatings including, poly-L-lysine (Kubovcikova et al., 2019), carboxydextran (Shi et al., 2019), PCL mat (Zhong et al., 2015), chitosan (Shete et al., 2014) and PEG (Dabbagh et al., 2019), which might be due to its greater capability in provision of well-dispersed SPIONs. Besides, the thermo-responsive nature of PCL biopolymer in the T_H range was considered as an extra benefit in the heating power enhancement.

SPIONs in single-domain state induce both Néel and Brownian relaxations under the AMF exposure to heat up the entire perimeter surrounding through the flipping motion of the magnetic moment within the crystal and the random motion of nanoparticles suspended in a solution, respectively. In general, when the nanoparticles diameter is below a critical range of 20-30 nm, the Néel relaxation time ' τ_N ' becomes predominant, whereas the Brownian relaxation time ' τ_B ' is considered as primarily heating mechanism for larger diameters. For particle diameters in the range of 20-30 nm, the effective relaxation time is defined as $\tau_{\text{eff}} = (\tau_N \tau_B) / (\tau_N + \tau_B)$ (Kafrouni & Savadogo, 2016). As a result, the core diameters of bare SPIONs and PCL-SPC₁₅ synthesized in this study designated that the produced heat was due to Néel relaxation. Moreover, the produced heat through the viscous friction between the rotating nanoparticles and their surrounding might be raised for larger particle diameter, implying a negligible effect of the Brownian mechanism. The anisotropy constant and particle aggregation also contribute in the heating mechanism. Deatsch and Evans (Deatsch & Evans, 2014) demonstrated that the dominant heating loss assigned to the one with faster relaxation time. PCL-SPC₁₅ with mean particle diameter of 15 nm was therefore indicated a shorter relaxation time of $\sim 10^{-7}$ s, meaning that τ_N might be occurred faster as compared to τ_B . However, τ_N was affected by the interparticle spacing as the energy barrier raised with enhancement of particle interactions. Therefore, the reduced dipolar interactions and increased interparticle

spacings via incorporation of surfactant and coating layers may result in hampered τ_N which is typically considered as the dominant heating loss mechanism in MHT.

Interestingly, the SAR values of the PCL-coated SPIONs are higher as compared to the bare SPIONs (section 4.3.6) owing to the presence PCL biopolymer coating layer around the SPIONs surface (in line with other previous reports (Kubovcikova et al., 2019; Reyes-Ortega, Delgado, Schneider, Checa Fernández, & Iglesias, 2018)), which not only preventing the particles agglomeration but also providing long-term stability of the particles in the colloidal dispersion and allow them to maintain their SPM nature in aqueous medium. Therefore, the best magnetic nanoheating agents regarding hyperthermia treatment are precisely the biopolymer-coated SPIONs as compared to the bare SPIONs due to the coated SPIONs are likely to have faster relaxation processes resulted in higher heating efficiency. Moreover, the thermo-responsive nature of PCL molecules is an additional benefit seems to assist this task.

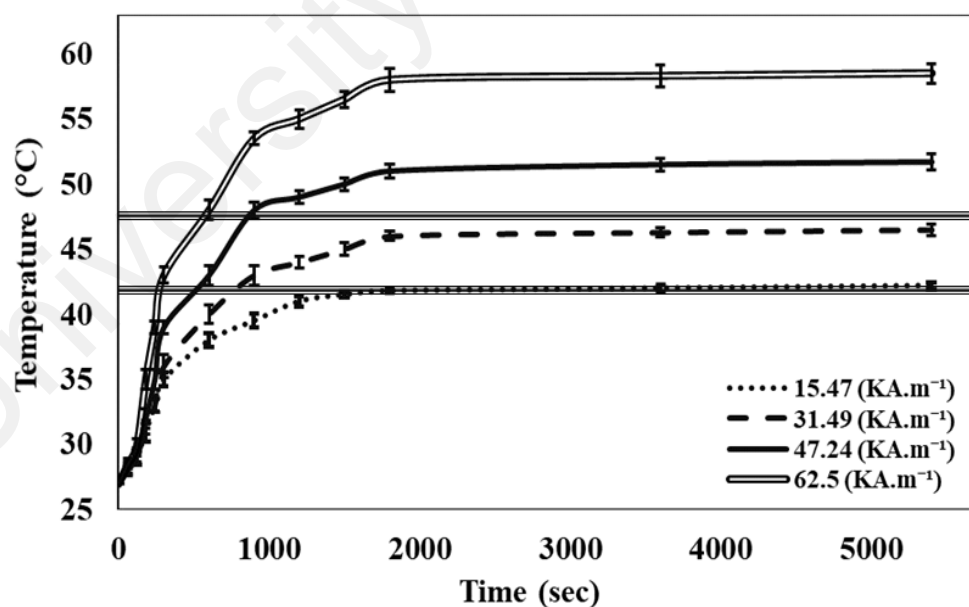


Figure 4.23: The thermal profile of PCL-SPC₁₅ at varied AMF strengths. The 31.49 kA.m⁻¹ magnetic strength could only induce heating power within the secure hyperthermia range (the band area)

4.4.9 In-Vitro Hyperthermia Test on HepG2 Cells

Figure 4.24 illustrates the comparison between the temperature profiles of the control group and the cell media containing $100 \mu\text{g.ml}^{-1}$ PCL-SPC₁₅ under the exposure of 31.49 and 47.24 kA.m^{-1} magnetic strengths over 900 s, which respectively raised the medium temperature to $43.2 \pm 0.3 \text{ }^\circ\text{C}$ and $46.1 \pm 0.5 \text{ }^\circ\text{C}$. The viability of HepG2 cells was quantified instantaneously by MTT assay on the control group and PCL-SPC₁₅ samples to prevent external factors effects. The cell viability responses of HepG2 cells were investigated in incubation interval 24 h shown in Figure 4.25. In spite of exposing to different AMF strengths, the control groups possessed the cell viabilities above 93% in comparison with the control group in the absence of AMF, indicating that the AMF applied in this research was in the safe range. Moreover, the cell viability results implied that neither SPIONs alone nor AMF alone with varied strengths could inhibit the cell growth, which were in a good agreement with other research (Quinto et al., 2015).

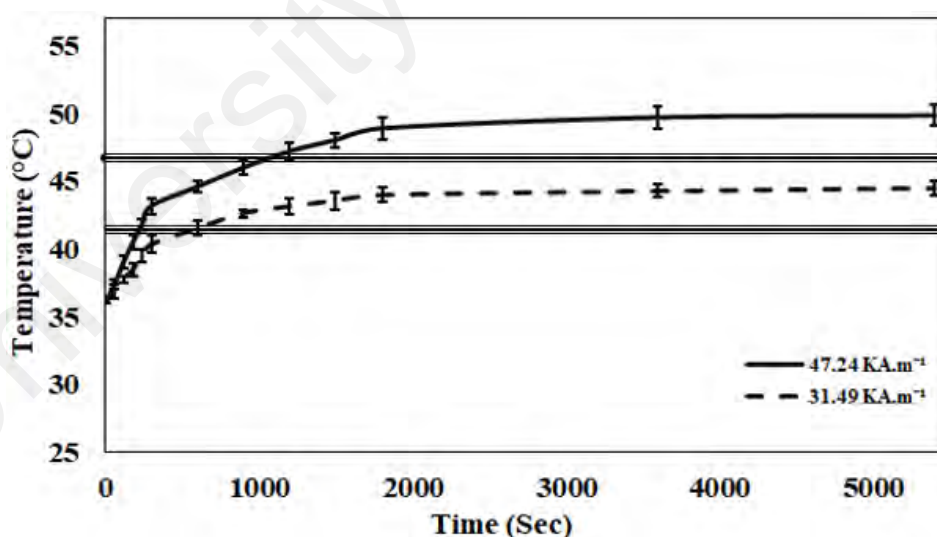


Figure 4.24: The temperature profile of HepG2 cells with PCL-SPC₁₅ during exposure to varied AMF strengths. The minimal magnetic field of 31.47 kA.m^{-1} could only render PCL-SPC₁₅ with adequate heating capability to retain the desirable T_H (the band area)

However, the cell viabilities were significantly lessened to $60.9 \pm 0.8\%$ and $40.1 \pm 0.9\%$ when the HepG2 cells were treated with PCL-SPC₁₅ and exposed to the AMF strengths of 31.49 and 47.24 kA.m⁻¹ in incubation interval of 24 h, respectively. Thereby, the principal mechanism for the cell growth inhibition was the produced heat by PCL-SPC₁₅ nanoparticles under AMF exposure. It assumed that the produced heat possesses adequate capability to increase the reactive oxygen species and thus denature cell division (Mondal et al., 2017). These significant reductions in cell viability of HepG2 treated with PCL-SPC₁₅ through induction heating process confirmed the hypothesis that this novel magnetic nanoheating agent comprised of SPIONs core and PCL biopolymer shell demonstrated a successful hyperthermia performance.

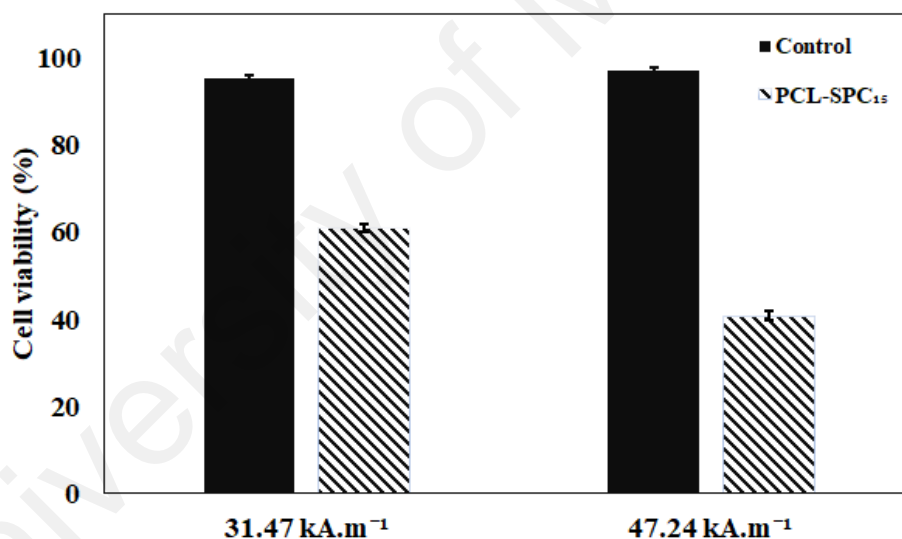


Figure 4.25: Cytotoxicity profiles of HepG2 cells treated with PCL-SPC₁₅ exposed to varied AMF strengths, as quantified by MTT assay

CHAPTER 5: CONCLUSION AND RECOMMENDATIONS

5.1 Conclusions

The aim of this research was to stabilize SPIONs using cationic CTAB and then functionalize them with a thermosensitive PCL biopolymer in order to enhance their in-vitro hyperthermia efficiency on HepG2 carcinoma cells under AMF exposure. Within limitations of this study, the following conclusions were made:

1. The proposed idea in this study was to produce IONPs under mild alkaline reagent and anaerobic condition, which resulted in nanoparticles with great stability and SPM behaviour without using any stabilizing agent. The obtained results indicated the significant contribution of alkaline reagents and synthesis environment on the physicochemical, morphological, and magnetic characteristics of the produced nanoparticles, where synthesis environment played a more significant role as compared to the alkaline reagent type on the particles crystallinity and magnetic behaviour. Overall, the use of mild NH_4OH alkaline reagent provided lower rates of particle formation and thus, higher crystallization and improved magnetic behaviour. On the other hand, by incorporating the strong NaOH reagent, higher zeta potential values and thus slightly lower aggregation tendencies were achieved. However, this effect was negligible when synthesis was carried out under the anaerobic environment. Therefore, in order to obtain nanoparticles with higher crystallinity and enhanced magnetic behaviour, as well as sufficient stability in aqueous medium, the synthesis process is recommended to be carried out using NH_4OH as the precipitating reagent under anaerobic environment.

2. Superparamagnetic iron oxide nanoparticles are commonly synthesized via co-precipitation of ferrous and ferric ions in an alkaline solution; however, reducing the amount of applied chemicals could lessen toxicity risks for cancer treatment purposes. Thereby, based on the high oxidation vulnerability of ferrous ions, the synthesis and optimization of SPIONs via a single-iron precursor route under four varied oxidative conditions were investigated. It was demonstrated that the physicochemical as well as magnetic properties of SPIONs may be purposefully tuned through alteration of oxidative conditions. The optimized SPIONs were produced when the O₂:N₂ flow ratio adjusted to 5:5 in synthesis environment. Thus, the SPIONs exhibited the highest crystallinity and superior magnetic behaviour with sufficient colloidal stability along with excellent cytocompatibility on HepG2 carcinoma cells. Induction heating experiments revealed a remarkable heating capability of the optimized SPIONs in a specific range of AMF strengths. Although the optimized SPIONs showed no cytotoxic effects, a potent cytotoxicity was induced by these particles on HepG2 cells under hyperthermia condition. Hence, these magnetic nanoheating agents could be considered as a promising candidate for cancer therapy purposes.

3. Magnetic hyperthermia therapy of cancer is a promising alternative for the current chemotherapy and radiation options, due to its targeting capability and lower systemic toxicity. However, agglomeration vulnerability of the nanoheating agents in biological media, low control over the heat generation and dissipation at the target region, and eschewed clearance by the renal and RES have been remained as the main challenges for clinical translation of this approach. Hence, the development of ad-micellar stabilized magnetic nanoheating agents with PCL biopolymer coating for in-vitro hyperthermia application was examined. The in-

in vitro investigations indicated a negligible influence of the biopolymer-coated SPIONs on cell viability of HepG2 cells at a maximum concentration. However, the significant hyperthermia efficiency of PCL-coated SPIONs was due to their intrinsic SPM property, stabilizing effect of CTAB ad-micelles, combined with the thermo-responsive nature of PCL biopolymer. The data presented here demonstrated the significant heating capability of PCL-coated SPIONs, which incurred a potent cytotoxic effect on HepG2 carcinoma cells under AMF exposures with appropriate strengths.

University of Malaya

5.2 Recommendations

Based on the finding of this research, further exploration of the following recommendations can be fruitful in extending magnetic hyperthermia therapy of cancer to medically relevant scenarios:

1. The development of magnetic drug delivery systems with active targeting of the carcinoma cells. In this approach, the thermosensitive performance of PCL coating could endow the magnetically thermal-triggered drug-releasing ability under AMF exposure. In fact, the cytotoxic effect of this magnetic nanoheating agent would be enhanced through the synergistic effects of hyperthermia as well as chemotherapy that induced by PCL-coated SPIONs and drugs, respectively. This will involve the use of both magnetic nanoparticles and drugs which can indeed consider as a promising cancer-therapeutic alternative modality to address the crucial issues of current chemotherapy.
2. Due to the direct interaction of the nanoparticles with the blood cells immediately after administration into biological medium, it is essential to determine hemocompatibility of biopolymer-coated SPIONs.
3. The stability tests as well as in-vivo comparative studies at both magnetic hyperthermia treatment alone and thermal-triggered drug-releasing must be performed to evaluate the in-vivo efficacy of the newly synthesized thermo-responsive product.
4. To perform a successful hyperthermia therapy, applying the AMF strength within the clinical safety limit is necessitate; hence, the substitution of SPIONs with Gadolinium and/or Zinc as a single core or even multi cores that possess Curie temperatures lower than Iron would be effective approach to conduct the self-controlled magnetic hyperthermia treatment.

REFERENCES

- Abu-Jdayil, B., Ghannam, M., & Nasser, M. S. (2016). The Modification of Rheological Properties of Bentonite-Water Dispersions with Cationic and Anionic Surfactants. *International Journal of Chemical Engineering and Applications*, 7, 75-80.
- Aggarwal, P., Hall, J., McLeland, C., Dobrovolskaia, M., & McNeil, S. (2009). Nanoparticle interaction with plasma proteins as it relates to particle biodistribution, biocompatibility and therapeutic efficacy. *Adv. Drug Deliv. Rev.*, 61(6), 428-437.
- Ahn, T., Kim, J. H., Yang, H.-M., Lee, J. W., & Kim, J.-D. (2012). Formation pathways of magnetite nanoparticles by coprecipitation method. *J. Phys. Chem. C*, 116(10), 6069-6076.
- Akin, Y., Obaidat, I., Issa, B., & Haik, Y. (2009). Ni_{1-x}Cr_x alloy for self controlled magnetic hyperthermia. *Cryst. Res. Technol.*, 44, 386-390.
- Alcantara, D., Lopez, S., García-Martin, M. L., & Pozo, D. (2016). Iron oxide nanoparticles as magnetic relaxation switching (MRSw) sensors: Current applications in nanomedicine. *Nanomed-Nanotechnol*, 12(5), 1253-1262.
- Alemi, P. S., Atyabi, S. A., Sharifi, F., Mohamadali, M., Irani, S., Bakhshi, H., & Atyabi, S. M. (2019). Synergistic effect of pressure cold atmospheric plasma and carboxymethyl chitosan to mesenchymal stem cell differentiation on PCL/CMC nanofibers for cartilage tissue engineering. *Polym. Adv. Technol.*, 30(6), 1356-1364.
- Ali, Mahmood, A., Khan, M. A., Chughtai, A. H., Shahid, M., Shakir, I., & Warsi, M. F. (2014). Impacts of Ni-Co substitution on the structural, magnetic and dielectric properties of magnesium nano-ferrites fabricated by micro-emulsion method. *J. Alloys Compd.*, 584, 363-368.
- Ali, Zafar, H., Zia, M., ul Haq, I., Phull, A. R., Ali, J. S., & Hussain, A. (2016). Synthesis, characterization, applications, and challenges of iron oxide nanoparticles. *Nanotechnol Sci Appl*, 9, 49-67.
- Amarjargal, A., Tijing, L. D., Park, C.-H., Im, I.-T., & Kim, C. S. (2013). Controlled assembly of superparamagnetic iron oxide nanoparticles on electrospun PU nanofibrous membrane: A novel heat-generating substrate for magnetic hyperthermia application. *Eur. Polym. J.*, 49(12), 3796-3805.
- Amiri-Aref, M., Raouf, J. B., Kiekens, F., & De Wael, K. (2015). Mixed hemi/ad-micelles coated magnetic nanoparticles for the entrapment of hemoglobin at the surface of a screen-printed carbon electrode and its direct electrochemistry and electrocatalysis. *Biosens. Bioelectron.*, 74, 518-525.
- Amirshaghghi, A., Yan, L., Miller, J., Daniel, Y., Stein, J. M., Busch, T. M., Cheng, Z., & Tsourkas, A. (2019). Chlorin e6-Coated Superparamagnetic Iron Oxide Nanoparticle (SPION) Nanoclusters as a Theranostic Agent for Dual-Mode Imaging and Photodynamic Therapy. *Sci. Rep.*, 9(1), 2613.

- Andreu, I., Natividad, E., Solozábal, L., & Roubeau, O. (2015). Same magnetic nanoparticles, different heating behavior: Influence of the arrangement and dispersive medium. *J. Magn. Magn. Mater.*, *380*, 341-346.
- Apostolov, A., Apostolova, I., & Wesselinowa, J. (2011). MO.Fe₂O₃ nanoparticles for self-controlled magnetic hyperthermia. *J. Appl. Phys.*, *109*, 083939-083939.
- Apostolova, I., & Wesselinowa, J. (2009). Possible low-TC nanoparticles for use in magnetic hyperthermia treatments. *Solid State Commun*, *149*, 986-990.
- Astefanoaei, I., Stancu, A., & Chiriac, H. (2017). Magnetic hyperthermia with Fe-Cr-Nb-B magnetic particles. *AIP Conf Proc*, *1796*(1), 040006-040012.
- Atkinson, W. J., Brezovich, I. A., & Chakraborty, D. P. (1984). Usable Frequencies in Hyperthermia with Thermal Seeds. *IEEE. Trans. Biomed. Eng.*, *BME-31*(1), 70-75.
- Azzaza, S., Alleg, S., Moumeni, H., Nemamcha, A. R., Rehspringer, J. L., & Greneche, J. M. (2006). Magnetic properties of nanostructured ball-milled Fe and Fe₅₀Co₅₀ alloy. *J. Phys. Condens. Matter*, *18*(31), 7257-7272.
- Baaziz, H., Tozri, A., Dhahri, E., & Hlil, E. K. (2016). Size-induced Griffiths phase-like in ferromagnetic metallic La_{0.67}Sr_{0.33}MnO₃ nanoparticles. *J. Magn. Magn. Mater.*, *403*, 181-187.
- Beji, Z., Sun, M., Smiri, L. S., Herbst, F., Mangeney, C., & Ammar, S. (2015). Polyol synthesis of non-stoichiometric Mn-Zn ferrite nanocrystals: structural /microstructural characterization and catalytic application. *RSC Advances*, *5*(80), 65010-65022.
- Berenbaum, A., Ginzburg-Margau, M., Coombs, N., Lough, A. J., Safa-Sefat, A., Greedan, J. E., Ozin, G. A., & Manners, I. (2003). Ceramics containing magnetic Co-Fe alloy nanoparticles from the pyrolysis of a highly metallized organometallic polymer precursor. *Adv. Mater.*, *15*(1), 51-51.
- Berkowitz, A. E., Schuele, W. J., & Flanders, P. J. (1968). Influence of Crystallite Size on the Magnetic Properties of Acicular γ - Fe₂O₃ Particles. *J. Appl. Phys.*, *39*(2), 1261-1263.
- Berry, S. L., Walker, K., Hoskins, C., Telling, N. D., & Price, H. P. (2019). Nanoparticle-mediated magnetic hyperthermia is an effective method for killing the human-infective protozoan parasite *Leishmania mexicana* in vitro. *Sci. Rep.*, *9*(1), 1059.
- Blanco-Andujar, C., Ortega, D., Southern, P., Nesbitt, S. A., Thanh, N. T., & Pankhurst, Q. A. (2016). Real-time tracking of delayed-onset cellular apoptosis induced by intracellular magnetic hyperthermia. *Nanomedicine*, *11*(2), 121-136.
- Boyer, C., Corrigan, N. A., Jung, K., Nguyen, D., Nguyen, T. K., Adnan, N. M., Oliver, S., Shanmugam, S., & Yeow, J. (2015). Copper-mediated living radical polymerization (atom transfer radical polymerization and copper (0) mediated polymerization): From fundamentals to bioapplications. *Chem. Rev.*, *116*(4), 1803-1949.

- Boyer, C., Whittaker, M. R., Bulmus, V., Liu, J., & Davis, T. P. (2010). The design and utility of polymer-stabilized iron-oxide nanoparticles for nanomedicine applications. *NPG Asia Mater.*, 2(1), 23-30.
- Bui, T. Q., Ton, S. N.-C., Duong, A. T., & Tran, H. T. (2018). Size-dependent magnetic responsiveness of magnetite nanoparticles synthesised by co-precipitation and solvothermal methods. *Journal of Science: Advanced Materials and Devices*, 3(1), 107-112.
- Busch, W. (1867). Aus der sitzung der medicinischen *Berl Klin Wochenschr*, 13(5), 137.
- Cabanas, A., & Poliakoff, M. (2001). The continuous hydrothermal synthesis of nanoparticulate ferrites in near critical and supercritical water. *J. Mater. Chem.*, 11(5), 1408-1416.
- Cai, W., & Wan, J. (2007). Facile synthesis of superparamagnetic magnetite nanoparticles in liquid polyols. *J. Colloid Interface Sci.*, 305(2), 366-370.
- Cao, G., & Wang, Y. (2011). Physical chemistry of solid surfaces. In *Nanostructures and Nanomaterials* (Vol. 2, pp. 19-60): World Scientific.
- Carrafiello, G., Lagana, D., Mangini, M., Fontana, F., Dionigi, G., Boni, L., Rovera, F., Cuffari, S., & Fugazzola, C. (2008). Microwave tumors ablation: principles, clinical applications and review of preliminary experiences. *Int J Surg*, 6, S65-S69.
- Carta, D., Mountjoy, G., Gass, M., Navarra, G., Casula, M. F., & Corrias, A. (2007). Structural characterization study of FeCo alloy nanoparticles in a highly porous aerogel silica matrix. *J Chem Phys*, 127(20), 204705.
- Çelik, Ö., Can, M. M., & Firat, T. (2014). Size dependent heating ability of CoFe_2O_4 nanoparticles in AC magnetic field for magnetic nanofluid hyperthermia. *J Nanopart Res*, 16(3), 2321-2327.
- Chatterjee, J., Bettge, M., Haik, Y., & Jen Chen, C. (2005). Synthesis and characterization of polymer encapsulated Cu–Ni magnetic nanoparticles for hyperthermia applications. *J. Magn. Magn. Mater.*, 293(1), 303-309.
- Chen, G., Roy, I., Yang, C., & Prasad, P. N. (2016). Nanochemistry and Nanomedicine for Nanoparticle-based Diagnostics and Therapy. *Chem. Rev.*, 116(5), 2826-2885.
- Cheung, A. Y. (1982). Microwave and radiofrequency techniques for clinical hyperthermia. *The British Journal of Cancer. Supplement*, 5, 16-24.
- Chin, A. B., & Yaacob, I. I. (2007). Synthesis and characterization of magnetic iron oxide nanoparticles via w/o microemulsion and Massart's procedure. *J Mater Process Technol*, 191(1–3), 235-237.
- Chiriac, H., Petreus, T., Carasevici, E., Labusca, L., Herea, D.-D., Danceanu, C., & Lupu, N. (2015). In vitro cytotoxicity of Fe–Cr–Nb–B magnetic nanoparticles under high frequency electromagnetic field. *J. Magn. Magn. Mater.*, 380, 13-19.

- Chomoucka, J., Drbohlavova, J., Huska, D., Adam, V., Kizek, R., & Hubalek, J. (2010). Magnetic nanoparticles and targeted drug delivering. *Pharmacol. Res.*, *62*(2), 144-149.
- Coey, J. M. D. (2011). Hard Magnetic Materials: A Perspective. *IEEE Trans. Magn.*, *47*(12), 4671-4681.
- Coley, W. B. (1891). Contribution to the knowledge of sarcoma. *Ann. Surg.*, *14*(3), 199-220.
- Cornell, R. M., & Schwertmann, U. (2006). *The iron oxides: Structure, properties, reactions, occurrences and uses*: John Wiley & Sons.
- Correlo, V., Boesel, L., Bhattacharya, M., Mano, J., Neves, N., & Reis, R. (2005). Properties of melt processed chitosan and aliphatic polyester blends. *Materials Science Engineering: A*, *403*(1-2), 57-68.
- Cregg, P. J., Murphy, K., & Mardinoglu, A. (2012). Inclusion of interactions in mathematical modelling of implant assisted magnetic drug targeting. *Appl. Math. Model.*, *36*(1), 1-34.
- Cruz, M. M., Ferreira, L. P., Ramos, J., Mendo, S. G., Alves, A. F., Godinho, M., & Carvalho, M. D. (2017). Enhanced magnetic hyperthermia of CoFe₂O₄ and MnFe₂O₄ nanoparticles. *J. Alloys Compd.*, *703*, 370-380.
- Dabbagh, A., Hedayatnasab, Z., Karimian, H., Sarraf, M., Yeong, C. H., Madaah Hosseini, H. R., Abu Kasim, N. H., Wong, T. W., & Abdul Rahman, N. (2019). Polyethylene glycol-coated porous magnetic nanoparticles for targeted delivery of chemotherapeutics under magnetic hyperthermia condition. *Int J Hyperthermia*, *36*(1), 104-114.
- Dai, Y., Su, J., Wu, K., Ma, W., Wang, B., Li, M., Sun, P., Shen, Q., Wang, Q., & Fan, Q. (2019). Multifunctional Thermosensitive Liposomes Based on Natural Phase-Change Material: Near-Infrared Light-Triggered Drug Release and Multimodal Imaging-Guided Cancer Combination Therapy. *ACS Appl. Mater. Interfaces*, *11*(11), 10540-10553.
- Dai, Z. R., Pan, Z. W., & Wang, Z. L. (2003). Novel Nanostructures of Functional Oxides Synthesized by Thermal Evaporation. *Adv. Funct. Mater.*, *13*(1), 9-24.
- Deatsch, A. E., & Evans, B. A. (2014). Heating efficiency in magnetic nanoparticle hyperthermia. *J. Magn. Magn. Mater.*, *354*, 163-172.
- Deraz, N. M. (2010). Size and crystallinity-dependent magnetic properties of copper ferrite nano-particles. *J. Alloys Compd.*, *501*(2), 317-325.
- Ding, Q., Liu, D., Guo, D., Yang, F., Pang, X., Che, R., Zhou, N., Xie, J., Sun, J., Huang, Z., & Gu, N. (2017). Shape-controlled fabrication of magnetite silver hybrid nanoparticles with high performance magnetic hyperthermia. *Biomaterials*, *124*, 35-46.
- Doll, T. A. P. F., Raman, S., Dey, R., & Burkhard, P. (2013). Nanoscale assemblies and their biomedical applications. *J R Soc Interface*, *10*(80), 20120740-20120754.

- Dutz, S., & Hergt, R. (2013). Magnetic nanoparticle heating and heat transfer on a microscale: Basic principles, realities and physical limitations of hyperthermia for tumour therapy. *Int J Hyperthermia*, 29(8), 790-800.
- Dutz, S., & Hergt, R. (2014). Magnetic particle hyperthermia—a promising tumour therapy? *Nanotechnology*, 25(45), 452001-452028.
- Edelstein, A. S., & Cammaratra, R. C. (1998). *Nanomaterials: Synthesis, Properties and Applications, Second Edition*: Taylor & Francis.
- Edmundson, M. C., Capeness, M., & Horsfall, L. (2014). Exploring the potential of metallic nanoparticles within synthetic biology. *New Biotechnology*, 31(6), 572-578.
- El-Gendy, A. A., Ibrahim, E. M. M., Khavrus, V. O., Krupskaya, Y., Hampel, S., Leonhardt, A., Büchner, B., & Klingeler, R. (2009). The synthesis of carbon coated Fe, Co and Ni nanoparticles and an examination of their magnetic properties. *Carbon*, 47(12), 2821-2828.
- Elfeky, S. A., Mahmoud, S. E., & Youssef, A. F. (2017). Applications of CTAB modified magnetic nanoparticles for removal of chromium (VI) from contaminated water. *J. Adv. Res.*, 8(4), 435-443.
- Eslami-Farsani, R., Hedayatnasab, Z., Khalili, S. M. R., & Soleimani, N. (2012). Mechanical characterization of nanoclay reinforced polypropylene composites at high temperature subjected to tensile loads. *Advanced Materials Research*, 488-489, 567-571.
- Eslami-Farsani, R., Reza Khalili, S. M., Hedayatnasab, Z., & Soleimani, N. (2014). Influence of thermal conditions on the tensile properties of basalt fiber reinforced polypropylene–clay nanocomposites. *Mater. Des.*, 53, 540-549.
- Espinosa, A., Di Corato, R., Kolosnjaj-Tabi, J., Flaud, P., Pellegrino, T., & Wilhelm, C. (2016). Duality of Iron Oxide Nanoparticles in Cancer Therapy: Amplification of Heating Efficiency by Magnetic Hyperthermia and Photothermal Bimodal Treatment. *ACS Nano*, 10(2), 2436-2446.
- Espinoza, S. M., Patil, H. I., San Martin Martinez, E., Casañas Pimentel, R., & Ige, P. P. (2019). Poly-ε-caprolactone (PCL), a promising polymer for pharmaceutical and biomedical applications: Focus on nanomedicine in cancer. *International Journal of Polymeric Materials and Polymeric Biomaterials*, 1-42.
- Evans, R. F. L., Fan, W. J., Chureemart, P., Ostler, T. A., Ellis, M. O. A., & Chantrell, R. W. (2014). Atomistic spin model simulations of magnetic nanomaterials. *J. Phys. Condens. Matter*, 26(10), 103202.
- Fantechi, E., Innocenti, C., Albino, M., Lottini, E., & Sangregorio, C. (2015). Influence of cobalt doping on the hyperthermic efficiency of magnetite nanoparticles. *J. Magn. Magn. Mater.*, 380, 365-371.
- Ferreira, C. L., Valente, C. A., Zanini, M. L., Sgarioni, B., Ferreira Tondo, P. H., Chagastelles, P. C., Braga, J., Campos, M. M., Malmonge, J. A., & de Souza Basso, N. R. (2019). Biocompatible PCL/PLGA/Polypyrrole Composites for Regenerating Nerves. *Macromol Symp*, 383(1), 1800028.

- Fersi, R., Mliki, N., Cabié, M., & Bessais, L. (2014). Intrinsic and extrinsic magnetic properties of nanocrystalline Pr₂(Co,Fe)₇. *Phys. Status Solidi A*, 211(4), 910-916.
- Frey, N. A., Peng, S., Cheng, K., & Sun, S. (2009). Magnetic nanoparticles: synthesis, functionalization, and applications in bioimaging and magnetic energy storage. *Chem. Soc. Rev.*, 38(9), 2532-2542.
- Fu, L., Liu, Z., Liu, Y., Han, B., Hu, P., Cao, L., & Zhu, D. (2005). Beaded Cobalt Oxide Nanoparticles along Carbon Nanotubes: Towards More Highly Integrated Electronic Devices. *Adv. Mater.*, 17(2), 217-221.
- Fukuda, K., Fujieda, S., S. K., Suzuki, S., & Jeyadevan, B. (2012). Low temperature synthesis of FePt alloy nanoparticles by polyol process. *J Phys Conf Ser*, 352(1), 012020.
- Gan, L., Lu, Z., Cao, D., & Chen, Z. (2018). Effects of cetyltrimethylammonium bromide on the morphology of green synthesized Fe₃O₄ nanoparticles used to remove phosphate. *Mater. Sci. Eng. C*, 82, 41-45.
- Garaio, E., Collantes, J. M., Garcia, J. A., Plazaola, F., Mornet, S., Couillaud, F., & Sandre, O. (2014). A wide-frequency range AC magnetometer to measure the specific absorption rate in nanoparticles for magnetic hyperthermia. *J. Magn. Mater.*, 368, 432-437.
- Gas, P. (2011). Essential facts on the history of hyperthermia and their connections with electromedicine. *Przegląd Elektrotechniczny*, 87(12), 37-40.
- Getzlaff, M. (2008). Introduction. In *Fundamentals of Magnetism* (pp. 1-6). Berlin, Heidelberg: Springer Berlin Heidelberg.
- Ghosh Chaudhuri, R., & Paria, S. (2012). Core/shell nanoparticles: classes, properties, synthesis mechanisms, characterization, and applications. *Chem. Rev.*, 112(4), 2373-2433.
- Gilchrist, R. K., Medal, R., Shorey, W. D., Hanselman, R. C., Parrott, J. C., & Taylor, C. B. (1957). Selective inductive heating of lymph nodes. *Ann. Surg.*, 146(4), 596-606.
- Giustini, A. J., Petryk, A. A., Cassim, S. M., Tate, J. A., Baker, I., & Hoopes, P. J. (2010). Magnetic nanoparticle hyperthermia in cancer treatment. *Nano LIFE*, 1(01n02), 17-32.
- Gómez Ruiz, B., Roux, S., Courtois, F., & Bonazzi, C. (2018). Kinetic modelling of ascorbic and dehydroascorbic acids concentrations in a model solution at different temperatures and oxygen contents. *Food Res. Int.*, 106, 901-908.
- Gonzalez-Fernandez, M. A., Torres, T. E., Andrés-Vergés, M., Costo, R., de la Presa, P., Serna, C. J., Morales, M. P., Marquina, C., Ibarra, M. R., & Goya, G. F. (2009). Magnetic nanoparticles for power absorption: Optimizing size, shape and magnetic properties. *J Solid State Chem*, 182(10), 2779-2784.
- Gordon, R. T., Hines, J. R., & Gordon, D. (1979). Intracellular hyperthermia. A biophysical approach to cancer treatment via intracellular temperature and biophysical alterations. *Med. Hypotheses*, 5(1), 83-102.

- Goswami, M. M., Dey, C., Bandyopadhyay, A., Sarkar, D., & Ahir, M. (2016). Micelles driven magnetite (Fe_3O_4) hollow spheres and a study on AC magnetic properties for hyperthermia application. *J. Magn. Magn. Mater.*, 417, 376-381.
- Gotić, M., Jurkin, T., & Musić, S. (2009). From iron (III) precursor to magnetite and vice versa. *Mater. Res. Bull.*, 44(10), 2014-2021.
- Gubin, S. P. (2009). Introduction. In *Magnetic Nanoparticles* (pp. 1-23): Wiley-VCH Verlag GmbH & Co. KGaA.
- Günlü, E., İşçi, S., Öztekin, N., Erim, F. B., Ece, Ö. I., & Güngör, N. (2006). Effect of cationic surfactant adsorption on the rheological and surface properties of bentonite dispersions. *J. Colloid Interface Sci.*, 303(1), 137-141.
- Guo, L., Chen, H., He, N., & Deng, Y. (2018). Effects of surface modifications on the physicochemical properties of iron oxide nanoparticles and their performance as anticancer drug carriers. *Chin Chem Lett*, 29(12), 1829-1833.
- Gupta, A. K., & Gupta, M. (2005). Synthesis and surface engineering of iron oxide nanoparticles for biomedical applications. *Biomaterials*, 26(18), 3995-4021.
- Hanini, A., Lartigue, L., Gavard, J., Kacem, K., Wilhelm, C., Gazeau, F., Chau, F., & Ammar, S. (2016). Zinc substituted ferrite nanoparticles with $\text{Zn}_{0.9}\text{Fe}_{2.1}\text{O}_4$ formula used as heating agents for in vitro hyperthermia assay on glioma cells. *J. Magn. Magn. Mater.*, 416, 315-320.
- Hayden, K. S., Park, K., & Curtis, J. S. (2003). Effect of particle characteristics on particle pickup velocity. *Powder Technol.*, 131(1), 7-14.
- Hedayatnasab, Z., Abnisa, F., & Wan Daud, W. M. A. (2017). Review on magnetic nanoparticles for magnetic nanofluid hyperthermia application. *Mater. Des.*, 123, 174-196.
- Hedayatnasab, Z., Abnisa, F., & Wan Daud, W. M. A. (2018). Investigation properties of superparamagnetic nanoparticles and magnetic field-dependent hyperthermia therapy. *IOP Conf Ser Mater Sci Eng*, 334(1), 012042.
- Hedayatnasab, Z., Dabbagh, A., Abnisa, F., Abu Ksaim, N. H., & Wan Daud, W. M. A. (2019). Synthesis of highly stable superparamagnetic iron oxide nanoparticles under mild alkaline reagents and anaerobic condition. *Nanosci Nanotechnol Lett*, 11(7), 985-990.
- Hedayatnasab, Z., Dabbagh, A., Abnisa, F., & Wan Daud, W. M. A. (2020a). Polycaprolactone-coated superparamagnetic iron oxide nanoparticles for in vitro magnetic hyperthermia therapy of cancer. *EUR POLYM J*, 133, 109789.
- Hedayatnasab, Z., Dabbagh, A., Abnisa, F., & Wan Daud, W. M. A. (2020b). Synthesis and in-vitro characterization of superparamagnetic iron oxide nanoparticles using a sole precursor for hyperthermia therapy. *Mater. Res. Bull.*, 132, 110975.
- Hedayatnasab, Z., Eslami-Farsani, R., Khalili, S. M. R., & Soleimani, N. (2013). Mechanical characterization of clay reinforced polypropylene nanocomposites at high temperature. *Fibers and Polymers*, 14(10), 1650-1656.

- Hergt, R., & Dutz, S. (2007). Magnetic particle hyperthermia—biophysical limitations of a visionary tumour therapy. *J. Magn. Magn. Mater.*, *311*(1), 187-192.
- Hergt, R., Dutz, S., Müller, R., & Zeisberger, M. (2006). Magnetic particle hyperthermia: Nanoparticle magnetism and materials development for cancer therapy. *J. Phys. Condens. Matter*, *18*(38), S2919-S2934.
- Hergt, R., Dutz, S., & Roder, M. (2008). Effects of size distribution on hysteresis losses of magnetic nanoparticles for hyperthermia. *J. Phys. Condens. Matter*, *20*(38), 385214-385225.
- Herring, N. P., Panda, A. B., AbouZeid, K., Almahoudi, S. H., Olson, C. R., Patel, A., & El-Shall, M. S. (2013). Microwave Synthesis of Metal Oxide Nanoparticles. In A. M. Carpenter, S. Mathur, & A. Kolmakov (Eds.), *Metal Oxide Nanomaterials for Chemical Sensors* (pp. 245-284). New York, NY: Springer New York.
- Hilger, I., Frühauf, K., Andrä, W., Hiergeist, R., Hergt, R., & Kaiser, W. A. (2002). Heating potential of iron oxides for therapeutic purposes in interventional radiology. *Acad Radiol*, *9*(2), 198-202.
- Hilger, I., & Kaiser, W. A. (2012). Iron oxide-based nanostructures for MRI and magnetic hyperthermia. *Nanomedicine*, *7*(9), 1443-1459.
- Hurrell, T., Lilley, K. S., & Cromarty, A. D. (2019). Proteomic responses of HepG2 cell monolayers and 3D spheroids to selected hepatotoxins. *Toxicol. Lett.*, *300*, 40-50.
- Iacovita, C., Florea, A., Dudric, R., Pall, E., Moldovan, A. I., Tetean, R., Stiuftuc, R., & Lucaciu, C. M. (2016). Small versus large iron oxide magnetic nanoparticles: hyperthermia and cell uptake properties. *Molecules*, *21*(10), 1357.
- Ibrahim, E. M. M., Abdel-Rahman, L. H., Abu-Dief, A. M., Elshafaie, A., Hamdan, S. K., & Ahmed, A. M. (2018). Electric, thermoelectric and magnetic characterization of γ -Fe₂O₃ and Co₃O₄ nanoparticles synthesized by facile thermal decomposition of metal-Schiff base complexes. *Mater. Res. Bull.*, *99*, 103-108.
- Iida, H., Takayanagi, K., Nakanishi, T., & Osaka, T. (2007). Synthesis of Fe₃O₄ nanoparticles with various sizes and magnetic properties by controlled hydrolysis. *Adv. Colloid Interface Sci.*, *314*(1), 274-280.
- Iqbal, Y., Bae, H., Rhee, I., & Hong, S. (2016a). Control of the saturation temperature in magnetic heating by using polyethylene-glycol-coated rod-shaped nickel-ferrite (NiFe₂O₄) nanoparticles. *J Korean Phys Soc*, *68*, 587-592.
- Iqbal, Y., Bae, H., Rhee, I., & Hong, S. (2016b). Magnetic heating of silica-coated manganese ferrite nanoparticles. *J. Magn. Magn. Mater.*, *409*, 80-86.
- Jakobi, J., Petersen, S., Menéndez-Manjón, A., Wagener, P., & Barcikowski, S. (2010). Magnetic Alloy Nanoparticles from Laser Ablation in Cyclopentanone and Their Embedding into a Photoresist. *Langmuir*, *26*(10), 6892-6897.
- Jana, N. R., Chen, Y., & Peng, X. (2004). Size- and Shape-Controlled Magnetic (Cr, Mn, Fe, Co, Ni) Oxide Nanocrystals via a Simple and General Approach. *Chem. Mater.*, *16*(20), 3931-3935.

- Jiang, W., Lai, K.-L., Hu, H., Zeng, X.-B., Lan, F., Liu, K.-X., Wu, Y., & Gu, Z.-W. (2011). The effect of $[\text{Fe}^{3+}]/[\text{Fe}^{2+}]$ molar ratio and iron salts concentration on the properties of superparamagnetic iron oxide nanoparticles in the water/ethanol/toluene system. *J Nanopart Res*, 13(10), 5135-5245.
- Joo, J., Kwon, S. G., Yu, J. H., & Hyeon, T. (2005). Synthesis of ZnO Nanocrystals with Cone, Hexagonal Cone, and Rod Shapes via Non-Hydrolytic Ester Elimination Sol-Gel Reactions. *Adv. Mater.*, 17(15), 1873-1877.
- Jordan, A., Scholz, R., Wust, P., Fähling, H., & Roland, F. (1999). Magnetic fluid hyperthermia (MFH): Cancer treatment with AC magnetic field induced excitation of biocompatible superparamagnetic nanoparticles. *J. Magn. Magn. Mater.*, 201(1-3), 413-419.
- Joshi, H. M., Lin, Y. P., Aslam, M., Prasad, P. V., Schultz-Sikma, E. A., Edelman, R., Meade, T., & Dravid, V. P. (2009). Effects of Shape and Size of Cobalt Ferrite Nanostructures on Their MRI Contrast and Thermal Activation. *J. Phys. Chem. C*, 113(41), 17761-17767.
- Julien, C. M., Ait-Salah, A., Mauger, A., & Gendron, F. (2006). Magnetic properties of lithium intercalation compounds. *Ionics*, 12(1), 21-32.
- Kafrouni, L., & Savadogo, O. (2016). Recent progress on magnetic nanoparticles for magnetic hyperthermia. *Progress in biomaterials*, 5(3-4), 147-160.
- Kandasamy, G., Soni, S., Sushmita, K., Veerapu, N. S., Bose, S., & Maity, D. (2019). One-step synthesis of hydrophilic functionalized and cytocompatible superparamagnetic iron oxide nanoparticles (SPIONs) based aqueous ferrofluids for biomedical applications. *J MOL LIQ*, 274, 653-663.
- Kandasamy, G., Sudame, A., Luthra, T., Saini, K., & Maity, D. (2018). Functionalized Hydrophilic Superparamagnetic Iron Oxide Nanoparticles for Magnetic Fluid Hyperthermia Application in Liver Cancer Treatment. *ACS Omega*, 3(4), 3991-4005.
- Karunamoorthi, R., Suresh Kumar, G., Prasad, A. I., Vatsa, R. K., Thamizhavel, A., Girija, E. K., & Fischman, G. (2014). Fabrication of a novel biocompatible magnetic biomaterial with hyperthermia potential. *J. Am. Ceram. Soc.*, 97(4), 1115-1122.
- Khalili, S. M. R., Eslami-Farsani, R., Soleimani, N., & Hedayatnasab, Z. (2014). Charpy impact behavior of clay/basalt fiber-reinforced polypropylene nanocomposites at various temperatures. *J. Thermoplast. Compos. Mater.*, 29(10), 1416-1428.
- Khoei, S., Bagheri, Y., & Hashemi, A. (2015). Composition controlled synthesis of PCL-PEG Janus nanoparticles: magnetite nanoparticles prepared from one-pot photo-click reaction. *Nanoscale*, 7(9), 4134-4148.
- Khot, V. M., Salunkhe, A. B., Thorat, N. D., Ningthoujam, R. S., & Pawar, S. H. (2013). Induction heating studies of dextran coated MgFe_2O_4 nanoparticles for magnetic hyperthermia. *Dalton Trans.*, 42(4), 1249-1258.
- Kim, T., Cho, E.-J., Chae, Y., Kim, M., Oh, A., Jin, J., Lee, E.-S., Baik, H., Haam, S., Suh, J.-S., Huh, Y.-M., & Lee, K. (2011). Urchin-shaped manganese oxide

nanoparticles as pH-responsive activatable T1 contrast agents for magnetic resonance imaging. *Angew. Chem.*, 50(45), 10589-10593.

- Kingsley, M. P., Desai, P. B., & Srivastava, A. K. (2015). Simultaneous electro-catalytic oxidative determination of ascorbic acid and folic acid using Fe₃O₄ nanoparticles modified carbon paste electrode. *J. Electroanal. Chem.*, 741, 71-79.
- Kittel, C. (1976). *Introduction to solid state physics* (Vol. 8): Wiley New York.
- Kline, T. L., Xu, Y.-H., Jing, Y., & Wang, J.-P. (2009). Biocompatible high-moment FeCo-Au magnetic nanoparticles for magnetic hyperthermia treatment optimization. *J. Magn. Magn. Mater.*, 321(10), 1525-1528.
- Knop, K., Hoogenboom, R., Fischer, D., & Schubert, U. S. (2010). Poly(ethylene glycol) in Drug Delivery: Pros and Cons as Well as Potential Alternatives. *Angew. Chem. Int. Ed.*, 49(36), 6288-6308.
- Kolhatkar, A. G., Jamison, A. C., Litvinov, D., Willson, R. C., & Lee, T. R. (2013). Tuning the magnetic properties of nanoparticles. *Int. J. Mol. Sci.*, 14(8), 15977-16009.
- Kubovcikova, M., Koneracka, M., Strbak, O., Molcan, M., Zavisova, V., Antal, I., Khmara, I., Lucanska, D., Tomco, L., Barathova, M., Zatovicova, M., Dobrota, D., Pastorekova, S., & Kopcansky, P. (2019). Poly-L-lysine designed magnetic nanoparticles for combined hyperthermia, magnetic resonance imaging and cancer cell detection. *J. Magn. Magn. Mater.*, 475, 316-326.
- Kumar, C. S. (2009). *Magnetic Nanomaterials*: John Wiley & Sons.
- Lahiri, B. B., Muthukumaran, T., & Philip, J. (2016). Magnetic hyperthermia in phosphate coated iron oxide nanofluids. *J. Magn. Magn. Mater.*, 407, 101-113.
- Lan, N. T., Duong, N. P., & Hien, T. D. (2011). Influences of cobalt substitution and size effects on magnetic properties of coprecipitated Co-Fe ferrite nanoparticles. *J. Alloys Compd.*, 509(19), 5919-5925.
- Laurent, S., Dutz, S., Häfeli, U. O., & Mahmoudi, M. (2011). Magnetic fluid hyperthermia: Focus on superparamagnetic iron oxide nanoparticles. *Adv. Colloid Interface Sci.*, 166(1-2), 8-23.
- Lee, J.-H., Jang, J.-t., Choi, J.-s., Moon, S. H., Noh, S.-h., Kim, J.-w., Kim, J.-G., Kim, I.-S., Park, K. I., & Cheon, J. (2011). Exchange-coupled magnetic nanoparticles for efficient heat induction. *Nat. Nanotechnol.*, 6, 418.
- Leteba, G. M., & Lang, C. I. (2013). Synthesis of Bimetallic Platinum Nanoparticles for Biosensors. *Sensors*, 13(8), 10358-10369.
- Li, W., Liu, Y., Qian, Z., & Yang, Y. (2017). Evaluation of Tumor Treatment of Magnetic Nanoparticles Driven by Extremely Low Frequency Magnetic Field. *Sci. Rep.*, 7, 46287-46295.
- Li, Z., Kawashita, M., Araki, N., Mistumori, M., & Hiraoka, M. (2011). Effect of particle size of magnetite nanoparticles on heat generating ability under alternating magnetic field. *Bioceram. Dev. Appl.*, 1, 1-4.

- Lin, X. M., Sorensen, C. M., Klabunde, K. J., & Hajipanayis, G. C. (1999). Control of Cobalt Nanoparticle Size by the Germ-growth Method in Inverse Micelle System: Size-dependent Magnetic Properties. *J. Mater. Res.*, *14*(04), 1542-1547.
- Liu, Fang, N., Li, C., Li, X., Liu, H., & Wu, J. (2017). A free-standing magneto-fluorescent $\text{La}_{1-x}\text{Sr}_x\text{MnO}_3@\text{ZnO}$ nanoparticle: Synthesis, properties and sharp Curie transition. *J. Alloys Compd.*, *693*, 518-526.
- Liu, L., He, Z., Zhao, Y., Sun, J., & Tong, G. (2018). Modulation of the composition and surface morphology of expanded graphite/Fe/Fe₃O₄ composites for plasmon resonance-enhanced microwave absorption. *J. Alloys Compd.*, *765*, 1218-1227.
- Lu, C., Chiu, H., & Liu, C. (2006). Removal of Zinc(II) from Aqueous Solution by Purified Carbon Nanotubes: Kinetics and Equilibrium Studies. *Ind. Eng. Chem. Res.*, *45*(8), 2850-2855.
- Lu, L.-Y., Yu, L.-N., Xu, X.-G., & Jiang, Y. (2013). Monodisperse magnetic metallic nanoparticles: synthesis, performance enhancement, and advanced applications. *Rare Metals*, *32*(4), 323-331.
- Lu, L. T., Dung, N. T., Tung, L. D., Thanh, C. T., Quy, O. K., Chuc, N. V., Maenosono, S., & Thanh, N. T. K. (2015). Synthesis of magnetic cobalt ferrite nanoparticles with controlled morphology, monodispersity and composition: the influence of solvent, surfactant, reductant and synthetic conditions. *Nanoscale*, *7*(46), 19596-19610.
- Lu, Q. M., Yue, M., Zhang, H. G., Wang, M. L., Yu, F., Huang, Q. Z., Ryan, D. H., & Altounian, Z. (2015). Intrinsic magnetic properties of single-phase Mn_{1+x}Ga ($0 < x < 1$) alloys. *Sci. Rep.*, *5*, 17086-17090.
- Mahmoudi, M., Sant, S., Wang, B., Laurent, S., & Sen, T. (2011). Superparamagnetic iron oxide nanoparticles (SPIONs): Development, surface modification and applications in chemotherapy. *Adv. Drug Deliv. Rev.*, *63*(1-2), 24-46.
- Maity, D., & Agrawal, D. C. (2007). Synthesis of iron oxide nanoparticles under oxidizing environment and their stabilization in aqueous and non-aqueous media. *J. Magn. Magn. Mater.*, *308*(1), 46-55.
- Mallory, M., Gogineni, E., Jones, G. C., Greer, L., & Simone Ii, C. B. (2016). Therapeutic hyperthermia: The old, the new, and the upcoming. *Crit. Rev. Oncol. Hematol.*, *97*, 56-64.
- Manakhov, A., Permyakova, E. S., Ershov, S., Sheveyko, A., Kovalskii, A., Polčák, J., Zhitnyak, I. Y., Gloushankova, N. A., Zajíčková, L., & Shtansky, D. V. (2019). Bioactive TiCaPCON-coated PCL nanofibers as a promising material for bone tissue engineering. *Appl. Surf. Sci.*, *479*, 796-802.
- Mary, J. A., Manikandan, A., Kennedy, L. J., Bououdina, M., Sundaram, R., & Vijaya, J. J. (2014). Structure and magnetic properties of Cu-Ni alloy nanoparticles prepared by rapid microwave combustion method. *T Nonferr Metal Soc*, *24*(5), 1467-1473.
- McBride, K., Cook, J., Gray, S., Felton, S., Stella, L., & Poulidi, D. (2016). Evaluation of $\text{La}_{1-x}\text{Sr}_x\text{MnO}_3$ ($0 \leq x < 0.4$) synthesised via a modified sol-gel method as mediators for magnetic fluid hyperthermia. *CrystEngComm*, *18*(3), 407-416.

- McNamara, K., & Tofail, S. A. M. (2015). Nanosystems: the use of nanoalloys, metallic, bimetallic, and magnetic nanoparticles in biomedical applications. *Phys. Chem. Chem. Phys.*, *17*(42), 27981-27995.
- Mody, V. V., Singh, A., & Wesley, B. (2013). Basics of magnetic nanoparticles for their application in the field of magnetic fluid hyperthermia. *European Journal of Nanomedicine*, *5*(1), 11-21.
- Mohapatra, J., Mitra, A., Tyagi, H., Bahadur, D., & Aslam, M. (2015). Iron oxide nanorods as high-performance magnetic resonance imaging contrast agents. *Nanoscale*, *7*(20), 9174-9184.
- Mondal, S., Manivasagan, P., Bharathiraja, S., Santha Moorthy, M., Nguyen, V. T., Kim, H. H., Nam, S. Y., Lee, K. D., & Oh, J. (2017). Hydroxyapatite coated iron oxide nanoparticles: A promising nanomaterial for magnetic hyperthermia cancer treatment. *Nanomaterials*, *7*(12), 426.
- Moroz, P., Jones, S. K., & Gray, B. N. (2002). Magnetically mediated hyperthermia: current status and future directions. *Int J Hyperthermia*, *18*(4), 267-284.
- Moroz, P., Pardoe, H., Jones, S. K., St Pierre, T. G., Song, S., & Gray, B. N. (2002). Arterial embolization hyperthermia: hepatic iron particle distribution and its potential determination by magnetic resonance imaging. *Phys. Med. Biol.*, *47*(9), 1591-1602.
- Morrish, A. H. (2001). The Magnetic Field. In *The Physical Principles of Magnetism* (pp. 1-30): John Wiley & Sons, Inc.
- Müller, R., Dutz, S., Neeb, A., Cato, A. C. B., & Zeisberger, M. (2013). Magnetic heating effect of nanoparticles with different sizes and size distributions. *J. Magn. Magn. Mater.*, *328*, 80-85.
- Muro-Cruces, J., Roca, A. G., López-Ortega, A., Fantechi, E., del-Pozo-Bueno, D., Estradé, S., Peiró, F., Sepúlveda, B., Pineider, F., Sangregorio, C., & Nogues, J. (2019). Precise Size Control of the Growth of Fe₃O₄ Nanocubes over a Wide Size Range Using a Rationally Designed One-Pot Synthesis. *ACS Nano*, *13*(7), 7716-7728.
- Nath, D., & Banerjee, P. (2013). Green nanotechnology – A new hope for medical biology. *Environ. Toxicol. Pharmacol.*, *36*(3), 997-1014.
- Nguyen, Chinnasamy, C., Yoon, S., Somu, S., Sakai, T., Baraskar, A., Mukerjee, S., Vittoria, C., & Harris, V. (2008). Functionalization of FeCo alloy nanoparticles with highly dielectric amorphous oxide coatings. *J. Appl. Phys.*, *103*, 07D532-507D532.
- Nguyen, & Kim, K. S. (2016). Controlled magnetic properties of iron oxide-based nanoparticles for smart therapy. *Kona Powder Part J*, *33*, 33-47.
- Nguyen, T. K., Duong, H. T. T., Selvanayagam, R., Boyer, C., & Barraud, N. (2015). Iron oxide nanoparticle-mediated hyperthermia stimulates dispersal in bacterial biofilms and enhances antibiotic efficacy. *Sci. Rep.*, *5*(1), 18385.

- Niederberger, M. (2007). Nonaqueous Sol–Gel Routes to Metal Oxide Nanoparticles. *Acc. Chem. Res.*, 40(9), 793-800.
- Obaidat, I., Issa, B., & Haik, Y. (2015). Magnetic Properties of Magnetic Nanoparticles for Efficient Hyperthermia. *Nanomaterials*, 5(1), 63-89.
- Oh, Y., Lee, N., Kang, H. W., & Oh, J. (2016). In vitro study on apoptotic cell death by effective magnetic hyperthermia with chitosan-coated MnFe_2O_4 . *Nanotechnology*, 27(11), 115101-115121.
- Pang, C. L. K. (2015). *Hyperthermia in Oncology*: CRC Press.
- Park, B.-H., Koo, B. S., Kim, Y. K., & Kim, M. K. (2002). The Induction of Hyperthermia in Rabbit Liver by means of Duplex Stainless Steel Thermosteds. *Korean J Radiol*, 3(2), 98-104.
- Park, J., Kang, E., Son, S. U., Park, H. M., Lee, M. K., Kim, J., Kim, K. W., Noh, H. J., Park, J. H., Bae, C. J., Park, J. G., & Hyeon, T. (2005). Monodisperse Nanoparticles of Ni and NiO: Synthesis, Characterization, Self-Assembled Superlattices, and Catalytic Applications in the Suzuki Coupling Reaction. *Adv. Mater.*, 17(4), 429-434.
- Patil, R. M., Thorat, N. D., Shete, P. B., Otari, S. V., Tiwale, B. M., & Pawar, S. H. (2016). In vitro hyperthermia with improved colloidal stability and enhanced SAR of magnetic core/shell nanostructures. *Mater. Sci. Eng. C*, 59, 702-709.
- Patsula, V., Moskvina, M., Dutz, S., & Horák, D. (2016). Size-dependent magnetic properties of iron oxide nanoparticles. *J Phys Chem Solids*, 88, 24-30.
- Pauli, W. (1967). On the connexion between the completion of electron groups in an atom with the complex structure of spectra. In *The Old Quantum Theory* (pp. 184-203): Pergamon.
- Peng, Guo, Y., Lv, H., Dou, X., Chen, Q., Zhao, J., Wu, C., Zhu, X., Lin, Y., Lu, W., Wu, X., & Xie, Y. (2016). Superparamagnetic reduced graphene oxide with large magnetoresistance: A surface modulation strategy. *Angew. Chem. Int. Ed.*, 55(9), 3176-3180.
- Peng, X., Wang, B., Yang, Y., Zhang, Y., Liu, Y., He, Y., Zhang, C., & Fan, H. (2019). Liver Tumor Spheroid Reconstitution for Testing Mitochondrial Targeted Magnetic Hyperthermia Treatment. *ACS Biomater. Sci. Eng.*, 5(3), 1635-1644.
- Pérido, E. A., Hemery, G., Sandre, O., Ortega, D., Garaio, E., Plazaola, F., & Teran, F. J. (2015). Fundamentals and advances in magnetic hyperthermia. *Appl. Phys. Rev.*, 2(4), 041302.
- Petit, C., & Pileni, M. P. (1999). Cobalt Nanosized Particles Organized in a 2D Superlattice: Synthesis, Characterization, and Magnetic Properties. *J. Phys. Chem. B*, 103(11), 1805-1810.
- Prasad, A. I., Parchur, A. K., Juluri, R. R., Jadhav, N., Pandey, B. N., Ningthoujam, R. S., & Vatsa, R. K. (2013). Bi-functional properties of $\text{Fe}_3\text{O}_4@YPO_4:\text{Eu}$ hybrid nanoparticles: hyperthermia application. *Dalton Transactions*, 42(14), 4885-4896.

- Qi, L., Song, C., Wang, T., Li, Q., Hirasaki, G. J., & Verduzco, R. (2018). Polymer-Coated Nanoparticles for Reversible Emulsification and Recovery of Heavy Oil. *Langmuir*, 34(22), 6522-6528.
- Quinto, C. A., Mohindra, P., Tong, S., & Bao, G. (2015). Multifunctional superparamagnetic iron oxide nanoparticles for combined chemotherapy and hyperthermia cancer treatment. *Nanoscale*, 7(29), 12728-12736.
- Rabin, Y. (2002). Is intracellular hyperthermia superior to extracellular hyperthermia in the thermal sense? *Int J Hyperthermia*, 18(3), 194-202.
- Raghunathan, A., Melikhov, Y., Snyder, J. E., & Jiles, D. C. (2010). Theoretical Model of Temperature Dependence of Hysteresis Based on Mean Field Theory. *IEEE Trans. Magn.*, 46(6), 1507-1510.
- Ranjbari, E., Hadjmohammadi, M. R., Kiekens, F., & De Wael, K. (2015). Mixed hemi/Ad-micelle sodium dodecyl sulfate-coated magnetic iron oxide nanoparticles for the efficient removal and trace determination of rhodamine-B and rhodamine-6G. *Anal. Chem.*, 87(15), 7894-7901.
- Rashid, A. u., Humayun, A., & Manzoor, S. (2017). MgFe₂O₄/ZrO₂ composite nanoparticles for hyperthermia applications. *J. Magn. Magn. Mater.*, 428, 333-339.
- Ravi, M., Song, S., Wang, J., Nadimicherla, R., & Zhang, Z. (2016). Preparation and characterization of biodegradable poly(ϵ -caprolactone)-based gel polymer electrolyte films. *Ionics*, 22(5), 661-670.
- Reddy, L. H., Arias, J. L., Nicolas, J., & Couvreur, P. (2012). Magnetic Nanoparticles: Design and Characterization, Toxicity and Biocompatibility, Pharmaceutical and Biomedical Applications. *Chem. Rev.*, 112(11), 5818-5878.
- Refait, P., & Génin, J. M. R. (1993). The oxidation of ferrous hydroxide in chloride-containing aqueous media and pourbaix diagrams of green rust one. *Corros. Sci.*, 34(5), 797-819.
- Reyes-Ortega, F., Delgado, Á. V., Schneider, E. K., Checa Fernández, B., & Iglesias, G. R. (2018). Magnetic nanoparticles coated with a thermosensitive polymer with hyperthermia properties. *Polymers*, 10(1), 10.
- Rivas Rojas, P. C., Tancredi, P., Moscoso Londoño, O., Knobel, M., & Socolovsky, L. M. (2018). Tuning dipolar magnetic interactions by controlling individual silica coating of iron oxide nanoparticles. *J. Magn. Magn. Mater.*, 451, 688-696.
- Robinson, I., Zacchini, S., Tung, L. D., Maenosono, S., & Thanh, N. T. K. (2009). Synthesis and Characterization of Magnetic Nanoalloys from Bimetallic Carbonyl Clusters. *Chem. Mater.*, 21(13), 3021-3026.
- Rosensweig, R. E. (2002). Heating magnetic fluid with alternating magnetic field. *J. Magn. Magn. Mater.*, 252, 370-374.
- Sakellari, D., Brintakis, K., Kostopoulou, A., Myrovali, E., Simeonidis, K., Lappas, A., & Angelakeris, M. (2016). Ferrimagnetic nanocrystal assemblies as versatile magnetic particle hyperthermia mediators. *Mater. Sci. Eng. C*, 58, 187-193.

- Salazar-Alvarez, G., Qin, J., Šepelák, V., Bergmann, I., Vasilakaki, M., Trohidou, K. N., Ardisson, J. D., Macedo, W. A. A., Mikhaylova, M., Muhammed, M., Baró, M. D., & Nogués, J. (2008). Cubic versus Spherical Magnetic Nanoparticles: The Role of Surface Anisotropy. *J. Am. Chem. Soc.*, *130*(40), 13234-13239.
- Saldívar-Ramírez, M. M., Sánchez-Torres, C. G., Cortés-Hernández, D. A., Escobedo-Bocardo, J. C., Almanza-Robles, J. M., Larson, A., Resendiz-Hernández, P. J., & Acuna-Gutiérrez, I. O. (2014). Study on the efficiency of nanosized magnetite and mixed ferrites in magnetic hyperthermia. *J Mater Sci Mater Med*, *25*(10), 2229-2236.
- Salunkhe, A. B., Khot, V. M., & Pawar, S. H. (2014). Magnetic hyperthermia with magnetic nanoparticles: A status review. *Curr Top Med Chem*, *14*(5), 572-594.
- Salunkhe, A. B., Khot, V. M., Ruso, J. M., & Patil, S. I. (2016). Water dispersible superparamagnetic Cobalt iron oxide nanoparticles for magnetic fluid hyperthermia. *J. Magn. Magn. Mater.*, *419*, 533-542.
- Santra, S., Kaittanis, C., Grimm, J., & Perez, J. M. (2009). Drug/Dye-Loaded, Multifunctional Iron Oxide Nanoparticles for Combined Targeted Cancer Therapy and Dual Optical/Magnetic Resonance Imaging. *Small*, *5*(16), 1862-1868.
- Sathe, T. R., Agrawal, A., & Nie, S. (2006). Mesoporous Silica Beads Embedded with Semiconductor Quantum Dots and Iron Oxide Nanocrystals: Dual-Function Microcarriers for Optical Encoding and Magnetic Separation. *Anal. Chem.*, *78*(16), 5627-5632.
- Sathya, A., Guardia, P., Brescia, R., Silvestri, N., Pugliese, G., Nitti, S., Manna, L., & Pellegrino, T. (2016). $\text{CoFe}_{3-x}\text{O}_4$ Nanocubes for Theranostic Applications: Effect of Cobalt Content and Particle Size. *Chem. Mater.*, *28*(6), 1769-1780.
- Schweiger, C., Hartmann, R., Zhang, F., Parak, W. J., Kissel, T. H., & Rivera-Gil, P. (2012). Quantification of the internalization patterns of superparamagnetic iron oxide nanoparticles with opposite charge. *J. Nanobiotechnology*, *10*(1), 28-28.
- Sebak, A. A. (2018). Limitations Of Pegylated Nanocarriers: Unfavourable Physicochemical Properties, Biodistribution Patterns And Cellular And Subcellular Fates. *Int. J. Appl. Pharm.*, *10*(5), 6-12.
- Shete, P. B., Patil, R. M., Thorat, N. D., Prasad, A., Ningthoujam, R. S., Ghosh, S. J., & Pawar, S. H. (2014). Magnetic chitosan nanocomposite for hyperthermia therapy application: Preparation, characterization and in vitro experiments. *Appl. Surf. Sci.*, *288*, 149-157.
- Shi, G., Takeda, R., Trisnanto, S. B., Yamada, T., Ota, S., & Takemura, Y. (2019). Enhanced specific loss power from Resovist® achieved by aligning magnetic easy axes of nanoparticles for hyperthermia. *J. Magn. Magn. Mater.*, *473*, 148-154.
- Silke, B., Helmut, B., Nina, M., Angelika, G., Eckhard, D., Wilhelm, H., Jens, B., Svetlana, Z., Natalie, P., Josef, H., Hartwig, M., Stephan, B., & Volker, K. (2006). Surface engineering of Co and FeCo nanoparticles for biomedical application. *J. Phys. Condens. Matter*, *18*(38), S2543-S2561.

- Simon, M. D., & Geim, A. K. (2000). Diamagnetic levitation: Flying frogs and floating magnets *J. Appl. Phys.*, 87(9), 6200-6204.
- Singh, N. P., Singh, L. P., Singh, N. R., & Srivastava, S. K. (2018). Photoluminescence properties of SrF₂:3Tb@BaF₂ nanoparticles and improved hyperthermia temperature achieved by core-shell nanohybrid SrF₂:3Tb@BaF₂/Fe₃O₄ materials. *Colloid Polym Sci*, 296(2), 355-365.
- Smolkova, I. S., Kazantseva, N. E., Makoveckaya, K. N., Smolka, P., Saha, P., & Granov, A. M. (2015). Maghemite based silicone composite for arterial embolization hyperthermia. *Mater. Sci. Eng. C*, 48, 632-641.
- Soleimani, N., Khalili, S. M., Farsani, R. E., & Hedayatnasab, Z. (2012). Mechanical properties of nanoclay reinforced polypropylene composites at cryogenic temperature. *J. Reinf. Plast. Compos.*, 31(14), 967-976.
- Spaldin, N. A. (2010). *Magnetic materials: fundamentals and applications*: Cambridge University Press.
- Stauffer, P. R. (2005). Evolving technology for thermal therapy of cancer. *Int J Hyperthermia*, 21(8), 731-744.
- Streffler, C., & Van Beuningen, D. (1987). The Biological Basis for Tumour Therapy by Hyperthermia and Radiation. In C. Streffler (Ed.), *Hyperthermia and the Therapy of Malignant Tumors* (pp. 24-70). Berlin, Heidelberg: Springer Berlin Heidelberg.
- Sugimoto, M. (1999). The past, present, and future of ferrites. *J. Am. Ceram. Soc.*, 82(2), 269-280.
- Sun, C., Lee, J. S. H., & Zhang, M. (2008). Magnetic nanoparticles in MR imaging and drug delivery. *Adv. Drug Deliv. Rev.*, 60(11), 1252-1265.
- Tailhades, P., Gillot, B., & Rousset, A. (1997). Mixed-valence defect ferrites : A new family of fine powders and thin films of spinel ferrites. *J Phys Colloq*, 07(C1), C1249-C1252.
- Thorat, N. D., Lemine, O. M., Bohara, R. A., Omri, K., El Mir, L., & Tofail, S. A. M. (2016). Superparamagnetic iron oxide nanocargoes for combined cancer thermotherapy and MRI applications. *Phys. Chem. Chem. Phys.*, 18(31), 21331-21339.
- Thorat, N. D., Patil, R. M., Khot, V. M., Salunkhe, A. B., Prasad, A. I., Barick, K. C., Ningthoujam, R. S., & Pawar, S. H. (2013). Highly water-dispersible surface-functionalized lsmo nanoparticles for magnetic fluid hyperthermia application. *New J Chem*, 37(9), 2733-2742.
- TrinhThang, T., Shinya, M., & NguyễnThiKim, T. (2012). Next generation magnetic nanoparticles for biomedical applications. In *Magnetic Nanoparticles* (pp. 99-126): CRC Press.
- Tudisco, C., Cambria, M., Giuffrida, A., Fulvia, S., Anfuso, D., Lupo, G., Caporarello, N., Falanga, A., Galdiero, S., Oliveri, V., Satriano, C., & Condorelli, G. (2018). Comparison between folic acid and gH625 peptide-based functionalization of

Fe₃O₄ magnetic nanoparticles for enhanced cell internalization. *Nanoscale Res. Lett.*, *13*(1), 45-54.

- Unni, M., Uhl, A. M., Savliwala, S., Savitzky, B. H., Dhavalikar, R., Garraud, N., Arnold, D. P., Kourkoutis, L. F., Andrew, J. S., & Rinaldi, C. (2017). Thermal Decomposition Synthesis of Iron Oxide Nanoparticles with Diminished Magnetic Dead Layer by Controlled Addition of Oxygen. *ACS Nano*, *11*(2), 2284-2303.
- Unterweger, H., Dézsi, L., Matuszak, J., Janko, C., Poettler, M., Jordan, J., Bäuerle, T., Szebeni, J., Fey, T., Boccaccini, A. R., Alexiou, C., & Cicha, I. (2018). Dextran-coated superparamagnetic iron oxide nanoparticles for magnetic resonance imaging: evaluation of size-dependent imaging properties, storage stability and safety. *Int. J. Nanomedicine*, *13*, 1899-1915.
- Von der Lühe, M., Weidner, A., Dutz, S., & Schacher, F. H. (2017). Reversible electrostatic adsorption of polyelectrolytes and bovine serum albumin onto polyzwitterion-coated magnetic multicore nanoparticles: implications for sensing and drug delivery. *ACS Appl. Nano Mater.*, *1*(1), 232-244.
- Wang, X., Zhou, J., Chen, B., Tang, Z., Zhang, J., Li, L., & Tang, J. (2016). Enhanced intracellular hyperthermia efficiency by magnetic nanoparticles modified with nucleus and mitochondria targeting peptides. *J. Nanosci. Nanotechnol.*, *16*(6), 6560-6566.
- Wei, W., Zhaohui, W., Taekyung, Y., Changzhong, J., & Woo-Sik, K. (2015). Recent progress on magnetic iron oxide nanoparticles: synthesis, surface functional strategies and biomedical applications. *Sci Technol Adv Mater*, *16*(2), 023501-023544.
- Weidner, A., Gräfe, C., Von der Lühe, M., Remmer, H., Clement, J. H., Eberbeck, D., Ludwig, F., Müller, R., Schacher, F. H., & Dutz, S. (2015). Preparation of core-shell hybrid materials by producing a protein corona around magnetic nanoparticles. *Nanoscale Res. Lett.*, *10*(1), 282-292.
- Wen, M., Liu, Q.-Y., Wang, Y.-F., Zhu, Y.-Z., & Wu, Q.-S. (2008). Positive microemulsion synthesis and magnetic property of amorphous multicomponent Co-, Ni- and Cu-based alloy nanoparticles. *Colloids Surf. A Physicochem. Eng. Asp.*, *318*(1-3), 238-244.
- Wenger, L. E., Tsoi, G. M., Vaishnav, P. P., Senaratne, U., Buc, E. C., Naik, R., & Naik, V. M. (2008). Magnetic properties of gamma-Fe₂O₃ nanoparticles precipitated in alginate hydrogels. *IEEE Trans. Magn.*, *44*(11), 2760-2763.
- White, C. W., Withrow, S. P., Sorge, K. D., Meldrum, A., Budai, J. D., Thompson, J. R., & Boatner, L. A. (2003). Oriented ferromagnetic Fe-Pt alloy nanoparticles produced in Al₂O₃ by ion-beam synthesis. *J. Appl. Phys.*, *93*(9), 5656-5669.
- Williams, E. H. (1926). The role of magnetism in valence. *Phys. Rev.*, *28*(1), 167-173.
- Wilson, D., & Langell, M. (2014). XPS analysis of oleylamine/oleic acid capped Fe₃O₄ nanoparticles as a function of temperature. *Appl. Surf. Sci.*, *303*, 6-13.
- Wu, Yang, X., & Yang, H. (2013). Magnetic properties of carbon-encapsulated Fe-Co alloy nanoparticles. *Dalton Trans.*, *42*(14), 4978-4984.

- Wu, S., Sun, A., Zhai, F., Wang, J., Xu, W., Zhang, Q., & Volinsky, A. A. (2011). Fe₃O₄ magnetic nanoparticles synthesis from tailings by ultrasonic chemical co-precipitation. *Mater. Lett.*, 65(12), 1882-1884.
- Wu, Y., Wang, Y., Luo, G., & Dai, Y. (2009). In situ preparation of magnetic Fe₃O₄-chitosan nanoparticles for lipase immobilization by cross-linking and oxidation in aqueous solution. *Bioresour. Technol.*, 100(14), 3459-3464.
- Wust, P., Hildebrandt, B., Sreenivasa, G., Rau, B., Gellermann, J., Riess, H., Felix, R., & Schlag, P. M. (2002). Hyperthermia in combined treatment of cancer. *Lancet Oncol.*, 3(8), 487-497.
- Xie, W., Guo, Z., Cao, Z., Gao, Q., Wang, D., Boyer, C., Kavallaris, M., Sun, X., Wang, X., Zhao, L., & Gu, Z. (2019). Manganese-Based Magnetic Layered Double Hydroxide Nanoparticle: A pH-Sensitive and Concurrently Enhanced T1/T2-Weighted Dual-Mode Magnetic Resonance Imaging Contrast Agent. *ACS Biomater. Sci. Eng.*
- Xu, Zhang, Y., Ma, M., Xia, J., Liu, J., Guo, Q., & Gu, N. (2007). Measurement of specific absorption rate and thermal simulation for arterial embolization hyperthermia in the maghemite-gelled model. *IEEE Trans. Magn.*, 43(3), 1078-1085.
- Xu, H., Zhang, Z., Shi, R., Liu, H., Wang, Z., Wang, S., & Peng, L.-M. (2013). Batch-fabricated high-performance graphene hall elements. *Sci. Rep.*, 3, 1207-1215.
- Yalcinkaya, E. E., Puglia, D., Fortunati, E., Bertoglio, F., Bruni, G., Visai, L., & Kenny, J. M. (2017). Cellulose nanocrystals as templates for cetyltrimethylammonium bromide mediated synthesis of Ag nanoparticles and their novel use in PLA films. *Carbohydr. Polym.*, 157, 1557-1567.
- Yazid, M. M., Olsen, S. H., & Atkinson, G. J. (2016). MFM study of a sintered nd-fe-b magnet: analyzing domain structure and measuring defect size in 3-D view. *IEEE Trans. Magn.*, 52(6), 1-10.
- Ye, J., He, W., Wu, Q., Liu, H.-L., Zhang, X.-Q., Chen, Z.-Y., & Cheng, Z.-H. (2013). Determination of magnetic anisotropy constants in Fe ultrathin film on vicinal Si(111) by anisotropic magnetoresistance. *Sci. Rep.*, 3, 2148-2154.
- Yin, Y., Hu, Z., Du, W., Ai, F., Ji, R., Gardea-Torresdey, J. L., & Guo, H. (2017). Elevated CO₂ levels increase the toxicity of ZnO nanoparticles to goldfish (*Carassius auratus*) in a water-sediment ecosystem. *J. Hazard. Mater.*, 327, 64-70.
- Yu, L., Liu, J., Wu, K., Klein, T., Jiang, Y., & Wang, J.-P. (2014). Evaluation of hyperthermia of magnetic nanoparticles by dehydrating DNA. *Sci. Rep.*, 4, 7216-7121.
- Zavisova, V., Koneracka, M., Kovac, J., Kubovcikova, M., Antal, I., Kopcansky, P., Bednarikova, M., & Muckova, M. (2015). The cytotoxicity of iron oxide nanoparticles with different modifications evaluated in vitro. *J. Magn. Magn. Mater.*, 380, 85-89.

- Zeng, H., Rice, P. M., Wang, S. X., & Sun, S. (2004). Shape-controlled synthesis and shape-induced texture of MnFe_2O_4 nanoparticles. *J. Am. Chem. Soc.*, *126*(37), 11458-11459.
- Zhang, Lee, I., Joo, J. B., Zaera, F., & Yin, Y. (2013). Core-shell nanostructured catalysts. *Acc. Chem. Res.*, *46*(8), 1816-1824.
- Zhang, Post, M., Veres, T., Jakubek, Z. J., Guan, J., Wang, D., Normandin, F., Deslandes, Y., & Simard, B. (2006). Laser-assisted synthesis of superparamagnetic Fe@Au core-shell nanoparticles. *J. Phys. Chem. B*, *110*(14), 7122-7128.
- Zhang, S., Tang, C., & Yin, C. (2015). Effects of poly(ethylene glycol) grafting density on the tumor targeting efficacy of nanoparticles with ligand modification. *Drug Deliv*, *22*(2), 182-190.
- Zhang, T., Thomas Gan, K. S., Lee, P., Ramanujan, R. V., & Rawat, R. S. (2006). Characteristics of FeCo nano-particles synthesized using plasma focus. *J. Phys. D*, *39*(10), 2212-2219.
- Zhang, X., Zhou, R., Rao, W., & Shanghai, P. R. (2006). Influence of precipitator agents NaOH and NH_4OH on the preparation of Fe_3O_4 nano-particles synthesized by electron beam irradiation. *J. Radioanal. Nucl. Chem.*, *270*, 285-289.
- Zhong, Y., Leung, V., Wan, L. Y., Dutz, S., Ko, F. K., & Häfeli, U. O. (2015). Electrospun magnetic nanofibre mats—A new bondable biomaterial using remotely activated magnetic heating. *J. Magn. Magn. Mater.*, *380*, 330-334.
- Zitoun, D., Pinna, N., Frolet, N., & Belin, C. (2005). Single crystal manganese oxide multipods by oriented attachment. *J. Am. Chem. Soc.*, *127*(43), 15034-15035.

LIST OF PUBLICATIONS AND PAPERS PRESENTED

Publications

1. **Ziba Hedayatnasab**, Faisa Abnisa, Wan Mohd Ashri Wan Daud. (2017). Review on magnetic nanoparticles for magnetic nanofluid hyperthermia application. *Materials & Design*, 123, 174-196. **(ISI-cited publication, Most cited article)**
2. **Ziba Hedayatnasab**, Ali Dabbagh, Faisal Abnisa, Noor Hayaty Abu Ksaim, Wan Mohd Ashri Wan Daud. (2019). Synthesis of Highly Stable Superparamagnetic Iron Oxide Nanoparticles under Mild Alkaline Reagents and Anaerobic Condition. *Nanoscience and Nanotechnology Letters*, 11(7), 985-990. **(ISI-cited publication)**
3. **Ziba Hedayatnasab**, Ali Dabbagh, Faisal Abnisa, Wan Mohd Ashri Wan Daud. (2020). Polycaprolactone-Coated Superparamagnetic Iron Oxide Nanoparticles Micelles for *In Vitro* Magnetic Hyperthermia Therapy of Cancer. *European Polymer Journal*, 133, 109789. **(ISI-cited publication)**
4. **Ziba Hedayatnasab**, Ali Dabbagh, Faisal Abnisa, Wan Mohd Ashri Wan Daud. (2020). Synthesis and In Vitro Characterization of Superparamagnetic Iron Oxide Nanoparticles Using a Sole Precursor for Hyperthermia Therapy. *Materials Research Bulletin*, 132, 110975. **(ISI-cited publication)**
5. **Ziba Hedayatnasab**, Ali Dabbagh, Faisal Abnisa, Hamed Karimian, Noor Hayaty Abu Ksaim, Wan Mohd Ashri Wan Daud. (2020). Synthesis, Characterization And In Vitro Analysis of Superparamagnetic Iron Oxide Nanoparticles for Targeted Hyperthermia Therapy. *Chemical Papers* **Accepted** (CHPA-D-19-01334R2). **(ISI-cited publication)**

Conference papers

1. **Ziba Hedayatnasab**, Faisal Abnisa, Wan Mohd Ashri Wan Daud. (2018). Investigation properties of superparamagnetic nanoparticles and magnetic field-dependent hyperthermia therapy. *IOP Conference Series: Materials Science and Engineering*, 334(1), 012042. **(Oral presentation by Mrs. Ziba Hedayatnasab, Best Presenter)**
2. **Ziba Hedayatnasab**, Ali Dabbagh, Faisal Abnisa, Hamid Reza Madaah Hosseini, Noor Hayaty Abu Kasim, Noorsaadah Abdulrahman, Wan Mohd Ashri Wan Daud. The Effects of Alkaline Reagent and Synthesis Atmosphere on the Chemical, Morphological, and Magnetic Characteristics of Magnetite Nanoparticles for Hyperthermia Treatment. *ISERD - 563rd International Conference on Medical and Health Sciences (ICMHS)*, Munich, Germany 3rd - 4th March 2019. **(Oral presentation, Best Presenter)**